Aalto-yliopisto
Kemian tekniikan
korkeakoulu

School of Chemical Technology
Degree Programme of Process System Engineering

Yan Chao

Hydrocarbon decomposition on oxygen permeable perovskite membranes

Master's thesis for the degree of Master of Science in Technology submitted for inspection, Espoo, 19, October, 2015.

Supervisor Professori Juha Lehtonen

Instructor Johanna Kihlman, M.Sc (Tech)

Aalto University
School of Chemical
Technology

Aalto University, P.O. BOX 11000, 00076 AALTO
www.aalto.fi
Abstract of master's thesis

Author	Yan Chao
Title of thesis	Hydrocarbon decomposition on oxygen permeable perovskite membranes
Department	Department of Biotechnology and Chemical Technology
Professorship	Industrial Chemistry — Code of professorship KEM-40
Thesis supervisor	Juha Lehtonen
Thesis advisor(s) / Thesis examiner(s)	Johanna Kihlman, M. Sc (Tech)
Date 19.10.2015	Number of pages 85+40 — Language English

Abstract

Synthesis gas ($CO+H_2$) can be produced via various pathways such as steam reforming, partial oxidation as well as autothermal reforming. Steam reforming is strongly endothermic and partial oxidation is weakly exothermic. By combing of the steam reforming and partial oxidation process can be operated at autothermal conditions (autothermal reforming). However, using the pure oxygen as oxidant is quite expensive and using the air would have the nitrogen content in the downstream processes. Oxygen permeable membrane enables the oxygen ions to be selectively transported through the membrane by blocking the nitrogen and other gases outside. In the literature part of the study, the mechanism and applications of the perovskite membranes as well as the preparation methods were introduced.

There were 12 membranes (A-H) tested in this thesis for toluene decomposition on the perovskite membrane under different temperatures, air flow rates, toluene amounts, bottom flow rate of toluene and nitrogen. Furthermore, the effect of the steam and gasification gas at atmospheric pressure were investigated. The results showed that the oxygen flux increased with the increased temperature and air flow rate. Higher bottom flow rate (2 l/min) of toluene and nitrogen results in lower oxygen flux value and the toluene amount has less effects on the oxygen permeability. Moreover, the oxygen flux reached to 3.03 ml/min*cm^2 at 900 ^oC, air flow rate of 0.45 l/min and total bottom flow of 0.5 l/min by adding the gasification gas, of which oxygen flux value of 1.8 ml/min*cm^2 for a normal run under the same condition. Regarding to the toluene conversion, it was clear that the toluene conversion increased with the increase of the temperature and it was higher with the gasification gases than with the steam. In summary, the oxygen fluxes were in the same range from 1.75 to 2.46 ml/min*cm^2 and C7 membrane had the highest oxygen flux and the optimal condition for the membrane was high temperature (900 ^oC), high air flow rate (0.45 l/min), with gasification gases and the optimal toluene amount dependent on the oxygen flux value.

Keywords Renewable Syngas, hydrocarbon decomposition, Oxygen permeable membrane,

Foreword

This master's thesis has been carried out at VTT Technical Research Centre of Finland between November 2014 to May 2015.

I would like to express my gratitude to Pekka Simell from VTT for offering me the possibility to make this master's thesis and his guidance and comment for my work. My thanks go to my instructor Johanna Kihlman for her advice and feedback. Moreover, I would like to acknowledge and extent my gratitude to my Professor Juha Lehtonen for his valuable advice and professional opinions. I am grateful to Mari-Leena Koskinen-Soivi and Katja Heiskanen for their patient guidance and teaching throughout the whole thesis.

Finally, thanks to my family for their encouragement and stimulating support during my studies and to my friends, Dong Jiachen, Zhang Jiaqiang and Karhan Ozdenkci who accompanied with me during my master studies.

Table of Contents

Nomenclature

Abbreviations

$A_2B_2O_7$	Pyrochlore
$A_2B_2O_5$	Brownmillerite
ABE	Metal-oxygen average bond energy
Al_2O_3	Alumina
BCFNO	$BaCo_{0.7}Fe_{0.2}Nb_{0.1}O_{3-\delta}$
BSCF	$Ba_{0.5}Sr_{0.5}Co_{0.8}Fe_{0.2}O_{3-\delta}$
BSCFO	$Ba_{0.5}Sr_{0.5}Co_{0.8}Fe_{0.2}O_{3-\delta}$
BSFZ	$Ba_{0.5}Sr_{0.5}Fe_{0.8}Zn_{0.2}O_{3-\delta}$
C_2H_2	Acetylene
CGO	Gadolinium Doped ceria
COG	Coke Oven Gas
CRR Mechanism	Combustion-reforming Mechanism
EDTA	Ethylenediaminetetraacetic Acid
GC	Gas Chromatograph
HIP	Hot isostatic pressing
MIEC	Mixed Ionic Electronic Conductors
OCM	Oxidative coupling of methane
POH	Partial Oxidation of Heptane to hydrogen
POM	Partial Oxidation of Methane to syngas
PPFR	Pressurized Plug Flow Reactor
$Sr_4Fe_{6-x}Co_xO_{13}$	Ruddlesden-Popper series

SOFC	Solid Oxide Fuel Cells
TCD-GC Chromatography	Thermal conductivity detector-Gas
TPOX	Thermal Partial Oxidation
YSZ	Yttrium Doped Zirconia

Symbols

a_o	Jump distance
A	Exponential factor;
C	Concentration of charge carries
Dv	Oxygen Vacancy Diffusion coefficient ($cm^2 s^{-1}$)
Ea	Activation energy
e’	Free Electrons
F	Faraday constant ($C.mol^{-1}$);
Fv	Lattice Free volume
J_{O2}	Oxygen permeation flux ($mol\ m^{-2}\ s^{-1}$)
L	Membrane thickness (m);
N_o	Number of oxygen ions per unit volume
O^x_o	Lattice oxygen
Δp	Pressure drop
P'_{O2}	Oxygen partial pressure at the LOW pressure side
P''_{O2}	Oxygen partial pressure at the high pressure side

γ	Geometric factor
r_A	Radius
R	Gas constant (J mol^{-1} K^{-1});
Rc	Cavity size
T	Temperature (K);
σ_{el}	Electronic conductivity;
σ_{ion}	Ionic conductivity ($\Omega^{-1}.cm^{-1}$);
Vm	Molar volume of the perovskite type ($cm^3.mol^{-1}$)
$[Vo^{\bullet\bullet}]$	Oxygen vacancy concentration
v_o	Jump odds
Z*e	Charge carries number

Subscripts

Cat	Catalyst

1. Introduction

Gasification of biomass is considered to be one of the most promising technology to produce syngas because the raw material is renewable and process is environmentally friendly [1]. Synthesis gas, which is mainly the mixture of carbon monoxide and hydrogen, can be produced via various pathways, for example, steam reforming, partial oxidation as well as autothermal reforming. The steam reforming process is endothermic which requires external heat sources to break down the hydrocarbon compounds to form H_2-rich gas. By contrast, the partial oxidation process is a weakly exothermic and it requires less energy and is less cost-intensive as well as provides a lower H_2: CO (2:1) ratio resulting in a more favourable composition for the synthesis of Fischer-Tropsch or methanol. Autothermal reforming is an alternative to steam reforming that combines of the steam reforming and partial oxidation reactions. However, using the oxygen as oxidant for partial oxidation or autothermal reforming process is quite expensive that will increase the investment cost. Separating the oxygen from the air could be favourable but it will increase the nitrogen content, of which is not suitable for the downstream processes such as Fischer-Tropsch. [2]

Oxygen permeable membranes enable the oxygen ions to be selectively transported through the membrane by blocking the nitrogen and other gases outside. It acts as a supplier of oxygen for the partial oxidation. The pure oxygen separated from the air by OPM is cheaper, economic, and environmentally friendly and no formation of NO_X in the reactor in theory takes place [3]. The core of the oxygen permeable membrane reactor is to combine both separation and reaction steps into one process making possible to get rid of expensive distillation [2].

Tar, which is the byproduct of the biomass gasification process, brings problems for the downstream process equipment including blockage or corrosion. The tar consists of the

aromatic compounds such as benzene, toluene and naphthalene. The tar can be removed by the oxidation reactions, which can be provided by Oxygen Permeable Membranes (OPM). Toluene was chosen as an example to represent the tar compounds in this study. [4]

The literature part of the thesis provides the mechanism and application of perovskite membranes as well as the manufacturing methods. The experiments were carried out between 700-950 ^{o}C at atmospheric pressure. The experiment was performed by exposing one side of the membrane to the air and the other side to the toluene. Both thermal conductivity detector-Gas Chromatography (TCD-GC) and Flame Ionization Detector-Gas Chromatography (FID-GC) were used for analysing the products. There were a total of 12 of perovskite membranes (A-H) that has been studied in the experiments. Different temperatures, air flow rates, total flow rates of toluene and nitrogen, toluene amounts, effect of the steam and gasification gases were evaluated for perovskite membranes in order to investigate the optimal reaction conditions. The main target was to compare several perovskite materials and find the optimal conditions for the best material, where the partial oxidation was the target reaction.

2. Oxygen Permeable Membrane

Mixed ionic electronic conductors (MIEC), also known as, dense ceramic oxygen permeable membranes, which exhibit both electronic and oxygen ionic conductivity, are capable of oxygen separation from air [5]. The partial pressure differences of the oxygen ions between two sides enable the oxygen ions to be selectively transported through the membrane. At the same time, counter transport of electronic charge carriers is required to maintain charger neutrality [6]. No external electrodes are required for transportation due to the electronic-ionic conductivity, but elevated membrane operation temperature (from 700°C to 1000 °C) is needed. Owning to the nature of oxygen vacancies, oxygen purities can be obtained with 100% selectivity at high temperatures, which means nitrogen or any other gas are blocked from the membranes [7].

The researches on the dense ceramic oxygen permeable membranes have gone through the steps from the fluorite-type compound to the perovskite-type compound [8]. Takahashi et al. [9] initially reported the fluorite-type Bi_2O_3-BaO for mixed ionic-electronic conductivity in 1976, of which novel applications of CaO or Y_2O_3-doped ZrO_2 (CeO_2) membranes have attracted a great attention in the research area during the last 30 years. However, these fluorite materials have low electronic conductivity and the first perovskite membrane $La_{1-x}Sr_xCo_{1-y}FeO_{3-\delta}$ was developed by Teraoka et al. [10] in 1985 to obtain high electronic-ionic and conductivity. In contrast, Perovskite materials have relatively high electronic conductivity (10^2-10^3 $S.cm^{-1}$), ionic conductivity and high oxygen permeability at elevated temperature. The MIEC also combines both separation process and catalytic oxidation conversion processes into single step for synthesis gas production. [11]

2.1 Theory (Mechanism)

The oxygen transportation mechanism across the membranes is a complicated physical-chemical process, which can be understood by the defect theory. The crystal lattice defects on the membrane material result in the existence of oxygen vacancies which enable anionic oxygen to be selectively transported; meanwhile electronics provide the electronic conductivity [8]. The driving force of dense membranes is the oxygen chemical potential gradient between two sides of the membrane. To simplify the process, the oxygen is first adsorbed, dissociated on the high oxygen chemical potential feed side and then transported across the ceramic material in the form of oxygen anions to low oxygen chemical potential (oxygen-lean side), finally associated and desorbed to form oxygen molecules. The oxygen transportation steps were shown in Figure 1: [13]

- Step 1. Diffusion: the oxygen molecules on the high oxygen chemical potential feed side diffuse to the membrane surface.
- Step 2. Adsorption: oxygen molecules adsorb on the high oxygen chemical potential membrane surface to form adsorbed oxygen.
- Step 3. Dissociation (surface reaction): the adsorbed oxygen disassociates to chemisorbed oxygen ions and occupies oxygen vacancies to form crystal lattice oxygen ions (O^{2-}).
- Step 4. Ionic transport (bulk diffusion): the oxygen ions are transported across the crystal lattices vacancies to oxygen-lean surface driven by oxygen chemical potential gradient.
- Step 5. Electronic transport (bulk diffusion): Meanwhile, counter transport of electronic charge carriers is required to maintain charger neutrality.
- Step 6. Association (surface reaction): the oxygen ions recombined with electrons to form oxygen molecules by releasing the electrons in the electronic conducting phase under the low oxygen chemical potential permeate side.

- Step 7. Desorption (surface reaction): the recombined oxygen molecules released from the permeate stream as pure oxygen.
- Step 8. Gas transport: the oxygen molecules on the low oxygen chemical potential feed side are formed new molecules.

The molecular diffusion of oxygen molecules in step 1 and 8 are independent of membrane characteristics, whilst step 4 and 5 involve the transportation of oxygen ions and electrons through the crystal lattice vacancies and carried out only at the elevated temperature. The steps 2-3 and 6-7 are the surface reaction steps which are controlled by surface dissociation/association kinetics, whereas the steps 4-5 are dependent on the intrinsic characteristic of the membrane materials and membrane thickness. Hence, it is clear that the oxygen permeability is essentially dominated by two factors, surface-exchange resistance on membranes interfaces and bulk diffusion of solid oxide state. [14]

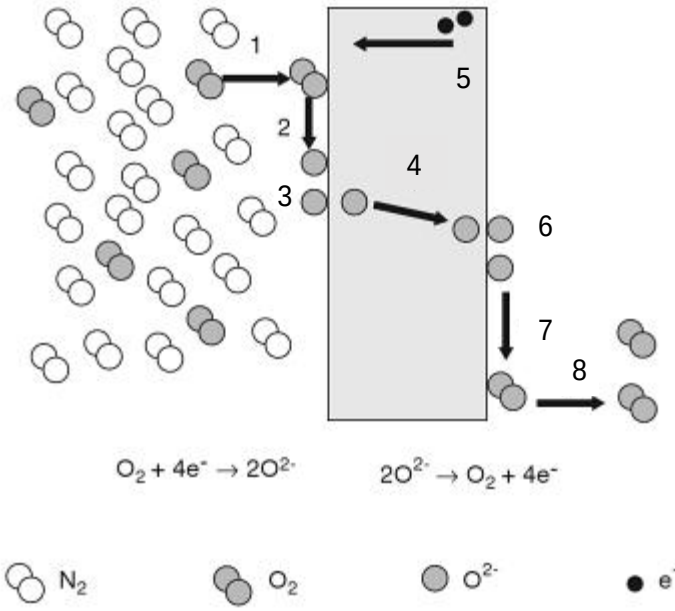

Figure 1. Schematic of oxygen transportation progressive steps through the perovskite membrane. [15]

2.1.1 Bulk diffusion

The oxygen permeability under oxygen chemical potential gradient is mainly dominated by the diffusion rate of oxygen ions through the lattice. The interaction between gas phase oxygen and lattice oxygen can be described by Kröger-Vink notation: [16]

$$O_2 + V_O^{\bullet\bullet} + 2e' \leftrightarrow O^x_o \quad (1)$$

Where, oxygen vacancies ($V_O^{\bullet\bullet}$), free electrons (e') and lattice oxygen (O^x_o). Oxygen vacancies provide the anionic oxygen to be selectively transported and compensated by electronic charges to maintain charge neutrality. In this equilibrium, oxygen vacancies are assumed to be ionized fully and the concentration of free electrons e' is negligible.

The oxygen permeability can be expressed by Wagner equation: [17]

$$J_{O_2} = -\frac{\mathrm{RT}}{4^2F^2L}\int_{lnP'O_2}^{lnP''O_2}\left[\frac{(\sigma_{el}\cdot\sigma_{ion})}{(\sigma_{el}+\sigma_{ion})}\right] dlnPO_2 \quad (2)$$

The ionic conductivity is calculated based on Nernst-Einstein relation: [18]

$$\sigma_{ion} = \frac{4\mathrm{F}^2\,[Vo^{\bullet\bullet}]\mathrm{Dv}}{RTVm} \quad (3)$$

In which J_{O2} is oxygen permeability in mol m^{-2} s^{-1}; R is the gas constant (J mol^{-1} K^{-1}); T is the temperature (K); F is the Faraday constant ($C.mol^{-1}$); L is the membrane thickness (m); σ_{el} is electronic conductivity; σ_{ion} is ionic conductivity ($\Omega^{-1}.cm^{-1}$); P''_{O2} and P'_{O2} are the oxygen partial pressure at the oxygen rich side and lean side; $[Vo^{\bullet\bullet}]$ is the concentration of oxygen vacancies in mole fraction, Dv is the oxygen vacancy diffusion coefficient (cm^2 s^{-1}) and Vm is the molar volume of the perovskite type ($cm^3.mol^{-1}$), respectively.

Consequently, according to Wagner equation it is obvious that the O_2 permeation rate depends on temperature, membrane thickness, the partial pressure differences

between oxygen rich and lean side as well as the ionic and electronic conductivity. The conductivity is the product of oxygen defect concentration, where the electrons concentration is negligible. According to Nernst-Einstein equation, the oxygen permeability is determined mainly by three factors: the oxygen vacancy concentration [$Vo^{\bullet\bullet}$] , the oxygen vacancy diffusion coefficient Dv and the temperature. The increase on the oxygen defect concentration will increase the oxygen permeability of the membranes.

The oxygen flux has inversely proportional relationship with the membrane thickness, which means decreasing the membrane thickness will lead an increasing of O_2 permeate rate. However, the oxygen permeate rate is not proportional to 1/L. The resistance to oxygen ions conduction for thinner membranes will be limited to a certain value. The decrease of membrane thickness will also affect the mechanical property of membranes. The value of Lc can be determined by: [19]

$$Lc = \frac{Dc}{Ks} \tag{4}$$

Where Dc represents oxygen anions diffusion coefficient and Ks is the oxygen surface exchange coefficient, respectively. Based on this equation, the membrane thickness is independent on the oxygen flux and oxygen conductivity; it only depend on oxygen anion coefficient and oxygen surface exchange coefficient. During the experiments, it has been found out that the membrane thickness is also determined by operating environment, for example, the temperature, O_2 partial pressure and preparation methods. However, decrease of the thickness of the membrane has less effect on the oxygen flux, if some catalytic material (Pt, Ag) is deposited on the membrane surface. [20]

2.1.2 Surface exchanges

If the reduction of membrane thickness has less effect on the ionic conductivity, surface-exchange reaction becomes the controlling step of the oxygen flux. In practice, the surface exchange reactions proceeding at the gas-oxide interface involve sequential steps of adsorption, dissociation, surface reaction, gas diffusion and finally recombined oxygen molecules. Consequently, the oxygen partial pressure difference is consumed by interfacial oxygen exchange. The mechanism of surface exchange is a complicated process, which may express as follows: [20]

$$O_2\,(g) \leftrightarrow O_2\,(ad) \tag{5}$$

$$O_2\,(ad) + e' \leftrightarrow O_2'\,(ad) \tag{6}$$

$$O_2\,(ad) + e' + S\,(ad) \leftrightarrow 2O'\,(ad) \tag{7}$$

$$O'\,(ad) + e' \leftrightarrow O''\,(ad) \tag{8}$$

$$O''\,(ad) + Vo^{\bullet\bullet} \leftrightarrow O^{x}_{o} \tag{9}$$

Equation (1) represents adsorption; (2) and (4) are charge transfer processes, (3) correspond to dissociation and (5) is the incorporation step in interfacial zones. The reverse reactions of re-oxidation of oxygen ions follow the same steps. The surface reactions are mainly governed by the charge transportation between oxygen to the oxide surface and the progressive steps will control the overall mechanism of the oxygen flux.

According to the Wagner's equation for bulk transport incorporated with surface reaction kinetics, the general flux equation for surface-exchange can be expressed as follows: [7]

$$J_{O_2} = -\frac{1}{1+(2L_C/L)}\frac{t_{el}\sigma_{ion}}{16F^2}\frac{\Delta\mu_{O_2}^{total}}{L} \tag{10}$$

Compared to Wagner's equation for bulk diffusion, the only difference is the membrane thickness and the flux is independent to L. Therefore, the value of Lc is the parameter for determining the influence of bulk or surface processes on the oxygen permeability. If the membrane thickness is greater than Lc (L>10Lc), bulk diffusion determines the oxygen flux. While the membrane thickness is significantly lower than Lc (L< 0.1Lc), the oxygen flux is dominated by surface exchange kinetics. If it is closer to Lc, the oxygen permeability is governed by both bulk diffusion and surface exchange [20].

The surface exchange kinetic could be enhanced by adding catalyst (Ni or noble metals) on the membrane surface, or by increasing the exchange surface rate, or by increasing the oxygen chemical potential gradient. However, the increase on the P_{O2} gradient will decrease the chemical stability and mechanical stability of the membranes. In conclusion, oxygen permeation rate dominated by the working condition, membrane thickness, the partial pressure differences, the electronic and ionic conductivity (oxygen vacancies concentration) and the surface catalytic kinetics. The overall controlling factor for oxygen permeability is shown below in figure 2. [20]

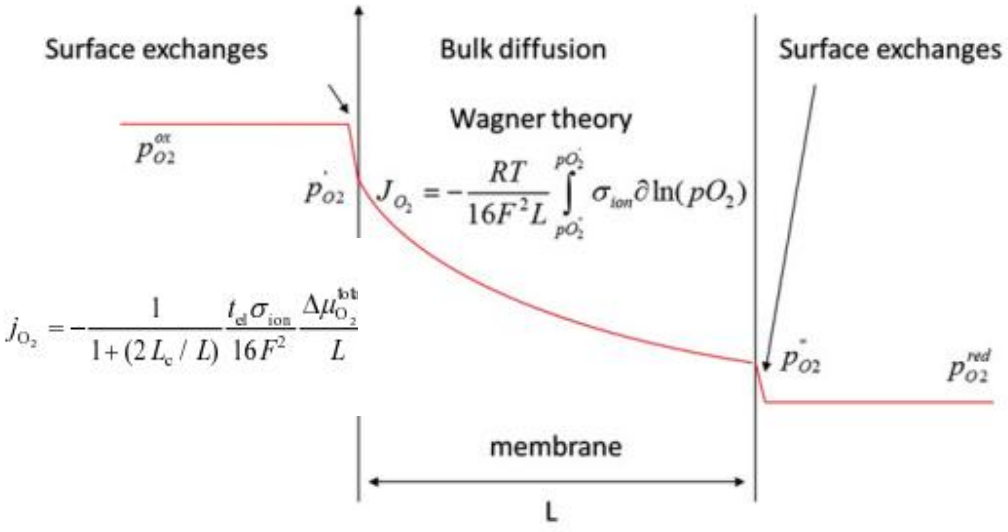

Figure 2. The overall mechanism for oxygen permeability [20]

2.2 MIEC Membrane Types and Structure

Mixed ionic electronic conductor displays the potential advantages for oxygen transportation, which results in high oxygen selectivity in theory. The two most promising compounds for oxygen permeability are fluorites and perovskites (single phase & double phase) in terms of the chemical structure. The compounds such as pyrochlore ($A_2B_2O_7$), brownmillerite ($A_2B_2O_5$), $Sr_4Fe_{6-x}Co_xO_{13}$, materials with $A_2BO_{4+\delta}$, bimevox compounds, Ruddlesden-Popper series ($An_{+1}B_nO_{3n+1}$) and orthorhombic K_2NiF_4-type series are also available for mixed conductor; of which the last two series belong to perovskite-related intergrowth structure. Since they are not so popular, it is not included in our discussion. Perovskite type compounds (single phase $ABO_{3-\delta}$ type) are the main subjects in this study [11].

2.2.1 Fluorite compounds

As previously mentioned, fluorite type compounds have high oxygen ions mobility due to their crystal structure. Fluorites contain a cubic packing of anions with half of the interstices occupied by the metal cations in the cubic (8-coordinate) holes [11] (Figure 3). The ideal ratio of the cation to anion must be 4.38 to maintain the cation-anion contact and closest packed cations in the fluorite structure. A smaller ratio will cause less closely packed of cations and a larger ratio will result in less cation-anion contact. This fluorite type material has the cations occupying all the cation sites, which provide the empty space for oxygen anions to form oxygen defects [21].

Recently, the research has focused on fluorite materials such as CaO, Y_2O_3 or Sc_2O_3 doped ZrO_2; Sm_2O_3, Gd_2O_3 or Y_2O_3 doped CeO_2 and SrO and Y_2O_3 or Er_2O_3 doped Bi_2O_3 for application of solid oxide fuel cells (SOFC). However, these fluorite materials have very low electronic conductivity resulting in low oxygen permeability. Hence, in order

to improve the electronic conductivity, the metals such as Pt, Pd, Au, Ag should be used as dopants to form high potential composite materials. Even though the electronic conductivity has been increased, the mixed ionic-electronic conductor for fluorite type is still unfavorable.

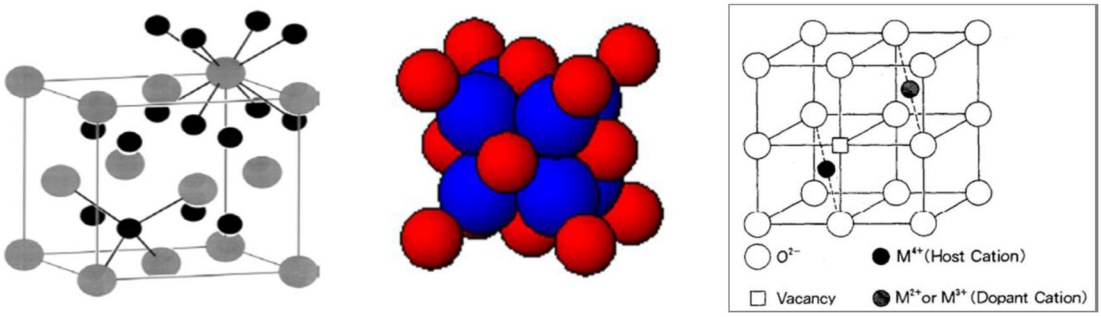

Figure 3. Structure of fluorite compounds [7].

2.2.2 Perovskite compound (single phase)

The most promising material of MIEC membranes is the perovskite type with the formula $ABO_{3-\delta}$ and it has gained greatest attention during the past. The ideal perovskite structure is cubic in which A has approximately same size with O ions and B site ions tend to be smaller. It can be described that B cations are located in the corners with 6-fold coordination and A cations with 12-fold coordination in the center and oxygen atoms are at the midpoints of the edges. (Figure 4) [21]. Perovskite material has symmetric cubic structure with the ratio of the A-O bond length to B-O bond length $\sqrt{2}$:1. Generally speaking, A-site ions can be alkali, rare-earth or alkaline-earth ions such as La^{3+}, Na^{1+}, Ca^{2+}, Sr^{2+} or Ba^{2+}. The B-sites are occupied by the transition metal ions such as Fe^{3+}, Co^{3+}, Ni^{2+} or Cu^{2+} [20]& [23].

The most common perovskite compounds are $A^{+}B^{5+}O_3$, $A^{2+}B^{4+}O_3$ and $A^{3+}B^{3+}O_3$. Recently, substitution of A and B sites by doping different elements has been investigated. The

idea is to increase the physical-chemical properties and oxygen permeability of membrane materials, of which the formula can be expressed by A_xA_{1-x} $B_yB'_{1-y}O_{3-\delta}$. The elements for chemical doping on the A site are aliovalent metals, of which a lower valence metal will increase the ionic conductivity. Doping higher valence metal in the A site decreases the ionic and doping same valence bigger radius will keep the ionic conductivity and at the same time increase the chemical stability in the reducing environment. The doped metals on the B-site are usually transition metals. The multivalence of the B-site ions mainly affects the electronic conductivity and stability of the material [23].

When an A-site metal ion is completely or partially replaced by metal ions with lower valence, it will lead to the increasing amount of oxygen vacancies that mainly affect oxygen ionic conductivity. Meanwhile, the aliovalent transition metal ions in B-site will change valence state to maintain the electronic neutrality to provide the electronic conductivity. Therefore, perovskite material performs both high oxygen ion conductivity and electronic conductivity. The high number of the oxygen vacancies will result in higher oxygen permeation flux. The higher number of defects can be achieved by doping of A-site ions with different valences. Doping elements with lower valence state (Cu or Ni ions) on B-site will increase the chemical/thermal stability of the membrane. The transformation of B can be explained below [20]:

$$B^{n+1} - O^{2-} - B^{(n-1)+} \longrightarrow B^{(n-1)+} - O^{-} - B^{(n-1)+} \longrightarrow B^{(n-1)+} - O^{2-} - B^{n+}$$

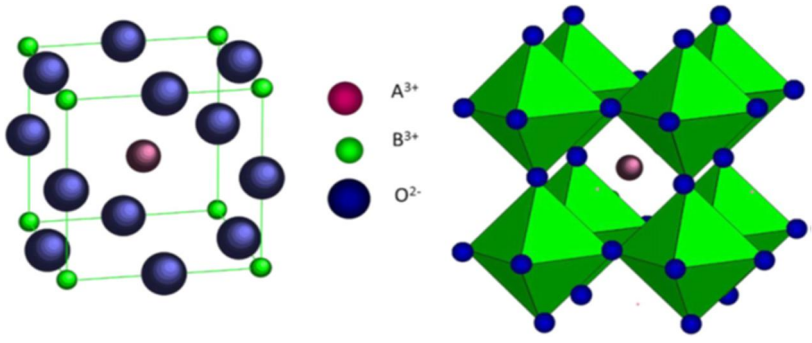

Figure 4. The ABO_3 structure of perovskite compounds [20].

2.2.3 Dense dual phase compounds

Longo et al. [24] initially reported mixed conducting dual-phase membranes in 1961 due to the fact that single-phase membranes, especially perovskite type, have low mechanical/thermal stability in the strong reducing environment. Therefore, dual phase compounds have been developed and extensively studied in order to enhance the overall membranes stability. Dual-phase membranes $A_2BB'O_6$ or double-perovskite type both exhibit magnetic and electronic properties. They consist both oxygen-ion and electronic conducting phases in which oxygen ions and electrons are transported in two independent passage. The oxygen-ion conducting phases are usually made of high oxygen-ion conducting and stable solid oxide electrolyte materials and the electronic conducting phases are electronic conductive oxides or noble metals. Usually, the fluorite-type membranes are used as ionic conducting phase, together with noble metals such as Pt, Au, Ag etc or pure electronic conducting oxides such as perovskite type or $MnFe_2O_4$ for electronic conducting phase to form $Ce_{0.8}Gd_{0.2}O_{1.9}$-$La_{0.7}Sr_{0.3}MnO_3$ dual phase [25].

Recently, doped Bi_2O_3 and Ag have been intensively studied for dual phase. The most common used oxygen-ion conducting phases are Y_2O_3 or CaO doped ZrO_2, which are all fluorite-type membranes. Solid oxide electrolytes such as yttrium doped zirconia (YSZ) and gadolinium doped ceria (CGO) have been used to improve the chemical stability in carbon dioxide atmosphere [26]. Double phase perovskite oxides such as Sr_2CaWO_6 and Sr_2MgWO_6 have shown potential advantages in long-term oxygen permeability and thermal stability [27]. However, the manufacturing of dual phase compounds are limited due to the incompatibility of the components that needs to be improved in the future.

2.3 Perovskite type MIEC Membranes

2.3.1 Characteristics of Pervoskite Membranes

The requirements for a good oxygen selective membrane are the capabilities for oxygen adsorption/desorption, oxygen diffusion and 100% oxygen selectivity. The oxygen is transported as follows:

$$O_2 \leftrightarrow O_2 \text{ adsorbed} \leftrightarrow O_2^- \text{absorbed} \leftrightarrow 2O^- \text{ adsorbed} \leftrightarrow 2O^{2-} \leftrightarrow 2O^{2-} \text{ lattice}$$

The radii of A- (r_A) and B-site (r_B) cations must fulfil the Goldschmidt tolerance factor (t) in order to form perovskite structure: [28][29]

$$t = \frac{(r_A + r_o)}{\sqrt{2}(r_B + r_o)} \quad (11)$$

When t=1, the perovskite is ideal cubic compound with stable cubic symmetry structure.

When t=0.75-1, the perovskite structure is maintained. Usually most of the perovskite structure has lower symmetry structures due to the distortion by the cation displacements, in which leads to bond lengths (A-O, B-O) shorter than in the ideal type. [30] &[31]

In reality, structure transformation under high oxygen chemical partial gradient leads to internal stress of membranes as a result of decrease the oxygen permeability. The tolerance factor, used for the adjustment of doping with different cations on A or B-sites for structure stability. Doping lower valence state of A-site will affect the defect formation and B-site cation valence dominates the structural stability. The possible structure transition from cubic to non-cubic can be calculated from the tolerance factor [30] & [31].

The perovskite type materials are considered to be electronic conducting membranes, of which the oxygen permeability depends on electronic/ionic conductivity of the

membranes. Therefore, to improve the oxygen ionic conductivity was the key to improve the oxygen flux. The ionic conductivity could also be expressed as follows: [30]

$$\sigma \text{ion T} = \text{A} \times \exp(-\frac{\text{Ea}}{\text{kT}}) \quad (12)$$

$$A = C\gamma(\frac{Z^2e^2}{k}){a_o}^2 v_o \cdot exp(\frac{\Delta Sm}{k}) \quad (13)$$

$$C = No[Vo^{\bullet\bullet}](1 - Vo^{\bullet\bullet}) \quad (14)$$

Where T represents absolute temperature as Kelvins; A is the exponential factor; E_a is the sum of activation energy of oxygen mobility and defect formation energy (J mol^{-1}), usually Ea=ΔH ($\Delta H\ for\ migration\ enthalypy$); C is concentration of charge carries; γ is geometric factor; Z*e charge carries number; a_o stands for jump distance; v_o is the jump odds; N_o is the number of oxygen ions per unit volume and $Vo^{\bullet\bullet}$ is the oxygen vacancy, respectively.

Based on equation (12), it is obvious that oxygen flux increases either by increase exponential factor or decreasing activation energy, if the temperature is fixed. Based on equation (8), the value of C is related to the concentration of oxygen vacancy, which fits on Nernst-Einstein relation. The increase of oxygen vacancies concentration leads to the rise of the value of A and therefore, the ionic conductivity will increase as well. It is important to emphasize that the Ea value will enhance the oxygen flux as well. Activation energy (Ea) is related to the cavity size (rc), lattice free volume (Fv) and metal-oxygen average bond energy (ABE). The equation is shown as follows:

$$rc = \frac{-{r_A}^2 + \frac{3}{4{a_o}^2} - \sqrt{2}\, a r_B + {r_B}^2}{2(r_A - r_B) + \sqrt{2}\, a_o} \quad (15)$$

$$Fv = a^3 - \frac{4}{3}\pi\lfloor {r_A}^3 + {r_B}^3 + (3 - \delta){r_o}^2 \rfloor \quad (16)$$

When the oxygen ions passing through the cavity in the membranes, they need to enter the narrow space in the center of two A cations and one B cation (Figure 5). The

r_c (r_c<1.1 Å) is the radius for that circle which is usually smaller than the radius of oxygen ions (r_o=1.4 Å). Hence, to pass the narrow space will require in relaxation effect of oxygen ions which needs high energy (activation energy Ea) to overcome the force for oxygen ion migration. The larger r_c will result in less relaxation effect and lower activation energy value. The increase of the radius of A and B will decrease the r_c value [30].

The lattice free volume (Fv) is the volume difference between the lattice and the total ions. The larger value of the lattice free volume means the larger space for oxygen mobility, which results in high oxygen permeability. The value of Fv increases with the rises of radius value of the A-site and B-site [30].

Metal-oxygen average bond energy (ABE) is the energy between A-O and B-O bond strength, which affects the oxygen vacancies. The less value of average metal-oxygen bond energy leads to the oxygen ions losing metal easily. The ABE value also affects both adsorption and dissociation steps and oxygen ionic bulk transportation. The higher oxygen ionic conductivity prefers lower average ABE value [30].

Therefore, the oxygen flux in the membrane can be increased either by partially doping metals on A-site to increase the oxygen vacancy or by choosing higher radius of A and B metal ions to lower the activation energy. Lower value of ABE is also important factor for increasing the ionic conductivity.

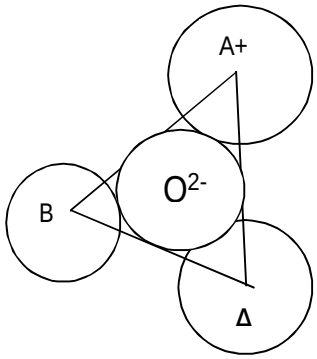

Figure 5. Oxygen ions transportation path.

Electrons are required to maintain charger neutrality and the mechanism process can be shown below [30]:

$$B^{n+}— O^{2-}—B^{(n+1)+} \rightarrow B^{(n+1)+} —O^{-}— B^{(n+1)+} \rightarrow B^{(n+1)+} — O^{2-}— B^{n+} \quad (17)$$

Some metal ions have high thermal expansion coefficient under a large oxygen chemical gradient or high temperature, causing the thermal expansion of the lattice volume promoted by the ionic radius change (e.g. Co^{2+}, Co^{3+} and Co^{4+}). As a result, the formation of cracks and membrane failure can take place during the operation. Under the reducing environment (H_2), the large amount of the oxygen defects cause the lattice expansion and phase transition, which results in structure distortion. When the perovskite-related membranes with doped alkaline earth metals are exposed to the CO_2 atmosphere, they may react with gas species like CO_2 resulting in the low chemical stability. The poor chemical stability under the high reducing environment, poor long-term oxygen permeability under the high oxygen chemical potential condition as well as low mechanical stability limits the practical applications. Therefore, it is wiser to dope the B-site with higher stabling metals (Fe, Cr, Zr, Ti or Mo) in order to restrain the transformation of the unstable metals, which increases the chemical/thermal stability of the membrane materials. [31]

2.3.2 Current situation of Single phase $ABO_{3-\delta}$ perovkite-type materials

2.3.2.1 Research progress

Since Teraoka et al. [1] has reported firstly dense ceramic perovskite oxides of $La_{1-x}Sr_xCo_{1-y}Fe_yO_{3-\delta}$ composition in the 1980s, various perovskite ($ABO_{3-\delta}$) types or related structures such as $SrFeCo_{0.5}O_x$, $Ba_{0.5}Sr_{0.5}Co_{0.8}Fe_{0.2}O_{3-\delta}$ and $La_xA_{1-x}Co_yFe_{1-y}O_{3-\delta}$ (A=Sr, Ba) have been studied. Considerable investments on the research of the dense ceramic membrane have been done in America, Japan and Netherlands. Numerous membranes have been reported, which partial substitution of Ca, Ba, Pr, Nd, Sm and Gd to A-site, and Sc, Ti, Cr, Mn, Ni, Cu, Zn, Al, Ga, Zr, Nb, Mo, Sn, Sb and W for doping of the B-site [20] & [23]. Almost all the alkaline metals and transition metals have been employed in the membranes. However, among these materials there are only few membranes suitable for practical applications because of the low thermal/chemical stability and poor mechanical strength. There are some materials that meet the practical requirements, for example, $Ba_{0.5}Sr_{0.5}Co_{0.8}Fe_{0.2}O_{3-\delta}$ with high oxygen permeability and thermal ability for short-term operations [32]. Cobalt-free membranes have been investigated such as $La_{0.6}Sr_{0.4}Ga_{0.6}Fe_{0.4}O_{3-\delta}$ to enhance the thermal stability. Recently, Harada reported $BaCo_{0.7}Fe_{0.2}Nb_{0.1}O_{3-\delta}$ having high oxygen-permeability and stability for long-term (700h) operations, and it has been widely used for coke oven gas oxidation under high oxygen chemical potential gradient in China [23].

2.3.2.2 Selection of perovskite material for oxygen permeation membrane

When selecting the perovskite material for the practical applications, five factors need to be considered: oxygen permeability, phase stability, thermal expansion, tolerance in reducing environment (H_2) and CO_2 resistance for application of oxygen separation in catalytic oxidation process. The oxygen permeability is dominated by the natural

property of the metal ions in A-site and doped metals for creating the more oxygen vacancies, while phase stability depends on the radius of both A and B-site which is judged by the calculation of the tolerance factor close to 1. The thermal expansion is affected by stability of multivalence state on the B-cations. The more stable of the metal oxides resulting in high stability and the easy transformation of the valence state causing low stability (Co^{2+}, Co^{3+}, Co^{4+}); Adding the lower valence state cations such as Fe and Cu to the original B-site cation will restrain the transformation of less stable metal ions as a result of lower the thermal expansion coefficient. Under the reducing environment, the membrane stabling, it is judged by the reaction with H_2. Normally, alkaline earth metal, rare earth metal and some high valence state metals will react with H_2. The resistance to the CO_2 is affected by the cations on A-metal, with alkaline earth metals (Ba^{2+}) easily reacting with CO_2 and water vapor [30].

The target of the selection of the membrane material is to provide high oxygen permeability, high phase stability under reducing atmosphere as well as sufficient mechanical strength. Therefore, there are several rules used to guide for development of the perovskite membrane materials, which is summarized below [30].

1) The selection of suitable doped metal cations to A or B-site should meet the tolerance factor in the range between 0.75-1 in order to maintain the structure stability. The more close to 1 will provide high phase stability, high ionic conductivity and electronic conductivity for practical applications.
2) The selection of the r_{A-} and r_{B-}site cations tend to be as large as possible. The large ionic radius leads to maximizing the lattice free volume, which would suppress the structure transition due to formed larger tolerance factor. Moreover, the metal with low average bonding energy (ABE) is favourable in order to obtain high ionic conductivity.
3) Doping higher valence metal in A site will decrease the ionic conductivity due to the reducing amount of oxygen lattice and doping same valence with bigger

radius will keep the ionic conductivity while increasing the chemical stability in reducing environment (Ba-Sr-Co-Fe-O). Therefore, A-site cations should be of large size and have low ABE value and low valence state.

4) For B-site cations, two types of cations are ideal: one which has higher valence in order to keep high thermal/chemical stability and structure stability and another one is transition metal ion for redox reactive. For the high valence stable metal cation in B-site, the amount of the stable metal is preferred to be low to improve the structure and thermal ability.

The previous subsections for the perovskite type materials can be summarized as follows:

Table 1. Selection of perovskite B-doped metal ions for oxygen permeation membrane [34]

Property	Metal
Oxygen ion conductivity	Co>Fe>Ga>Mn>Cr>Ti
Electronic conductivity	Co>Fe>Mn>Cr>Ga>Ti
Oxygen surface exchange coefficient	Co>Fe>Ga>Mn>Cr>Ti
Thermal expansion coefficient	Co>Fe>Mn>Cr>Ga>Ti
Chemical expansion coefficient	Co>Fe>Mn>Cr>Ga>Ti
CO_2 tolerance	Ti>Ga>Cr>Mn>Fe>Co
Creep rate	Ti>Ga>Cr>Mn>Fe>Co
A-site Low activation energy (Ea) (high oxygen flux)	Ba, Sr, Ca, Bi, Pb
A-site High activation energy (Ea) (high stability)	La, Y, Pr, Nd
B-site Low activation energy (Ea) (high oxygen flux)	Co, Mg, Zn, Mn, Bi, Cu, Ni
B-site High activation energy (Ea) (high stability)	Al, Cr, Zr, Ti, Mo, V,

2.3.2.3 Current situation and future development

Although it has been significant progress in dense ceramic oxygen membranes in the past decades, there are still some challenges need to be overcome to reach a technical utilization of ceramic membrane for practical applications. The current membranes are still unfavourable due to the low oxygen flux value and stability which limits their applications. The future improvements of membrane are listed as follows [35] & [36]:

1) Membrane Materials: the increase the oxygen permeability flux value through surface modification either by adding supported layer or microstructure modification changing surface exchange kinetics. The stability under the reducing environment and CO_2 tolerance are other urgent issues for further improvements and double-perovskite membranes or dual phase membranes are recommended.
2) Membrane Manufacturing: the preparation methods, sintering parameters and materials shape (disk, tube, capillaries and hollow) needs to be further improved, which is discussed in the following section.
3) Chemical reaction: the catalytic activity of these oxides is generally insufficient for selective oxidation; hence suitable catalysts such as nickel are necessary for the application of dense ceramic reactors in large-scale practical usage.

3. Membrane preparation methods

Three sequential steps: preparation of powders, shape-forming of membranes and sintering of membranes are employed for membrane preparation. Three synthesis methods (solid state, Co-precipitation and sol-gel methods) are frequently used to produce MIEC powders. Other less common methods such as hydrothermal methods, spray and freeze drying, plasma spraying, electronic beam evaporation and arc vaporization are also reported [37]. Typically powder possesses relatively large pores (i.e. diameters larger than 1um). Ceramic shape forming processes involves compaction (densification) of precursor powders to produce dense ceramic membranes, followed by sintering process. The mechanical property (strength) and morphology (grain size, grain boundary and size distribution) of the membrane depends on the form of raw materials, the nature of the process (preparation methods) and preparation conditions (pH, temperature, additives, duration, and atmosphere) leading to effect on oxygen permeability.

3.1 Preparation of powders

Solid-state reaction: the solids (oxides, carbonates, hydroxides or salts), with the desired metal ions are mixed together by mechanical process of grinding and mixing, usually applying a ball mill, followed by the subsequent calcination for a given time (3-10 hours) at the temperature (800 ºC-1100ºC). A sufficient amount of agent of some volatile organic liquid (acetone or alcohol) is added to aid the homogenization prior to the mixing and the powder is dominated by starting materials and grinding. Solid-state reaction is a frequent method to produce the conventional powders because of the easy-controlling and low cost. However, the high calcination temperature may cause

the growth of the intermediate products leading to deactivation, and the homogeneity and the purity of the power are relatively poor. [11] & [19]

In the Co-precipitation, the aqueous solution with the desired cations are mixed together by adding a precipitation agent (H_2O_2, KOH or Na_2CO_3), followed by filtration, drying and subsequent calcination at high temperature (600ºC-800ºC) to obtain final products. The morphology and the physical characteristics of the desired products are adjusted by the control of concentration, temperature and atmosphere (pH) as well as mixing rates to get materials in an exact stoichiometric composition. Co-precipitation is an ancient technique which require lower temperature and shorter reaction time than solid-state reaction and shows better homogeneity and higher power purity. This technique is popular because of the fast reaction, easy controlling and requires less amount of energy. However, both the solid-state and co-precipitation cannot achieve the uniform dispersion of different metals. The inhomogeneities of the powders might occur in the co-precipitation method. Meanwhile, a doping agent could be mixed into the solution in order to obtain the better compositional homogeneity and addition of surfactants and a capping agent are required to adjust the partial size. [19]

In the sol-gel method (Citrate-EDTA method), the metal alkoxides or nitrates containing the desired cations are mixed together and they undergo hydrolysis and condensation reactions to form hydroxides or oxides (sol), followed by the agglomeration and evaporation for the production of an amorphous-like gel, which is dehydrated and subsequently thermally decomposed in low temperature to obtain desired powders. The citric acid-ethylenediaminetetraacetic acid (EDTA) is the most popular method in the sol-gel preparation family due to its advantages of excellent chemical homogeneity, lack of carbonates, high relative density and powder purity. In citreate-EDTA method, the complexation of metal alkoxides are mixed together by adding chelating agent (citric acid, EDTA or glycine) to prevent partial segregation of metal components, followed by aging (syneresis) and calcination (100 ºC-200 ºC). The pH and temperature

affect the degree of the complexation, the productivity and morphology of sol as well as the final properties of desired gel products. Compared with solid-state reaction and co-precipitation, sol-gel method shows the properties of high purity and fine powder and requires low calcination temperature. Therefore, it has been widely applied for synthesizing fluorite and peroviskite-based compounds. [19]

3.2 Shape-forming of membranes

Pressing, solvent casting (phase inversion) and plastic extrusion are the three basic shaping processes for ceramics powders, of which the most noted methods are pressing and extrusion. Pressing process applies relatively high pressures into the porous aggregates to ensure the strength of the body. Isostatic pressing and hot isostatic pressing are frequently used. Isostatic pressing produces uniformly compacted membrane with extremely high mechanical strength resulting membrane pore diameter of 1-10 nm range [37]. Hot isostatic pressing (HIP) gives additional densification which provides the characteristics of open porosity, narrow pore size distribution, high mechanical strength and higher fluid permeability [37]. Plastic forming with extrusion processes involves the mixing of powders and plastic paste, followed by deaeration and deagglomeration. The paste is forced through a constricting die at a given speed controlled by the piston pressure to obtain elongated shapes of constant cross-section. The solvent casting or phase inversion is typically used in ultrafiltration membranes for converting the polymer solution into gel. In slip casting, the suspension mixture of the properly sized particles, dispersants, binders and plasticizers (slip) are ball-milled, deaerated and poured into a porous mould, followed by compaction on the mold walls by capillary force. Tape casting is a well-established practice for making porous mould in microelectronics to fabricate films in the range of 0.01 to 1mm thick. [39]& [40] & [41]

3.3 Sintering

Sintering leads to densification of a compacted green body and provides the disk, tubular or hollow-fiber shaped membranes with the required mechanical strength by means of heat treatment (>1000ºC) for a certain time. The achievement of the state of minimum free enthalpy is the major driving force of the sintering process and the membrane undergoes pore elimination, grain growth, material diffusion, evaporation, condensation, dissolving and precipitation when the temperature and time are increased. Higher temperature is required to increase the number of saturated chemical bonds in the crystal lattice and enable material transport (diffusion), which leads to the improvement of the mechanical properties of the membrane [42].

The microstructures (grain size and grain boundary) and properties of membrane depended on the sintering temperature, dwelling time, ramping rates as well as the sintering atmosphere, which leads to effect on the oxygen permeability reported by researchers. S. Diethelm et. al has reported that when the temperature of duration of treatment was increased in the preparation of $La_{0.5}Sr_{0.5}FeO_{3-\delta}$ membrane, the grains grew larger and the grain boundary decreased, which leads to lower oxygen flux due to the increase of the activation energy in the bulk diffusion [42]. Karton et. al has also reported that $LaCoO_{3-\delta}$ membrane oxygen flux will decrease with the rise of the grain size due to formation of blocking layers at the grain boundaries in the high temperature resulting in decrease of the oxygen ionic conduction [43] &[44].

4. Hydrocarbon decomposition on oxygen perovskite membrane

Synthesis gas or syngas (H_2+CO) can be produced by biomass gasification and subsequent steam reforming of hydrocarbons in the gasification gases. The steam reforming requires external heat sources to break down the hydrocarbon compounds to form H_2-rich gas. It produces the high H_2/CO (3:1) ratio, which is not suitable for the downstream processes such as Fischer-Tropsch synthesis. In contrast, the partial oxidation is a weakly exothermic reaction via the introduction of enough oxygen into the feed for converting the fuel into carbon monoxide and hydrogen in a short residence time. It is less energy and cost-intensive as well as provides a lower H_2: CO (2:1) ratio resulting in a more favourable composition for the synthesis of Fischer-Tropsch or methanol. However, it has drawbacks of lower yields due to the oxidation of CO and H_2. [2]

Autothermal reforming (equation 18) is the combination of the partial oxidation reaction and steam reforming processes that using the air or pure oxygen and steam as oxidants. It takes the advantages of both, in which the heat released by the exothermic oxidation reaction is cooperated with heat required for the endothermic steam reforming at contemporaneously increasing of the hydrogen yield. If the heat released by the exothermic oxidation is balanced with the heat for endothermic, the reaction proceeds under the energy neutral conditions; if the heat from the oxidation reaction is larger than the heat required for the endothermic steam reforming, the temperature would balance by itself and no external heat is needed.

$$C_nH_mO_p + aO_2 + bH_2O \rightarrow cH_2 + dCO_2 \qquad (18)$$

Although partial oxidation based on air is more favorable than steam reforming, the downstream process contents nitrogen. Therefore, a source of pure oxygen is needed to avoid conventional cryogenic separation of unnecessary gases. An alternative route

is to apply MIEC membrane reactor, which provides the pure oxygen separation and can be combined with the catalytic partial oxidation process reducing the capital cost potentially by 45%. Hydrocarbon decomposition on the oxygen pervsokite membrane involves three consecutive steps: oxygen separation, partial oxidation and steam reforming/mixed reforming. [45]

4.1 Process overview

4.1.1 Oxygen separation from perovskite membrane reactor

In the current industrial applications, the reforming processes include huge separation steps with high investment and operation costs. The core of the oxygen permeable membrane reactor is to combine both separation and reaction steps into one process making possible to get rid of expensive separation by distillation. Oxygen permeable membrane (OPM) acts as a supplier of oxygen for the partial oxidation. The pure oxygen separated from the air by OPM is cheaper and environmentally way friendly to produce pure oxygen. There is no formation of NO_X in the reactor in theory due to the high selectivity of oxygen and the impermeability to nitrogen. It reduces the energy and capital cost significantly and makes the hydrocarbon gas conversion to alternative fuel more feasible. It is much safer than the conventional reactor, operating within the explosion limits can be avoided and oxygen can be pre-mixed with natural gas for reducing the blockage by hot spots. [45]

Pure oxygen separated from the air is further used in the catalytic oxidations and various type of inert gas is employed as sweep gas such as He, Ar etc. The idea of having the sweeping gas in the oxygen membrane reactor is to ensure that enough oxygen sources are available in the oxygen-enriched side and to enlarge the partial pressure gradient leading to high oxygen permeability. The sweeping gas has positive effect on the oxygen flux value and it increases with the increase of the oxygen partial pressure gradient. [36]

In the oxygen permeable reactor, there are various types of active oxygen species acting as the reactant in the reaction zone, for example, O_{2ad}, O, O^-, O_2^-, O_2^{2-}, O^{2-}, O_2^-, etc; the lattice oxygen on the membrane surface also provides the catalytic property to activate the hydrocarbon [46]. The oxygen permeable membrane provides the oxygen selectively separated from air, while its catalytic property is less important if there is a reforming catalyst present in the reactor. It distributes the oxygen uniformly with controllable partial pressure gradient and oxygen permeation rate. As a result, the undesired weakness of the conventional co-feeding reactor can be avoided [46].

4.1.2 Partial oxidation of hydrocarbon on the perovskite membrane

Partial oxidation process involves two types of oxidation, which are the thermal partial oxidation (TPOX) and catalytic partial oxidation (CPOX). TPOX, which is widely used in converting the methane to hydrogen-rich syngas, proceeds with air or oxygen in the temperature range between 1200-1400 °C with absence of catalysts. The products are carbon monoxide and hydrogen and the general reaction equation is shown below. In the industrial practical applications of TPOX, the air-fuel ratio is higher than stoichiometric ratio in order to prevent the coke formation. Methane is oxidized with oxygen to form carbon monoxide and hydrogen, while aromatic hydrocarbons are cracked to form alkenes under the high temperature. [47]

$$C_nH_m + n/2\ O_2 \rightarrow n\ CO + m/2\ H_2, \quad \Delta H^o_{298K} < 0 \qquad (19)$$

In CPOX, the temperature is reduced to the range between 750-900 °C due to the presence of catalyst. The introduction of the catalyst will increase the syngas (hydrogen and carbon monoxide) selectivity and decrease the production of by-product leading to less coke formation. [48].

At the relatively high temperature, the hydrocarbons or aromatic compounds will cause the thermal cracking due to their low stability. The formation of the short-chain carbon of alkane or alkene is favored leading to the coke formation finally; further oxidation of short-chain carbon compounds form the gas products of CO, CO_2, CH_4, H_2O and C_nH_m etc. Therefore, it is necessary to add the catalyst in the membrane reactor to prevent the coke formation from long-chain hydrocarbons. Meanwhile, the selectivity of the hydrogen and carbon monoxide increases, whereas the hydrocarbon compound performs relatively inert and low synthesis gas selectivity is obtained in the absence of the catalyst. [49]

4.1.3 Steam reforming/Mixed reforming of hydrocarbon on perovskite membrane

The gases produced from the partial oxidation over the catalyst on the membrane are mainly CO, H_2, and some CO_2 and H_2O. The resulted gases diffuse to the membrane surface again and react with the lattice oxygen to form additional H_2O and CO_2 to increase the oxygen permeability, of which follows the process of mixed reforming. The mixed reforming is achieved after the partial oxidation and it involves the reactions of steam reforming (CH_4+H_2O), water-gas shift ($CO+H_2O$), methanation ($CO+H_2$ or CO_2+H_2), dry reforming ($C_nH_mO_p + CO_2$), autothermal reforming ($C_nH_mO_p + O_2 + H_2O$) and $C_nH_mO_p + CO_2 + H_2O$. The possible reactions are shown below: [50]

Steam Reforming:

$$CH_4+H_2O \rightarrow CO+H_2 \qquad \Delta H^o_{298K}=206 \text{ KJ/mol} \tag{20}$$

$$C_nH_mO_p+ H_2O \rightarrow CO+H_2 \quad \Delta H^o_{298K}>0 \tag{21}$$

Water gas-shift:

$$CO+H_2O \leftrightarrow CO_2 + H_2 \qquad \Delta H^o_{298K}= -41.2 \text{ KJ/mol} \tag{22}$$

Methanation:

$$CO+3H_2 \rightarrow CH_4+H_2O \qquad \Delta H^o_{298K}= -217 \text{ KJ/mol} \tag{23}$$

$$CO_2+4H_2 \rightarrow CH_4+2H_2O \qquad \Delta H^o_{298K}= -178 \text{ KJ/mol} \tag{24}$$

Dry reforming:

$$CH_4+CO_2 \rightarrow 2CO+2H_2 \tag{25}$$

$$C_nH_mO_p+ CO_2 \rightarrow CO+H_2 \quad \Delta H^o_{298K}>0 \tag{26}$$

4.2 Reaction mechanisms of hydrocarbons on the perovskite membrane

4.2.1 Partial oxidation of methane

Recently, the partial oxidation of methane (POM) in the perovskite membrane $Ba_{0.5}Sr_{0.5}Co_{0.8}Fe_{0.2}O_{3-\delta}$ (BSCFO) reactor has been intensively studied [51]. As shown in Figure 6, one side of the membrane was exposed to the compressed air from the bottom and methane and helium are from the other side [52]. Two different of membrane reactors were applied to investigate the performance of catalyst on the membrane, of which of the configuration A (OCM reactor) operated without the additional catalyst and reactor B (POM reactor) with the catalyst of LiLaNiO/ γ-Al_2O_3 with 10wt% of nickel loading packed above the membrane (Figure 8) [53]&[54].

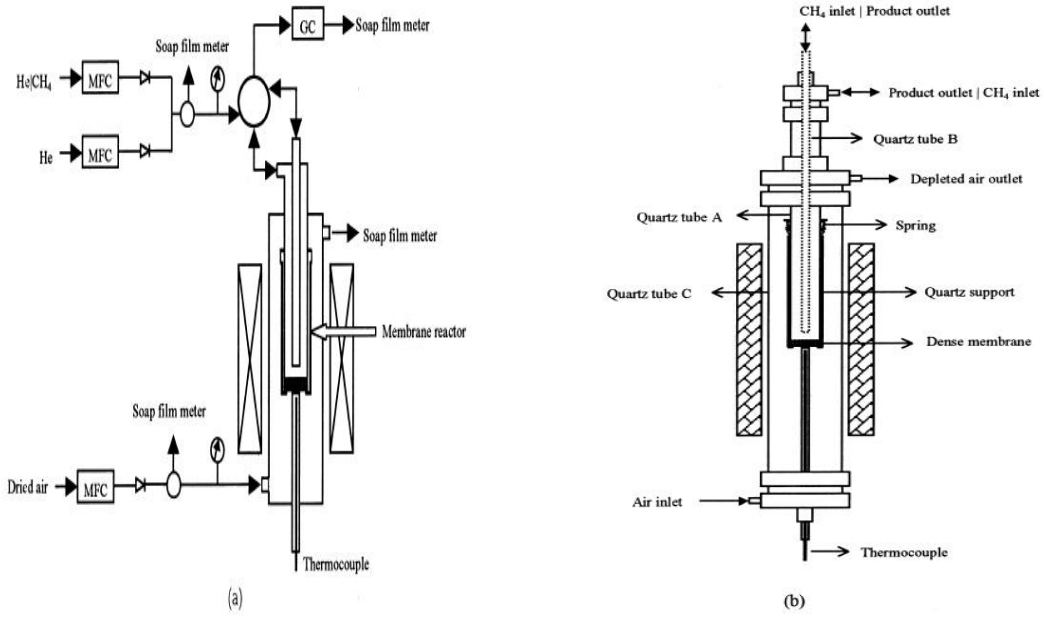

Figure 6. (a) Experimental setup of POM; (b) detailed [53] & [54].

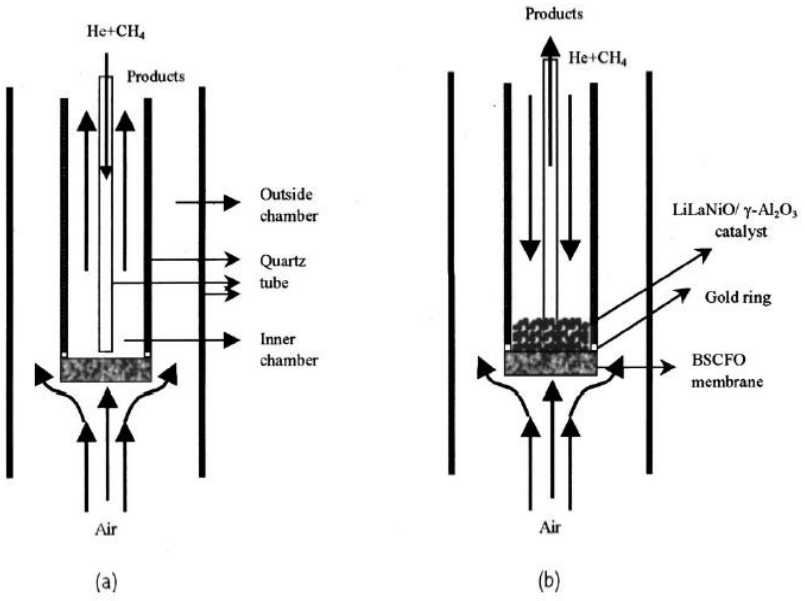

Figure 7. (A) Experimental setup of OCM without catalyst for OCM experiment (B) with catalyst of LiLaNiO/ γ -Al2O3 with 10wt% of nickel for POM [53]&[54].

The mechanisms of POM to hydrogen and carbon monoxide have been conflicted in two versions. One is the direct partial oxidation mechanism (DPO mechanism), which includes dissociation of methane into adsorbed carbon and H_2 over the surface of the catalyst, the H radius recombination to molecular H_2 and the remaining carbon reacting with oxygen to form CO. The other is the combustion-reforming mechanism (CRR mechanism) where the CH_4 is first oxidized to CO_2 and H_2O followed by subsequent steam reforming and dry reforming. [54] & [55]

In the OCM reactor, the catalytic behaviour of the BSCFO was investigated at high temperature of 800-900 °C with the air exposed from the bottom and CH_4 on the top in the reactor. The air flow rate was 300 ml/min and 0.21 atm of oxygen partial pressure gradient. The results showed that species of C_2H_4, C_2H_6, H_2O, CO_2, O_2, and CO were present in the reaction chamber, while it was also found numerous amount of the unreacted molecular oxygen in the products with C_2 selectivity of 48.2-72.8% and the

methane conversion of 3.25-0.65%. It is reasonable to understand: there are various types of active oxygen species, for example O_{2ad}, O, O^-, O_2^-, O_2^{2-}, O^{2-}, O_2^-, etc acting as oxidizer at the membrane surface. The methane will react directly with the lattice oxygen without presence of the catalyst on the surface of the membrane. However, it is unfavourable that methane reacts with the lattice oxygen on the membrane in the absence of catalyst, since the membrane is really inert due to its stable chemical structure of tetrahedral molecule with four equivalent C-H bonds and no double-bond or triple bond in the structure. [56] & [57]. Although the catalyst is not presented on the membrane surface, the perovskite membrane has some catalytic properties that enables the small amount of methane to react with oxygen. [53] [55] & [58]

For the POM reaction, the catalyst LiLaNiO/α-Al_2O_3 was packed into the reactor and air and methane were inserted into both sides in the temperature of 850°C with the flow rate of 300 and 34.99 ml/min. There were CO, CO_2, H_2O, H_2, H_2O but no C_2H_4 or C_2H_6 detected in the chamber. The methane conversion of 98.5%, CO selectivity of 93%, 1.93-1.97 of H_2/CO ratio and 10.45 ml /cm^2 min oxygen permeability were achieved [53] & [54]. After adding the catalyst LiLaNiO/ γ -Al_2O_3 on the surface of the $Ba_{0.5}Sr_{0.5}Co_{0.8}Fe_{0.2}O_{3-\delta}$ (BSCFO) membrane, CH_4 dissociates over Ni^o sites forming hydrogen H* and CH_3* surface species. The dissociation H* was recombined to form H_2 and react with lattice oxygen on the membrane surface to form water. The carbon (or CH_3* species) reacted with water (OH*) at the interface to form carbon monoxide and hydrogen (Figure 8). The possible reaction pathway is shown below: [59]

$$CH_4 + Ni^o \rightarrow Ni.....C + 2H_2 \quad (27)$$

$$CH_4 \rightarrow CH_3^* + H^* \quad (28)$$

$$H + H \rightarrow H_2 \quad (29)$$

$$2H^* + O_2 \rightarrow H_2O \quad (30)$$

$$C + H_2O \rightarrow CO + H_2 \quad (31)$$

The compounds of synthesis gas were then diffused on the surface of the membrane to react with the lattice oxygen for additional production of hydrogen, carbon monoxide, water and carbon dioxide. The oxygen permeability of the membrane is greatly enhanced due to the additional consumes of the oxygen on the reaction side of the membrane led to increasing the oxygen chemical partial gradient. The presence of strong reducing gases of H_2 and CO will cause the oxygen flux value increase as well. Meanwhile, the methane conversion and the selectivity of H_2 and CO were increasing significantly [59].

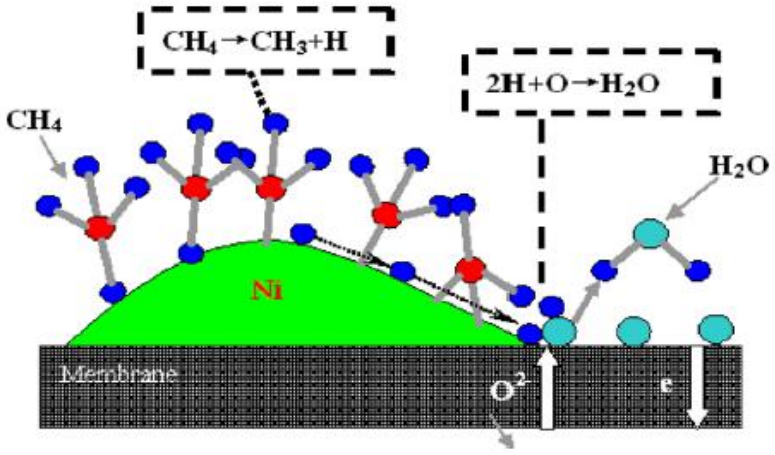

Figure 8. The reaction mechanism of CH_4 dissociation on the BCFNO membrane reactor [59].

4.2.2 Mixed reforming of heptane on the perovskite membrane

Mixed reforming of heptane was performed in a membrane reactor of $Ba_{0.5}Sr_{0.5}Co_{0.8}Fe_{0.2}O_{3-\delta}$ (BSCFO) with certain amount of steam, oxygen and helium for the hydrogen production. One side of the membrane was exposed to air from the top (air flow rate of 200 l/min), while the heptane reforming mixture and helium were inserted from the other side under the 0.21 atm of oxygen partial pressure gradient. The catalyst LiLaNiO/ γ-Al_2O_3 was packed above the membrane and experiment under the temperature of 850 °C (Figure 9). [60]

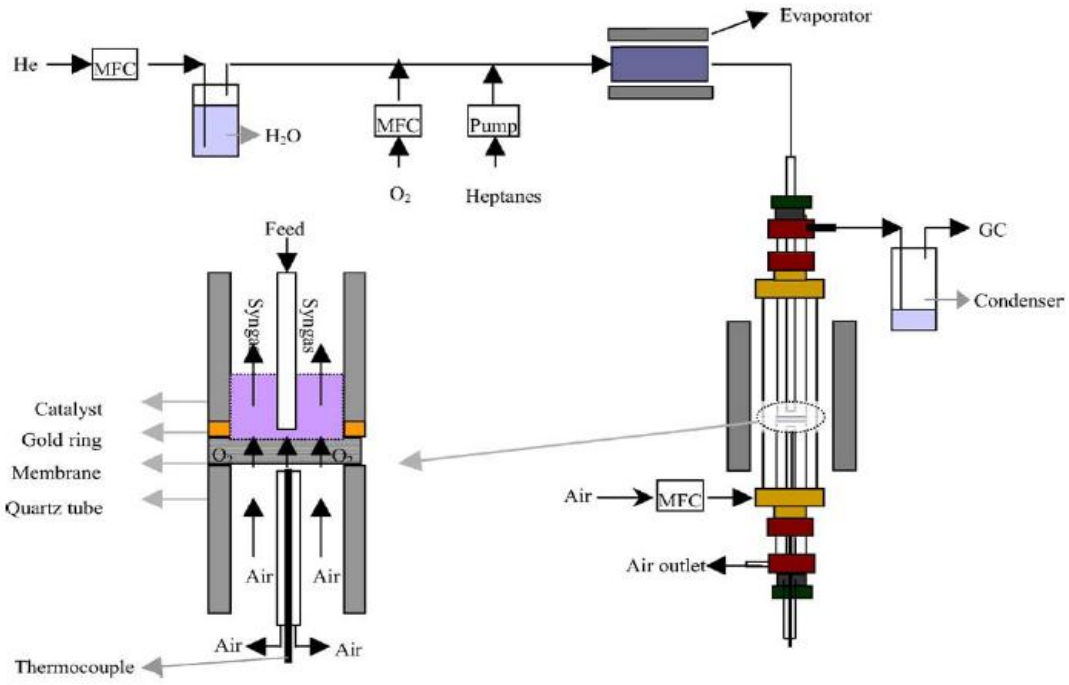

Figure 9. Experimental setup of mixed reforming of heptane [60].

The BSCFO membrane was tested in long-term operation of 100h under the gradient of air/He to keep the stability. The results showed heptane conversion of 100%, 91-93% of CO selectivity and 95-97% of H_2 selectivity were achieved after 100 h. The oxygen permeability was maintained at 11.5 ml/cm^2 min that is excellent stability in the high reducing environment with the presence of the catalyst. The air flow rate and the

temperature affected the oxygen flux value, which could be adjusted during the operations. [60] & [61]

The mechanism of the heptane reaction is proposed by Xiong el al [60] as follows: Without the catalyst: there are various types of active oxygen species, for example O_2ad, O, O^-, O^{2-}, O_2^{2-}, O_2^-, O_2^-, etc acting as oxidizer at the membrane surface. The absorbed heptane on the membrane surface will initially react with the lattice oxygen to form CO and CO_2 with the selectivity of being CO_2 is less than that of CO. CO_2 was considered to be obtained from CO by oxidation. Meanwhile, a large amount of the unreacted heptane and oxygen were detected on the surface, which means that the oxygen permeability flux was low at the moment. Also the perovskite membrane (BSCFO) has the low catalytic property that enables the small amount of heptane to react with oxygen [60] & [62].

When the small amount of catalyst LiLaNiO/α-Al_2O_3 was introduced to the reactor, the active sites of $NiAl_2O_4$ were reduced to Ni^o. Under the high temperature, the C-C bond of heptane will thermally crack and dissociate into hydrogen H* and surface CH_3-R* species. The dissociated H* was recombined to form H_2 or reacted with permeated oxygen to form water. The carbon (or CH_3-R* species) reacted with water (OH*) to form CO and H_2. The formation of CO_2 was probably due to the further oxidation of the CO or the oxidation of coke on the surface. Moreover, there were large amount of the short-chain hydrocarbons, e.g.C_2H_4, CH_4, C_2H_6, on the surface of the membrane due to the thermal cracking, as a result of much higher coke deposition tendency on the membrane. Compared with the partial oxidation of methane, the oxidation of the heptane suffered from the coke formation problems, which can be decreased by the adding the catalyst. At last, the conversion of the heptane as well as the selectivity of CO and H_2 will increase. The oxygen permeability was highly enhanced by the reduction of H_2 and CO. [59]

Finally, the components of synthesis gas are diffused on the membrane surface to react with the lattice oxygen over the catalyst for additional production of H_2, CO, H_2O and CO_2, followed by the mixed reforming of heptane with O_2, water-gas-shift reaction, methanation, reverse water-gas-shift reaction, dry reforming and autothermal reforming etc. The final products were H_2, CO, CO_2, H_2O and some alkanes or alkenes. [59]

4.2.3 Mixed reforming of coke oven gas on the perovskite membrane

Coke oven gas (COG), which mainly contains of hydrogen, methane, carbon monoxide, carbon dioxide and less amounts of other substances (toluene and benzene), is a by-product of coke-making process and it is the most attractive source for syngas or hydrogen production. Only small amount of the coke oven gas is synthetized as fuel, while most of COG is burned and discharged into the atmosphere directly resulting in air pollution in China. Therefore, the converting COG for hydrogen production as clean energy by using oxygen permeable membrane has received increasing attention all over the world, especially in China. [59]

The experiment of COG reforming on a $BaCo_{0.7}Fe_{0.2}Nb_{0.1}O_{3-\delta}$ (BCFNO) reactor with a certain amount of NiO/MgO catalyst on the membrane surface was investigated. One side of the membrane was exposed to compressed air and the other side was inserted with COG gases (58.7% H_2, 31% CH_4, 7.3% CO, 3% CO_2). The flow rate of compressed air was 200 ml/min and for COG was controlled to 100 ml/min under the high chemical oxygen pressure gradient of 0.21(oxygen-rich) to 0.01 (oxygen-lean) atm. The experiment apparatus is shown below in Figure 10. [59]

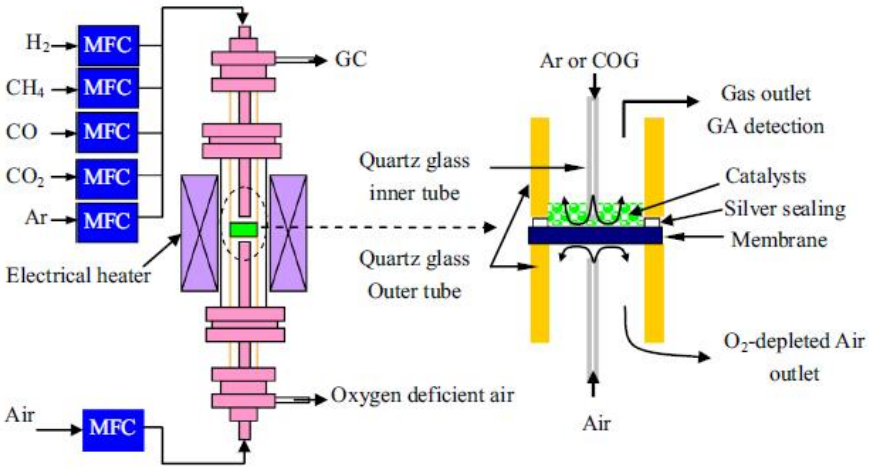

Figure 10. The experiment setup of BCFNO membrane reactor for coke oven gas reforming [59]

The results showed that the oxygen permeability flux (17.2 ml $cm^{-2}min^{-1}$) under the COG was greater than in normal condition with air/CH_4 (3.8 ml $cm^{-2}min^{-1}$) due to the presence of strong reducing gases of CO and H_2 to be immediately converted by permeated. The selectivity of H_2 and CO increased from 56.6%, 91.3% to 75.1% and 108.2%. The original carbon dioxide in COG was converted to carbon monoxide through the reforming reactions of methane. The packed catalyst of NiO/MgO had less effect on the oxygen permeability, while it effected the selectivity of H_2 and CO. [59]

The mechanism of the COG in the membrane reactor was also proposed by Yang et al [59] (Figure 11). The original H_2 in the COG first dissociated on the membrane surface and reacted with the lattice oxygen or ionic oxygen to form water, meanwhile, very minor amount of CH_4 dissociated over the Ni^o sites to form H_2 and surface active carbon for the production of additional H_2O again by the reaction with O_2. The formed H_2 reacted with oxygen to produce H_2O again. The remaining CH_4 reacted with produced H_2O by steam reforming to form H_2 and CO over the catalyst bed. The oxygen permeability was controlled by the amount of the H_2 and the catalyst improved the selectivities of CO and H_2 by steam reforming of CH_4.

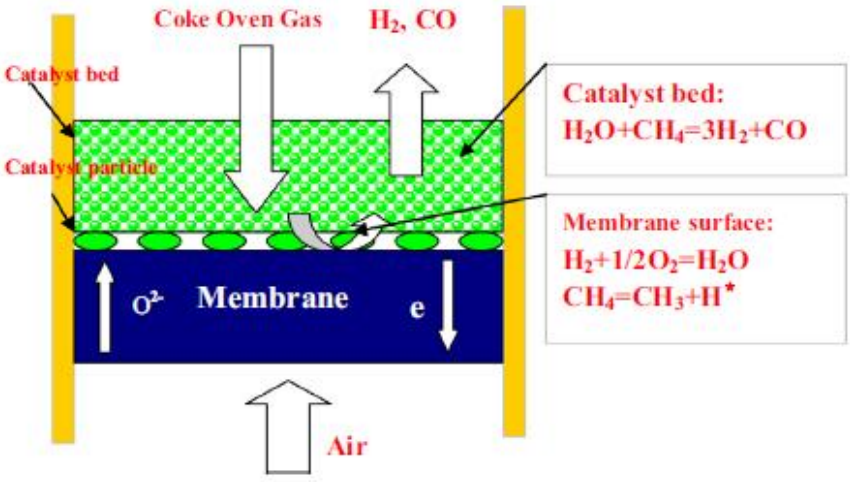

Figure 11. The mechanism of COG in the BCFNO membrane reactor [59].

4.2.4 Mixed reforming of toluene on the perovskite membrane

Tar content in syngas from gasification process is undesirable and causes a serious problem of the downstream equipment blockage and corrosion, therefore, to remove the tar by oxygen permeable membrane is required to be investigated [63]. There is lack of recent literature studies for the toluene decomposition on the oxygen permeable membrane and only few studies exist. Xiong et al [60] investigated toluene decomposition on the $Ba_{0.5}Sr_{0.5}Co_{0.8}Fe_{0.2}O_{3-\delta}$ (BSCFO) membrane with small amount of catalyst LiLaNiO/α-Al_2O_3 for 100 h operation between 800 to 950 °C together with certain amount of steam, oxygen and helium. The results showed oxygen permeability flux value of 12.1 ml/cm^2 min (at 950 °C). The largest problem was the coke formation on the catalyst surface due to the formation of the short-carbon chains products e.g. alkenes, methane or C_2H_2 caused by the thermal cracking of the aromatic hydrocarbons under the high temperature.

The mechanism of the toluene decomposition on the membrane surface followed oxidation-reforming processes, which can be surmised to follow the previous mechanism of methane, heptane and coke oven gas (Figure 12) Initially, the toluene reacted with the various types of active oxygen species, for example O_2ad, O, O^-, O^{2-}, O_2^{2-}, O_2^-, O_2^-, etc on the membrane surface to form carbon monoxide, hydrogen and less amount of CO_2 and H_2O. Additionally, due to the thermal cracking of toluene takes place via two reactions:

$$C_6H_5CH_3 \rightarrow C_6H_5CH_2 + H \quad (32)$$

$$C_6H_5CH_3 \rightarrow C_6H_5 + CH_3 \quad (33)$$

The subsequently cracking via $C_6H_5CH_2 \rightarrow C_6H_5 \rightarrow C_4H_3 \rightarrow C_2H_2$

$$C_6H_5CH_2 \leftrightarrow C_2H_2 + C_5H_5 \quad (34)$$

$$C_6H_5 \leftrightarrow C_2H_2 + C_4H_3 \quad (35)$$

There might be nearly 90 different kinds of the side products e.g. C_2H_2, C_2H_4, C_4H_2, C_3H_6, C_3H_4, C_5H_6, C_6H_6 and heavy species like xylene and ethylbenzene formed on the membrane surface at various temperatures. All of these unpredicted and unexpected compounds lead to the coke formation on the surface of the catalyst, which can be minimized by the adjustment of flow rate, temperature and steam to carbon ratio.

After adding the catalyst on the membrane surface, there are mainly six species in the outlet gas: H_2, CO, CH_4, H_2O, CO_2 and C_nH_n. The following reactions are assumed to take place on the surface of the catalyst/membrane:

- H_2 is first dissociated over the Ni^o surface into H* and reacted with the lattice to form steam. ($2H + O_2 \rightarrow H_2O$)
- CO is absorbed on the Ni^o sites and reacted with the produced H_2O to form CO_2 and H_2O by water-gas shift. ($CO + 3H_2O \rightarrow CO_2 + H_2O$)
- CH_4 is partially dissociated over Ni^o sites forming hydrogen H* and surface CH_3* species. The dissociated H* is recombined to form H_2 or to react with lattice oxygen on the membrane surface to form water. The carbon (or CH_3* species) can react with water (OH*) to form CO and H_2. The carbon will might react with water to form CO and H_2 as well. The formed hydrogen will react with oxygen to form the H_2O again. The remained CH_4 will react with produced H_2O in steam reforming to form H_2 and CO over the catalyst bed ($CH_4 \rightarrow CH_3^* + H^*$; $H + H \rightarrow H_2$; $2H^* + O_2 \rightarrow H_2O$, $H_2 + O_2 = H_2O$, $C + H_2O \rightarrow CO + H_2$, $CH_4 + H_2O = H_2 + CO$)
- CO_2 is formed due to the further oxidation of the CO or the oxidation of coke formed on the surface.
- C_nH_m undergoes further thermal cracking of toluene over the catalyst to coke, which accumulated on the catalyst surface or reacted with H_2O to form more CO and H_2 leading to reduced coke formation. ($C + H_2O \rightarrow CO + H_2$)

Therefore, the products are mainly CO, H_2 and H_2O or less amount of CO_2 and CH_4 etc. , of which the catalyst promote the selectivity of the CO and H_2.

Finally, the produced gases are again diffused on the membrane surface to react with the lattice oxygen over the catalyst for additional product of H_2, CO, H_2O and CO_2, followed by the mixed reforming of C_nH_m with O_2, water-shift reaction, methanation, reversed water-gas-shift reaction, dry reforming and autothermal reforming etc. The final products are H_2, CO, CO_2 and H_2O. The high oxygen permeability flux value will achieved by the strong reducing gases of H_2, CO and mixed reforming processes, of which the selectivity of CO and H_2 will be increased as well.

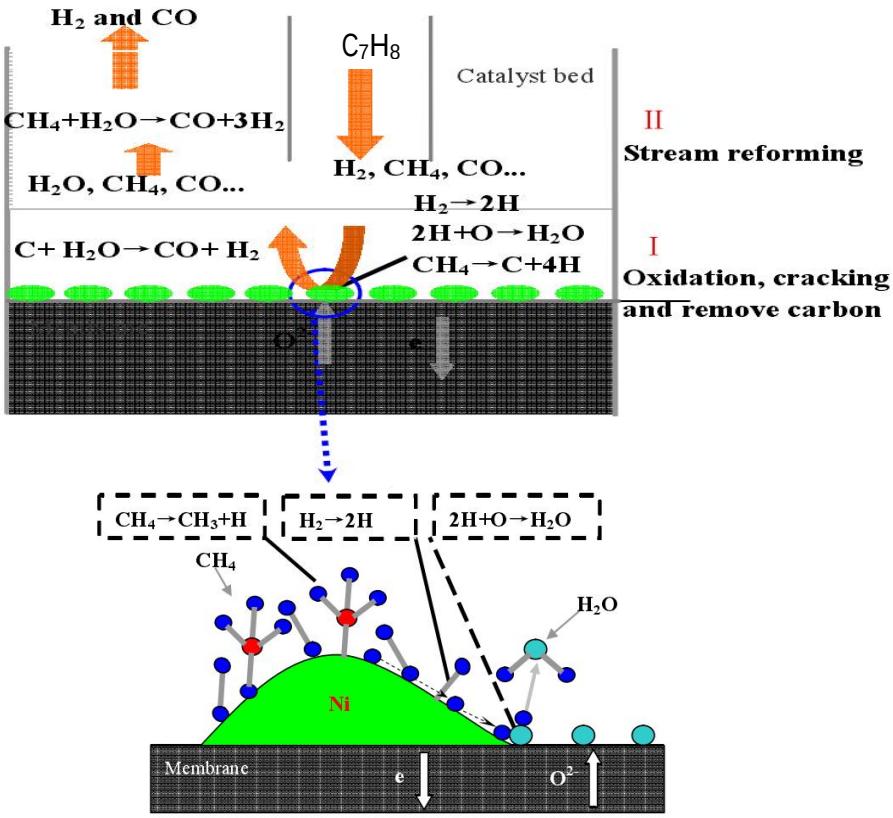

Figure 12. Reaction mechanism of toluene [60]

4.4 Reaction parameters of the toluene decomposition in the membrane reactor

4.4.1 Effect of reaction temperature

The temperature will affect the following things: oxygen permeability flux value, selectivity of the H_2, CO and CO_2, the conversion of CH_4, the toluene decomposition products (short-chain carbon species) and the catalyst deactivation.

The oxygen flux value dependence on the temperature in the toluene reforming has been reported by Xiong et al. [56]. The oxygen permeability increases from 4.25 to 12.1 ml/cm^2 min at 800°C to 950 °C in mixed reforming of heptane to syngas on the $Ba_{0.5}Sr_{0.5}Co_{0.8}Fe_{0.2}O_{3-\delta}$ (BSCFO). The experiment shows the oxygen flux value in heptane reforming increases with the increase of the temperature, whereas due to the increase of the oxygen ions diffusion rate leading the increase the oxygen vacancies controlled by bulk diffusion (Figure 13). [59]

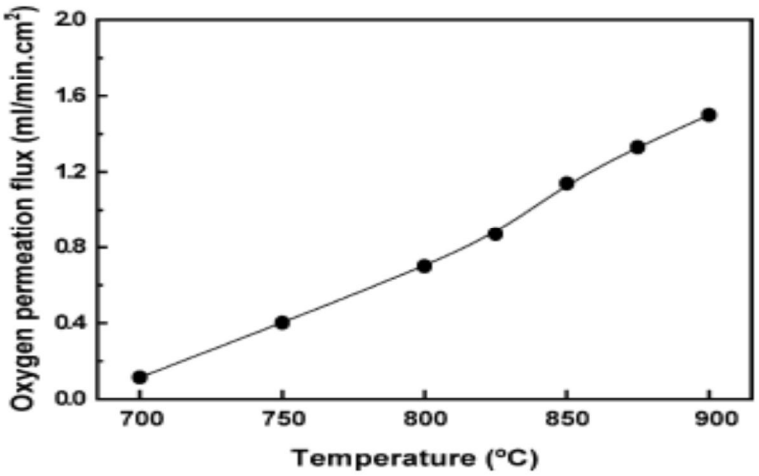

Figure 13. Effect of reaction temperature on the oxygen flux value of heptane on the $Ba_{0.5}Sr_{0.5}Co_{0.8}Fe_{0.2}O_{3-\delta}$ (BSCFO). (Air flow rate: 200 ml/min, helium flow rate, 30 ml/min) [60]

The compositions of the products are drastically dependent on the temperature due to the differences in the reaction rates and chemical equilibriums (Figure 14). At the temperature between 800-950 °C, toluene was completely converted. Based on the figure, it is obviously that the selectivity of H_2 and CO_2 increased constantly with the increase of the temperature, while the selectivity of methane and CO declined with the increase of the temperature. At the lower temperature (800°C), some alkene (C_2H_2) existed which was not shown in the figure. The oxygen flux value at 800°C was at lowest and the oxygen transport was not efficient enough to completely convert all C_7H_8 to CO and H_2. It is also well-known that the thermal decomposition of hydrocarbon is favored at high temperatures. Therefore, a certain amount of alkene was observed on the membrane. With the increasing temperature, the oxygen flux increases and it leads to increase of the selectivity of the H_2. However, the actual ratio between the O/C is higher in the operation, which means there are more oxygen available than the reaction required resulting in the less production of CO and more production of CO_2. Another reason was that the WGS reaction is favored causing the increased production of CO_2. Therefore, the increase of the temperature has a favorable effect on the production of H_2. [60]

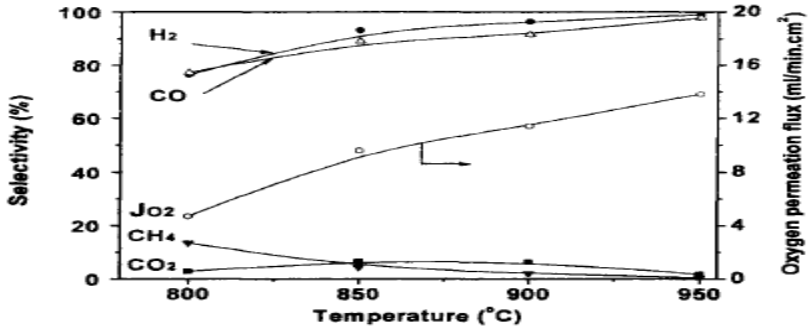

Figure 14. Effect of the temperature (V_{air}=200ml/min, W/C=0.38, He/C=1.8) [56]

The catalyst deactivation is also affected by the temperature, i.e. the increasing of the temperature inhibits the deactivation of the catalyst due to the promotion of the

gasification of the coke precursors. The longer chain hydrocarbon results in various type of coke formation in wider temperature range which is unpredictable. [60]

4.4.2 Effect of air flow rate

The air flow rate has an influence on the oxygen permeability, the selectivity of the H_2 and CO and the methane conversion, which is shown in Figure 15.

The oxygen permeability increased from 4 to 7 ml/cm^2 min with the air flow changing from 50 to 400 ml/min, however, the oxygen permeability remained constant at 7 ml/cm^2 min and had only slightly changes with the air flow rate above 200 ml/min. It means that the exchange of the oxygen on the air side was not the rate controlling step of the oxygen permeation with the air flow rate above 200 ml/min at 850 °C. Therefore, it was better to fix the air flow rate to 200 ml/min. [60]

The selectivity of the H_2 and CO_2 was increased with the increasing of air flow rate, while the selectivity of the CO and CH_4 was decreased. With the increasing of the air flow rate, the oxygen permeability started to increase. The excess oxygen caused the further oxidation of the CO to CO_2. Meanwhile, the WGS reaction produced CO_2 as well. Therefore, it resulted in the lower production of CO and increased production of CO_2. With the air flow rate above 200 ml/min, the oxygen flux value remained constant and the selectivity of the H_2, CO, CO_2 and CH_4 stayed constant as well. [60]

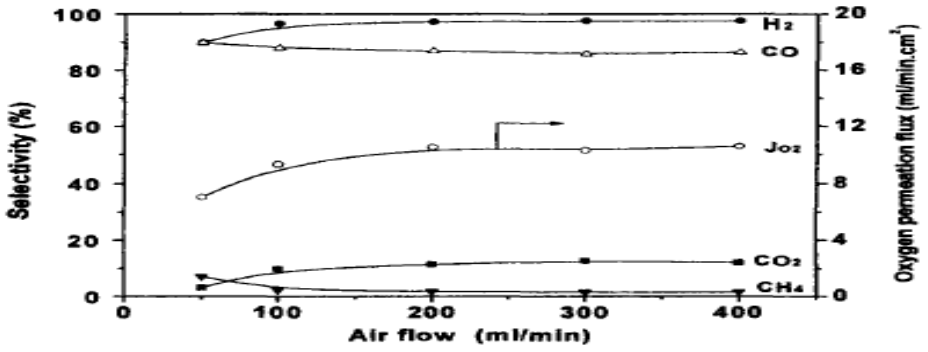

Figure 15. The effect of the air flow rate of toluene (T=850°C, W/C=0.38, He/C=1.8) [60]

4.4.3 Effect of steam to carbon ratio

Steam is employed not only for production of the additional H_2, CO and CO_2, but also to prevent the coke formation on the catalyst. Xiong et al. has reported that a higher S/C ratio leads to high hydrogen and carbon dioxide production but lower the production of carbon monoxide and methane (Figure 16). It is due to the water-gas shift reaction, steam reforming of CO and the methanation reaction increased the selectivity of CO_2 with a high S/C ratio. In addition, the oxygen permeability flux value increased with the increasing S/C ratio. [64]

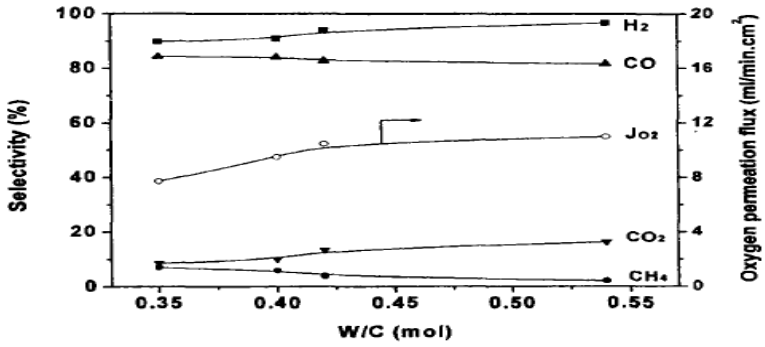

Figure 16. Steam to carbon feed ratio (T=850°C, V_{air}=200ml/min, He/C=1.8). [66]

However, it was also found that there is no significant effect on the H_2 and CO_2 yield as well as the oxygen flux value by further increasing the S/C ratios. The oxygen permeability flux value sustained stable (7 ml/cm^2 min) with the S/C ratio of 0.5. It can be explained by the coke formation on the catalyst as a result of the blocking of the oxygen transformation through the membrane.

Moreover, the S/C ratio should not be too high, which could lead to the negative effects on the reaction, the H_2 production yield and energy efficiency. The large amount of the water causes the excess energy required for the heating and results in waste of energy. Therefore, there are two factors to be considered in order to optimize the S/C ratio: [65]

(1) S/C ratio is recommended to be high enough to prevent the coke formation.

(2) S/C ratio is not recommended be too high to prevent the extra heating of H_2O.

4.4.4 Effect of the catalyst

The adding of the catalyst on the surface of the membrane has a significant effect on the oxygen permeability, methane conversion as well as the selectivity of the H_2 and CO. Due to the lack of literature studies for the toluene decomposition, the performance of $BaCo_{0.7}Fe_{0.2}Nb_{0.1}O_{3-\delta}$ (BCFNO) for coke oven gas conversion to syngas coupled with nickel-based catalyst (figure 17) is presented here. [66]

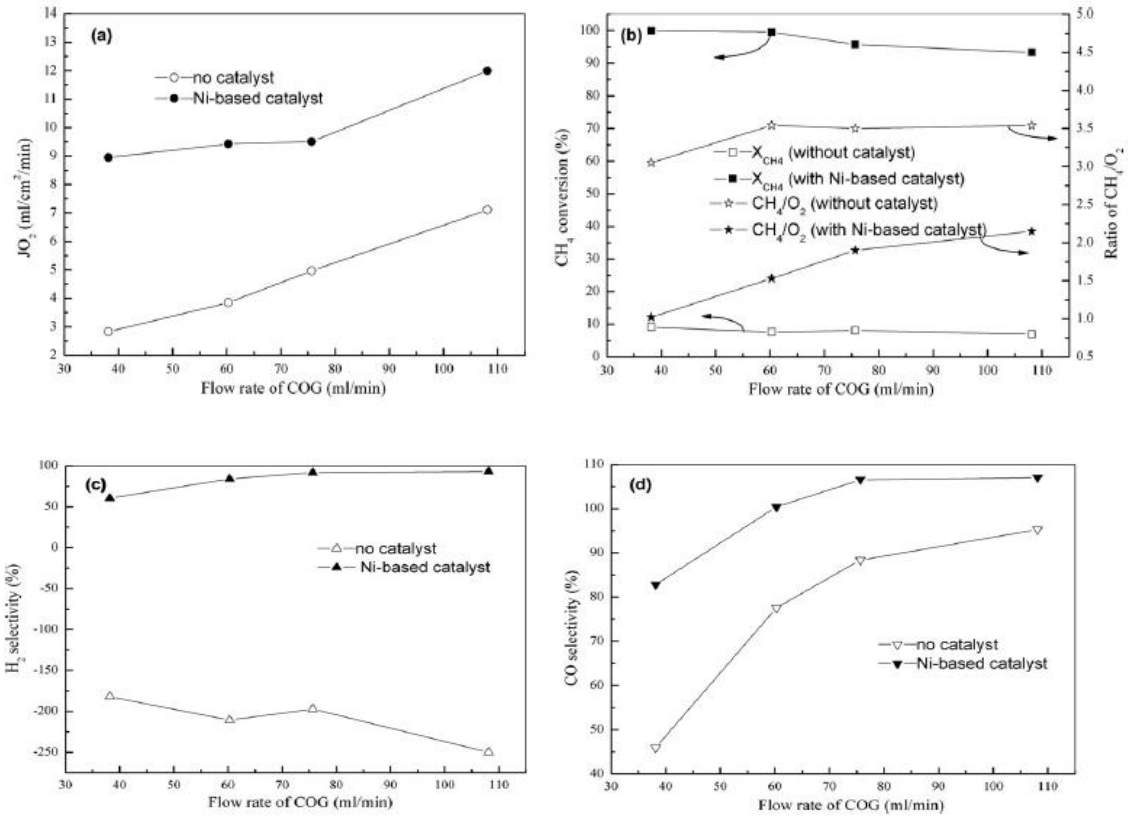

Figure 17. The performances of the $BaCo_{0.7}Fe_{0.2}Nb_{0.1}O_{3-\delta}$ (BCFNO) for coke oven gas without catalyst and with nickel-based catalyst. (Air low rate: 92.9ml/min, reaction temperature, 1148K) [66]

The oxygen permeability coupled with nickel-based catalyst increased even twice more than in the normal membrane reactor as shown in the Figure 18. It was due to the fact that the addition of catalyst activated for the oxidation reactions of reducing species such as hydrogen, carbon monoxide and CH_4 as a result of the additional consumption of oxygen for high oxygen permeability. The catalyst performance on the product selectivity and conversion should be specially highlighted: the methane conversion was increased from 10% to 90% and the selectivity of H_2 and CO was significantly increased with Ni-catalyst. [55]

4.4.5 Long-term test of mixed reforming

The ideal dense oxygen permeation membrane reactor should possess the excellent oxygen permeability as well as the stability under the reducing environment. However, the coke formation as well as the low chemical and mechanical strength can lead to an unstable ceramic membrane reactor. The performance of the $Ba_{0.5}Sr_{0.5}Co_{0.8}Fe_{0.2}O_{3-\delta}$ (BSCFO) was investigated over the duration of 100h at 850 °C for the toluene decomposition. The results shows that the BSCFO membrane maintains its physical structure, which is proved by the high oxygen permeability and excellent phase stability and chemical/mechanical stability under the reducing environment. [67]

Furthermore, the stable performance of the membrane for toluene decomposition was related to the optimization of the temperature (850 °C), S/C ratio (0.38), air flow rate (200 ml/min) as well as the existence of the catalyst (LiLaNiO/ $\gamma -Al_2O_3$). The oxygen permeability of 10 ml/cm^2 min, as well as the 90-92% selectivity of CO and for 95-97% H_2 and CH_4 conversion of 95-99% were achieved (Figure 18). [67]

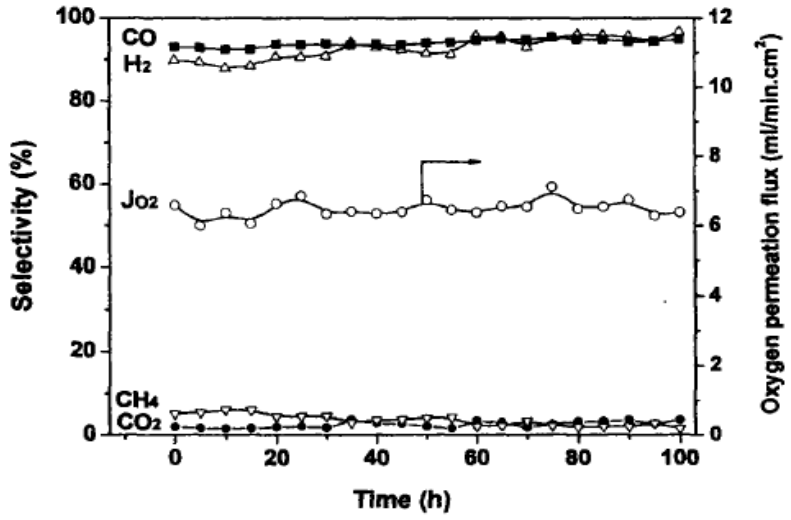

Figure 18. The long run of mixed reforming reaction of toluene in the membrane reactor. (T=850°C, V_{air}=200ml/min, He/C=1.8) [67]

EXPERIMENTAL PART

The objective of the experimental work was to find optimal conditions for hydrocarbon decomposition on the oxygen permeable perovskite membrane in order to remove the tar from gasification gases. One side of the membrane was exposed to the air, while the other side was exposed to the tar and nitrogen. Oxygen, which was permeated through the membrane from the synthetic air, acted as oxidizer to convert the hydrocarbon into synthesis gas by the oxidation reaction. The simplest mono-substituted aromatic compound, toluene, was chosen as an example to represent the tar compounds in this experimental study.

The experiments were performed at temperatures between 700-950 ^{o}C and at atmospheric pressure. There were a total of eight different types of perovskite membranes (A-H) that were tested in the experiments. Different temperatures, air flow rates, total flow rates of toluene and nitrogen, toluene amounts as well as the effect of the steam and gasification gases were evaluated for perovskite membranes in order to investigate the optimal reaction conditions. The main target was to compare several perovskite materials and find the optimal conditions for the best material, where the toluene partial oxidation was the target reaction.

5. Material and research methods

5.1 Experimental setup

The reactor system used for the experiments was a tubular reactor presented in Figure 19. Accordingly, the Inconel alloy metal reactor was placed in the centre surrounded by the three-zone furnace. The gas coming from the top was synthetic air with 80% of N_2 and 20% of O_2 (total flow of 200-450 ml/min) and only oxygen could permeate through the membrane to the reaction side leaving the nitrogen and other impurities outside of

the reactor to the vent. The toluene was fed by isocratic pump at a constant rate to the bottom of the reactor. The nitrogen, which was used to protect the system, and toluene were brought into the reactor with the total flow of 200-2000ml/min. The inlet gases flow rates were controlled by mass flow controllers, which have been calibrated beforehand. Both sides of the membrane were maintained at atmospheric pressure. The down part gases reacted with the oxygen permeated from the top through the membrane to form carbon monoxide, carbon dioxide, methane, and other hydrocarbons by oxidation. A portion of the gas was sampled to GC analyser equipped with TCD (Thermal conductivity detector) and FID (flame ionization detector) detectors for the products measurements. The rest of the gases went through the gas cooler and to the vent. The bypass line was designed to measure the concentration of the feed gas to ensure the composition and stability of the inlet gas. A thermocouple was placed to the bottom of membrane reactor to measure the reactor temperature. The PI diagram of the whole system was shown in figure 20.

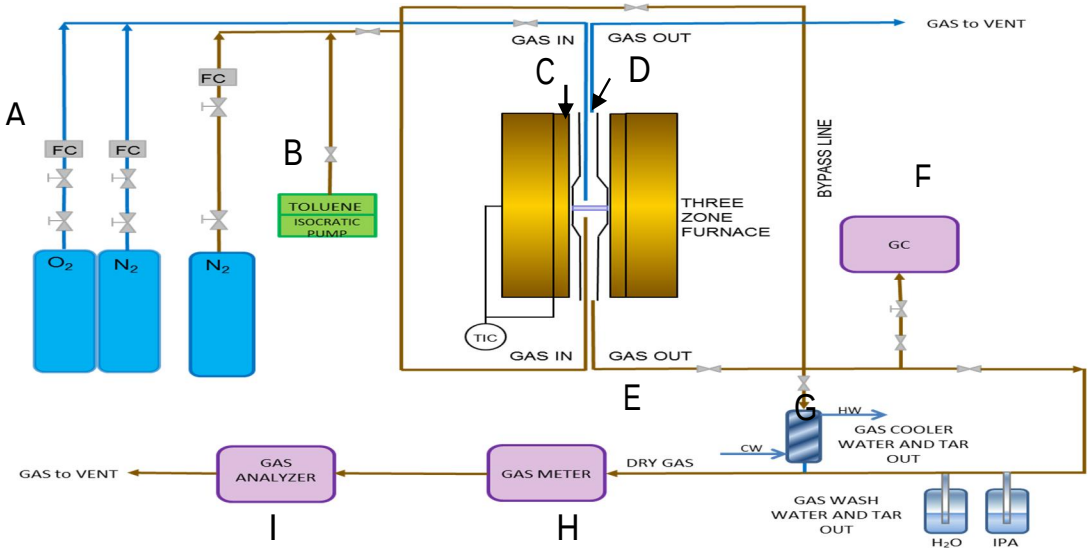

Figure 19. Pressurized plug flow reactor: A) FC: Flow control B) Isocratic pump: Agilent series 1200, 100% C_7H_8 liquid. C) Oven: Carbolite 3-zone oven, max. temperature 1000 ^oC D) metal reactor with membrane. E) Thermocouple F) GC: Gas Chromatograph G) Condenser H) Gas Meter I) Gas analyser (VTT figure).

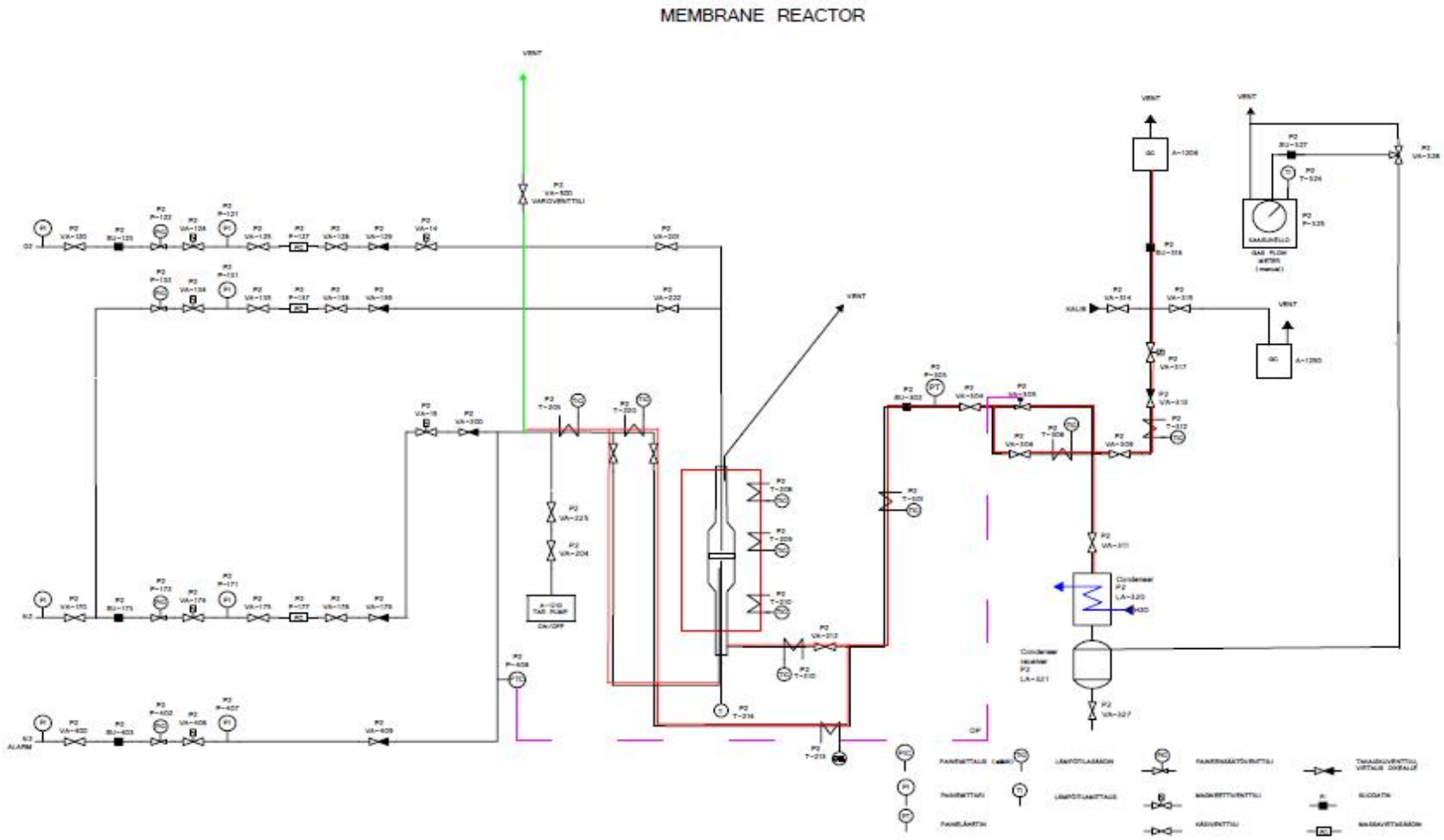

Figure 20. Schematic representation of the hydrocarbon decomposition on the oxygen perovskite membrane reactor system. (VTT figure)

5.2 Reactor System

The membrane reactor was assembled by three parts: a dense ceramic membrane in the middle, an Inconel alloy metal tube with protruding hole on the top and a bottom Inconel tube with two legs of springs for sealing (Figure 21). The membrane was placed between the gaskets on the both ends of the top and bottom for sealing and it was controlled by adjusting the lengths of the springs by tightening and loosening the screws on the top from the both sides. When the membrane reactions proceeded, one side of the membrane was exposed to the synthetic air from the top through a 6mm (in diameter) Inconel pipe and the nitrogen and other impurities went out to the vent through the protruding hole. The reaction gas mixture of toluene and nitrogen was flowed to the other side of the membrane to the bottom through a 6mm (in diameter) Inconel pipe and left to the vent through gas washing bottle. The membrane was supported by alumina substrate disc and it had the effective inner surface area and the thickness around 2.45 cm^2 and 0.3 cm, respectively.

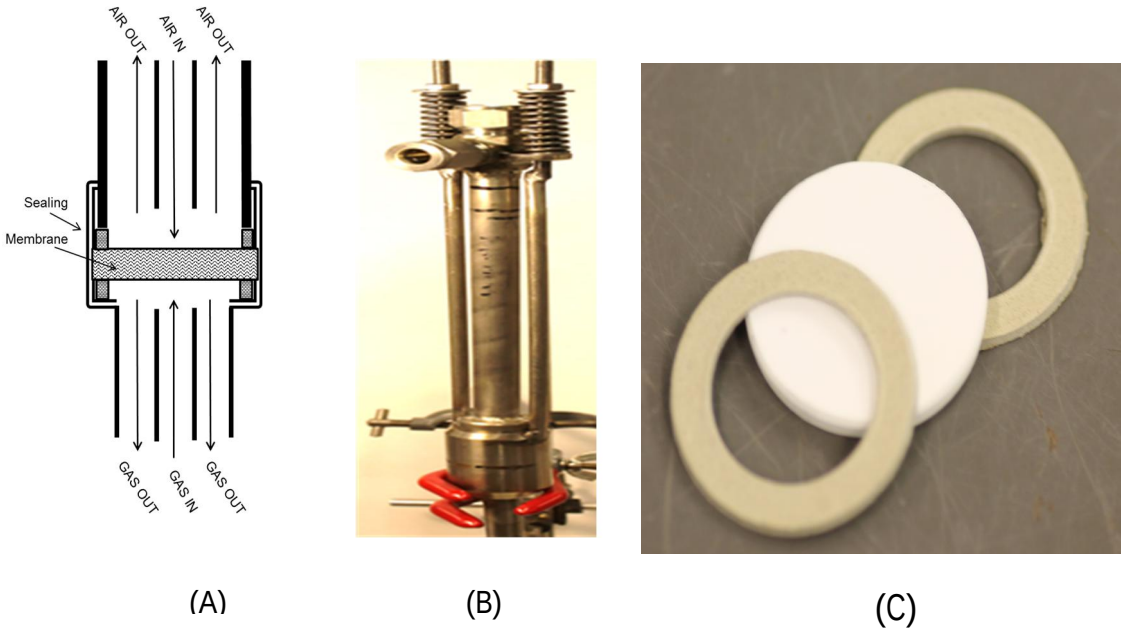

(A) (B) (C)

Figure 21. (A) Metal reactor (B) Steel reactor (C) Gasket (thermal 866 thickness (1mm), 17.5 (inner diameter) * 25.5 mm (outer diameter) and membrane (VTT figures).

Both thermal conductivity detector-Gas Chromatography (TCD-GC) and Flame Ionization Detector-Gas Chromatography (FID-GC) were used for analysing the products. TCD was applied to measure the light gases, for example, hydrogen, oxygen, nitrogen, carbon monoxide, carbon dioxide, methane and other light hydrocarbons (acetylene, ethylene and ethane). The heavier hydrocarbons and light hydrocarbons could be both detected by FID-GC. The FID-GC measured the wet gas composition and the TCD-GC measured the dry gas composition.

FID-GC was equipped with two columns; column 1 was HP-5 (5% phenyl Methyl Siloxan: Agilent 19091J-413) and column 2 was HP-PLOT-Q (Agilent 19091P-Q04). Gas mixtures was passed through the HP-5 column (FRONT signal, FIDA) and after 8.6 mins it went through the HP-PLOT-Q column (Back signal). The oven temperature program was set up to 100 ^{o}C for 9 mins at 20 ^{o}C/min and 250 ^{o}C for 12 mins. The FID-GC was flushed with nitrogen at the room temperature until the baseline was stable and then the heating was started for the method. The samples were taken automatically and the inlet and outlet of the hydrocarbons were analysed by FID-GC. The gases were calibrated every time to ensure the accuracy of the results in order to reduce the analysis errors (Appendix B). The FID-GC was flushed with nitrogen again overnight after finishing the experiment, so called 'stand-by method', to remove the hydrocarbons or coke from the column.

The Micro-GC (TCD-GC) (Varian CP-4900 Micro-GC), so called thermal conductivity detector, typically analysed small hydrocarbon gases by comparing the differences in the thermal conductivity between the carrier gas and the sample components. A mixture of sample compound was flowed through the gas column and within a considerably short period of time of 3 minutes for sampling. It involved four channels, of which only the first two channels were used for analysing the products in our experiment.

5.3 Experiment configuration

5.3.1 Pre-test 1: Gasket leakage (Blank Quartz membrane)

The gaskets were placed on the top and bottom of the membrane for sealing and both were tightened by adjusting the springs on the top. The gasket leakage is the main problem in the membrane testing and it was investigated by placing the blank quartz membrane inside of the reactor and feeding nitrogen to the bottom in order to observe pressure drop by pressure indicators (Figure 22). A flow rate (0.3 l/min) of nitrogen was fed to the bottom and it was shown that there was no pressure drop. Thus, such conclusion could be drawn that the reactor passed the leakage. Furthermore, the nitrogen flow rate was increased from 0.5 l/min, 0.7 l/min, 1 l/min, 1.2 l/min, 2 l/min, 2.2 l/min, 2.4 l/min, 2.6 l/min, 2.8 l/min to3 l/min in order to check if the gaskets can with stand the increasing flow rate. The oven temperature was increased to 700 ^{o}C, 800 ^{o}C and 900 ^{o}C keeping 2 hours at each temperature (6h in total) in order to observe the temperature effect on the gaskets and finally the oven was cooled down to 30 ^{o}C. The results showed that the gaskets stayed intact with the membrane, therefore, it can be concluded that the gasket could endure both high and low temperature as well as high flow rate.

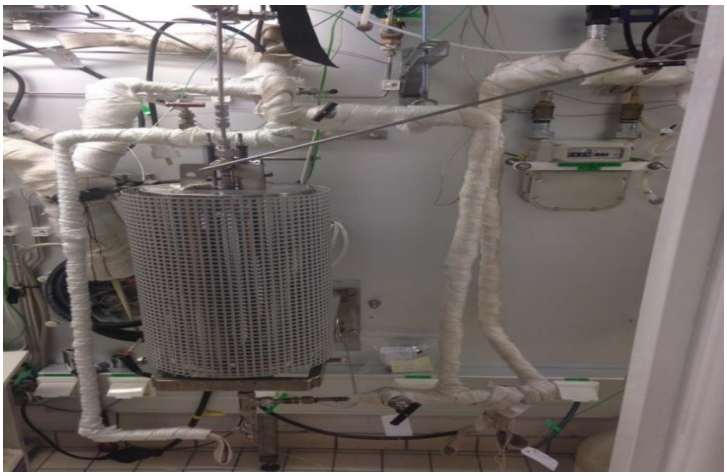

Figure 22. Pressurized plug flow reactor (VTT figure).

5.3.2 Pre-test 2: Alumina (Al_2O_3) support testing

The membrane was supported by an alumina substrate; therefore, it was important to check the characteristics of the substrate. Two factors were tested in this pre-test: the durability of support under the high temperature (800-900 ^oC) and the oxygen permeability through the substrate material. The durability test was performed by flowing the nitrogen from the top and bottom of the reactor, while the oven temperature was raised to 700 ^oC, 800 ^oC, 900 ^oC and kept for half an hour at each temperature and then cooled down to 30 ^oC in order to observe the cooling effects. It was shown that there was no breakage of the alumina substrate indicating that it would with stand high temperature and cooling effects.

The oxygen permeability test of the alumina substrate was carried out by changing the air flow on the top (0.2 l/min to 0.45 l/min) and pure nitrogen (0.35 l/min or 0.45l/min) on the bottom in order to monitoring the oxygen flow through the membrane to get a background value for the later experiment. The result was analysed by TCD-GC. It was obvious that the oxygen amount increased with the increasing of the air flow rate (0.2 l/min or 0.4 l/min) and nitrogen flow rate (0.35 l/min or 0.45 l/min) has less effect on the oxygen permeability (Table 2). A stabilization error of TCD-GC could have caused the 0.86 % of oxygen permeability at 900 ^oC with the air flow rate of 0.25 l/min and bottom flow (nitrogen and toluene) of 0.35 l/min.

Table 2. Oxygen permeability of alumina at high temperature.

Oven T (°C)	Air flow (l/min)	C_7H_8 &N_2 (l/min)	O_2 amount (%)
800	0,20	0,45	0,49 %
	0,25	0,45	0,47 %
	0,30	0,45	0,37 %
	0,40	0,45	0,51 %
900	0,20	0,45	0,33 %
	0,25	0,45	0,46 %
	0,30	0,45	0,51 %
	0,40	0,45	0,37 %
	0,45	0,45	0,47 %
900	0,20	0,35	0,46 %
	0,25	0,35	0,86 %
	0,30	0,35	0,50 %
	0,40	0,35	0,52 %

5.3.3 Pre-test 3: High temperature toluene cracking

Toluene tends to be thermally cracked under high temperature approximately above 600 °C, therefore, the products of the toluene cracking were checked at the temperature between 800 to 950 °C in order to compare the results with those from the oxygen permeability test. The test was performed by placing the blank quartz membrane inside of the reactor and feeding the nitrogen and toluene (0.4 l/min) to the bottom. The oven programme was raised from 800-900-950 °C, and at each setpoint the outlet gas was analysed by FID-GC. The results (Table 3) showed that the toluene was cracked into heavier hydrocarbons with increasing the temperatures and the number of identified heavier hydrocarbons compounds increased from 11 to 32 from 800 to 950 °C. The amount of the cracking products (benzene, methane and ethylene) also increased with the increasing temperature. Therefore, it can be concluded that the higher temperature was, the more it cracked.

Table 3. High temperature toluene thermal cracking.

Oven T (°c)	Heavier hydrocarbon	C_7H_8 (Out) vol%	C_6H_6 (Out) ppm	CH_4 (Out) ppm	C_2H_4(Out) ppm	H_2 (%)	CH_4 (%)
800	11 kinds	51	16	14	0	0,0	0,0
850	15 kinds	48	63	59	0,0	0,2	0,0
900	26 kinds	43	211	206	8,7	0,2	0,0
950	32 kinds	37	945	931	42,6	0,4	0,1

5.4 Execution of experiments

There were total twelve (named A3, B6, B9, C7, D3, E3, F16, G10, H13, H14, H15, H16) different perovskite membranes tested in the temperature between 700-950 ^oC and at atmospheric pressure in the experiment. The first eight membranes (named A-G) were tested by feeding the air from the top and toluene (52.7%) and nitrogen (47.3%) (Total flow rate: 0.4 l/min) to the bottom of the reactor. The air flow rate (total flow: 0.2 l/min to 0.45 l/min) and the temperature (700-950 ^oC) were varied in order to find the optimal conditions for the maximum oxygen flux value.

The rest four membranes (H 13, H14, H15, H16) belonging to one series (similar type with G) were evaluated mainly for the effects of the bottom flow rate (total flow rate of toluene and nitrogen (0.5 l/min to 2l/min), toluene amount (3000 ppm to 10000 ppm) as well as for the effects of the steam and gasification gas in order to find the highest oxygen flux and the toluene decomposition conversion. H13 membrane was tested under the bottom flow rate from 0.5 l/min to 2l/min, while H14 was tested to investigate different toluene amounts and the effect of the steam (H_2O: 12.43%; C_7H_8: 3000ppm and 10000 ppm). Finally, the gasification gas (wet gas composition: CO 10.9 vol %, CO_2 13.1 vol %, H_2 9.6 vol %, N_2 47.6 vol %, C_2H_4 0.87 vol %, C_7H_8 0.25 vol %, CH_4 5.24 vol %, H_2O 12.4 vol %) were added to the bottom at a constant flow rate (0.4 l/min). Two membranes (H15 and H16) were tested for long-term sequences (40 hours:

700 ºC for 10 h, 900 ºC for 10h, 800 ºC for 10h and 700 ºC for 10h), of which H15 was for the gasification sequence and H16 for the steam sequence.

Before starting the experiment, the pressure test was carried out by flushing the nitrogen from the top and the bottom. Gas leakage, if present, could be detected by monitoring the pressure in the control screen. Then the oven temperature was raised to 700 ºC with the help of flowing the nitrogen from the top and bottom to protect the system. The quality of the membrane was evaluated by performing the oxygen test (how much of the oxygen was permeated) and nitrogen test beforehand. The oxygen test was performed by feeding the synthetic air from the top and nitrogen from the bottom, while nitrogen permeability was tested by flowing the synthetic air from the top and carbon dioxide from the bottom. In order to ensure the stability and reliability of the results, the inlet concentration of the toluene was tested through the by-pass line by FID-GC before turning the toluene to the bottom. The temperature set points were tested in the order of 700 ºC, 900, 800 ºC and 700 ºC. Each time, three stable samples were taken from FIC-GC and TCD-GC. In addition, the outlet dry gas flow was measured through the gas flow meter by adjusting the value and timer, where the flow measurements contributed a small error for the results.

5.5 Calculation methods

Toluene conversion and oxygen flux were the most important parameters to assess the performance of the membrane. The tar is generated from the gasification gas and it was a complex mixture of organic compounds ranging from the light compounds to heavy hydrocarbons, for example, benzene being one of the heavy polyaromatic compounds. Toluene mainly cracked to benzene and light hydrocarbons on the membrane at high temperature and there was no other heavier hydrocarbons than benzene founded in FID-GC. Therefore, tar conversion and selectivity of toluene to benzene can be calculated from inlet and outlet amounts (ppm) in the equation 38. The oxygen flux was calculated based on the sum of the molar flow rate of carbon monoxide, carbon dioxide, unreacted oxygen and corresponding amount of water by assuming the complete combustion reaction.

$$\text{Tar conversion}=\frac{\mathrm{In}_{\mathrm{toluene\ (ppm)}}-\mathrm{Out}_{(\mathrm{toluene+benzene})(ppm)}}{\mathrm{In}_{\mathrm{toluene}}(ppm)} \quad (36)$$

$$\text{Selectivity toluene to benzene}=\frac{\mathrm{Out}_{\mathrm{benzene}}(ppm)}{\mathrm{In}_{\mathrm{toluene\ (ppm)}}-\mathrm{Out}_{\mathrm{toluene(ppm)}}} \quad (37)$$

$$\text{Oxygen flux}=\frac{\mathrm{F_{CO}}+\mathrm{F_{CO2}}+\mathrm{F_{O2unreacted}}+\mathrm{F_{H2O}}}{\mathrm{oxygen\ membrane\ area}}\ \mathrm{ml/min*cm^2} \quad (38)$$

6. Results and Discussion

The objective of the experimental work was to find the optimal conditions for the hydrocarbon decomposition on the oxygen permeable perovskite membrane and study the performance of the perovskite membrane materials for oxygen permeability. The activity of the membranes was dependent on the reaction conditions, therefore, the effects of the temperature, the air flow rate, the bottom flow rate of the nitrogen and toluene, the toluene amount, the steam, and the gasification gas were tested. Also a long-term test and comparison between the normal run and runs with steam and gasification gas was carried out. Finally, the optimal reaction conditions for the perovskite membrane material are proposed according to the results.

6.1 Effect of the temperature

The first 8 membranes (A-G) were tested under the reaction conditions of 52.7% toluene (47.3% of N_2) with total flow rate of 0.4 l/min by changing the air flow rate (from 0.2 l/min to 0.45 l/min) at four temperatures between 700 °C and 950 °C. The outlet gas compositions (vol %) and the oxygen flux values for the A-G membranes were in the same range, therefore, B6 membrane was selected for the discussion and the results for membrane B6 are given in table 4. The rest of the results for A-G are presented in the Appendix B. TCD-GC analysis was carried out for the measurements of the outlet gas composition (vol %). It was not possible to calculate toluene conversions for A-G membranes due to the lack of FID-GC analysis data for the first eight membranes.

Table 4. The reaction conditions and outlet gas composition with B6 membrane

	INPUT			OUTPUT(%)				
Temperature	Air flow	C_7H_8 & N_2	Toluene amount	H_2	CO	CO_2	CH_4	O_2 Flux
	(l/min)	(l/min)	(%)					(ml/min*cm^2)
700 ºC	0,20	0,40	52,7	0,08	0,30	0,89	0,00	1,59
	0,30	0,40	52,7	0,10	0,30	0,90	0,00	1,79
	0,45	0,40	52,7	0,10	0,30	0,99	0,00	1,77
800 ºC	0,30	0,40	52,7	0,40	0,60	1,00	0,00	1,85
	0,45	0,40	52,7	0,43	0,70	1,10	0,00	2,43
900 ºC	0,20	0,40	52,7	0,77	0,60	0,93	0,00	2,01
	0,30	0,40	52,7	0,71	0,90	0,98	0,03	2,12
	0,45	0,40	52,7	0,68	0,90	1,10	0,02	2,22
950 ºC	0,40	0,40	52,7	0,83	1,06	0,90	0,10	2,10
	0,45	0,40	52,7	0,95	1,20	0,90	0,10	2,25

It is obvious that with the increase of the temperature from 700 ºC to 950 ºC, the oxygen flux increased from 1.77 ml/min*cm^2 to 2.25ml/min*cm^2 at the air flow rate of 0.45 l/min (Figure 23). It was consistent with Xiong et al. who reported the oxygen flux depends on the temperature [1] & [2]. The rise of the temperature increased the diffusion rate of the oxygen ions leading to the increase of the oxygen vacancies controlled by bulk diffusion. The oxygen fluxes of A-G membranes in this study were in the range between 1.5 ml/min*cm^2 to 2.5ml/min*cm^2 in the temperature range of 700 to 950 ºC, which was quite similar with the value reported in the literature of 1.1 ml/min*cm^2 for 700 ºC [5]&[6].

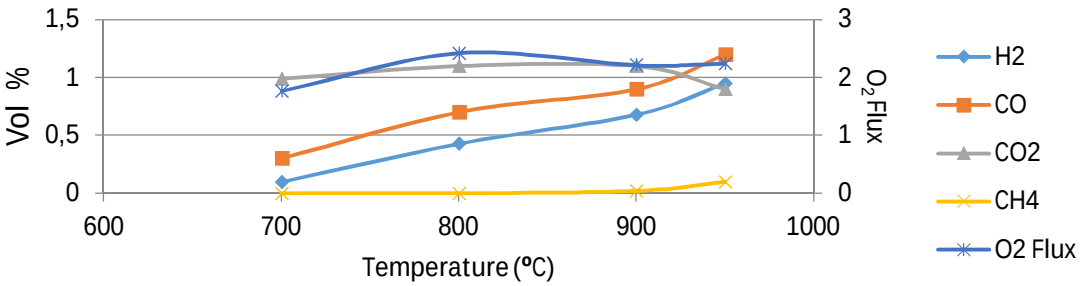

Figure 23. Effect of the temperature on the oxygen permeation flux as well as the outlet gas composition of B6 membrane (Air flow rate: 0.45 l/min).

At 700 ºC, the oxygen chemical potential gradient between oxygen-rich and oxygen-lean side is the main driving force that enables the oxygen to be transported through the membrane. Because small amount of carbon monoxide and carbon dioxide were generated and it was assumed that a small amount of oxygen was permeated through the membrane. The permeated oxygen reacted with the toluene to form carbon monoxide and carbon dioxide with the amount of the carbon dioxide being higher than carbon monoxide. It can be explained that carbon dioxide was coming from two pathways, one was from the complete combustion and the other was the oxidation of the carbon monoxide. The reaction was more favourable to the production of the carbon dioxide. Small amount of the hydrogen might have been produced by the partial oxidation of the toluene.

At the temperatures from 700 ºC to 900 ºC, only a small increase in the concentration of carbon dioxide (from 0.89% to 1.1%) was observed but the amount of the carbon monoxide started to climb up (from 0.3% to 0.9%). However, the amount of the carbon dioxide was still higher than carbon monoxide. It can be explained that the oxygen flux increased with the increasing of the temperature resulting in higher amount of carbon monoxide. The other reason might be that the water-gas shift reaction made the contribution for the production of the carbon monoxide. At the high temperature, thermal decomposition of hydrocarbon (C_7H_8) produced lighter hydrocarbons, which reacted with oxygen to form more carbon monoxide. The amount of carbon dioxide was still greater than carbon monoxide that might due to the complete combustion reaction. The oxygen permeated from the membrane and reacted with the toluene to have the complete combustion. Further oxidation of the carbon monoxide to carbon was assumed to have minor contribution in the carbon dioxide production. The water-gas shift and the thermal decomposition of the hydrocarbon (C_7H_8) at high temperature formed the products of C_2H_6, C_2H_4 etc, which reacted with oxygen to form not only carbon monoxide and carbon dioxide.

At 900 °C to 950 °C, methane (CH_4) was found in the products as result of the toluene cracking at high temperature forming lighter hydrocarbons. At 950 °C, the toluene cracked more to methane than it did at 900 °C, being consistent with the toluene cracking pre-test. Methane might also be generated by methanation reaction. Therefore, it can be concluded that the hydrocarbon cracked more at higher temperature.

At 950 °C, it was interesting that the amount of carbon monoxide was higher than the amount of the carbon dioxide. The carbon monoxide climbed up from 0.3 % to 1.2 % at 700 °C to 950 °C. It can be explained by that at 950 °C, the oxygen flux started to increase with the increasing temperature and it supplied more oxygen to produce more carbon monoxide. The carbon dioxide has been converted to carbon monoxide through the reactions of the reverse water-gas shift. The formed hydrocarbon react with carbon dioxide probably contributing to the carbon monoxide as well. And also at the high temperature, more steam was formed to promote the reaction of steam reforming for additional carbon monoxide. Therefore, the increase of the temperature had a favorable effect on the production of the carbon monoxide rather than carbon dioxide.

The oxygen flux increased with the temperature rising from 700 to 950 °C due to the temperature effect resulting in the high oxygen chemical gradient between the two sides of the membrane. As the temperature increased, the oxygen ions had been consumed and more oxygen started to permeate through the membrane. It reacted with the toluene to form carbon monoxide, carbon dioxide, hydrogen, methane as well as lighter hydrocarbons. At 700 °C, the reaction was more favorable for the production of the carbon dioxide due the chemical equilibrium as well as the further oxidation of the carbon monoxide. Afterwards, the amount of the carbon monoxide exceeded the amount of carbon dioxide. Moreover, the amount of the hydrogen as well as methane grow larger with the increasing of the temperature, which can be understood by the

higher temperature resulting in the higher thermal cracking of the hydrocarbon (toluene).

6.2 Effect of the air flow rate.

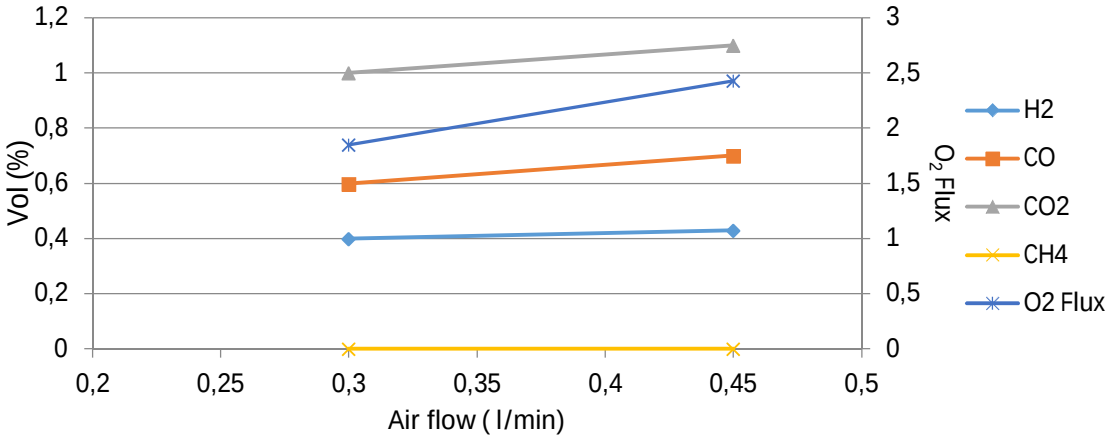

Figure 24. The effect of the air flow rate on the oxygen flux of the membrane (B6) and the outlet gas composition, T=800 ºC, air flow from 0.3 l/min to 0.45 l/min, $V_{toluene+N2}$= 0.4 l/min

Figure 24 shows the influence of the air flow rate on the perovskite B6 membrane at 800 ºC. Obviously, with the increasing of the air flow rate, the oxygen flux and outlet gas composition increased correspondingly. The oxygen flux increased from 1.85 ml/min*cm^2 to 2.43 ml/min*cm^2, when the air flow rate increased from 0.3 l/min to 0.45 l/min at 800 ºC. It can be understood that increased air flow rate led to higher exchange rate of the oxygen ions on the air side of the membrane, which was the controlling step of the oxygen permeation. The high air flow rate increased the oxygen chemical gradient between the air side and permeated side of the membrane and resulted in the increased oxygen permeation through the membrane.

In the experiment with B6 membrane, the total air flow rate was 0.3 l/min (20 vol% of oxygen: 0.06 l/min; 80 vol% of nitrogen: 0.24 l/min). The total flow rate of nitrogen and toluene was 0.4 l/min, which 0.21 l/min for C_7H_8 and 0.19 l/min for N_2. The actual amount of the oxygen fed into the reactor was 0.06 l/min at air flow rate of 0.3 l/min. If all the oxygen was assumed to go through the membrane, the amount of the oxygen flux was supposed to be 24.4 ml/min*cm^2 (60 ml/min divided by the area of the membrane 2.46 cm^2), whereas the oxygen flux in this experiment for B6 was only 1.85 ml/min*cm^2. If the partial oxidation was assumed to be the main reaction, the amount of the carbon monoxide was supposed to be 15.3% according the partial oxidation reaction of toluene. The carbon dioxide could be calculated separately based on the equation of the full combustion, which was supposed to be 7.6% of carbon dioxide. The reason for this difference between the theoretical and experimental values could be that the perovskite membrane did not allow all the oxygen to permeate, which might be caused by two reasons. In the air feeding on the top to the membrane reactor, all the oxygen was supposed to permeate the membrane into the reactor leaving nitrogen and other impurities outside the reactor to the vent. However, the flow with huge amount of the nitrogen could also took some part of the oxygen out to the vent. As a result, only small amount of the oxygen went through the membrane to the reactor because of the low residence time of the oxygen. The oxygen flux is also highly dependent on the perovskite membrane materials and different perovskite membranes have different oxygen permeability value.

When the air flow increased from 0.3 l/min to 0.45 l/min, the carbon monoxide increased from 0.6 % to 0.7% and the amount of the carbon dioxide increased from 1% to 1.1%. The oxygen flux increased from 1.85 ml/min*cm^2 to 2.43 ml/min*cm^2. This illustrates that the increase of the air flow rate led to the increase pressure on the air side of the membrane which resulted in higher oxygen flux. Therefore, it was obvious that the oxygen flux and outlet gas composition was affected by the air flow rate.

6.3 Effect of the total flow rate of nitrogen and toluene

In the experiment, different total flow rates of toluene and nitrogen (2 l/min, 1 l/min and 0.5 l/min) were applied for H13 membrane at temperatures between 700 ºC to 950 ºC. The results of the outlet composition gas and oxygen flux are presented in Table 5.

Table 5. The effect of the total flow rate of the nitrogen and toluene on H13 membrane (air flow: 0.45 l/min)

	INPUT		OUTPUT(%)				O_2 FLUX
Temperature	C_7H_8&N_2	Toluene amount	H_2	CO	CO_2	CH_4	(ml/min*cm^2)
ºC	(l/min)	(ppm)	vol%	vol%	vol%	vol%	
700ºC	2,00	2643,00	0,01	0,00	0,06	0,00	0,60
800ºC	2,00	2643,00	0,00	0,00	0,08	0,00	0,80
900ºC	2,00	2643,00	0,04	0,00	0,10	0,00	1,01
950ºC	2,00	2643,00	0,04	0,00	0,10	0,00	1,00
700ºC	1,00	3174,00	0,02	0,02	0,14	0,00	0,76
900ºC	1,00	3174,00	0,09	0,00	0,21	0,00	1,16
700ºC	0,50	2957,00	0,04	0,02	0,48	0,00	1,51
800ºC	0,50	2957,00	0,07	0,01	0,39	0,00	1,22
900ºC	0,50	2957,00	0,34	0,30	0,47	0,00	1,80

Based on the table 5, it is clear that when the total flow changed from 2 l/min to 0.5 l/min, the oxygen flux increased with the decrease of the total flow. The oxygen flux was 1.51 ml/min*cm^2 at the total flow of 0.5 l/min at 700 ºC, which was three times more than the total flow of 2 l/min (0.6 ml/min*cm^2) at the air flow rate of 0.45 l/min. It might be due to the higher flow rate of bottom flow (toluene & nitrogen), which resulted in the short residence time for toluene, which led to insufficient reaction time for toluene and oxygen. The oxygen has permeated through the membrane; however, the continuously flowing toluene from the bottom feed with higher flow rate did not have enough time to react with oxygen. On the other hand, toluene acted as an activating component for the membrane, the oxygen was accumulated near the membrane side and the more toluene reacted with the oxygen led to more oxygen

chemical gradient as a result of high oxygen flux. Therefore, too short residence time for toluene led to insufficient amount of the toluene reacting with the oxygen, which resulted in lower value of the oxygen flux.

At the total flow of 2 l/min (toluene and nitrogen), only a small amount of carbon dioxide was found and no carbon monoxide was detected in the outlet gas composition between 700 ^{o}C to 950 ^{o}C for H13 membrane. It meant that there was only a small amount of oxygen permeated through the membrane and the reaction was more favourable to form carbon dioxide. When the total flow changed from 2l/min to 1 l/min, carbon dioxide started to increase and a small amount of carbon monoxide was formed. It meant that more oxygen permeated through the membrane and the reaction was still more favourable to the complete combustion and less favourable with the partial oxidation. When the total flow of the toluene and nitrogen changed to 0.5 l/min, both of the carbon dioxide and the carbon monoxide continued to increase. Hydrogen continued to increase with lower total flow rate of the toluene and nitrogen because of toluene cracking more with longer residence time. Therefore, it could be concluded that the lower flow rate of the toluene and nitrogen resulted in higher oxygen flux value.

6.4 Effect of the toluene

Three different concentrations of toluene, which were 52.6 vol % of toluene (47.3 vol % of N_2) with the total flow rate of 0.4 l/min, 3000 ppm of toluene with higher total flow rate of 0.5 l/min and 10560 ppm of toluene with the total flow rate of 0.5 l/min, were investigated for comparison by keeping the constant top air flow rate. The results are shown in Table 6.

Table 6. The effect of the toluene with the constant air flow of 0.45 l/min.

	INPUT			OUTPUT(%)				O_2 FLUX
Membrane	Temperature	C_7H_8 &N_2	Toluene amount	H_2	CO	CO_2	CH_4	(ml/min*cm^2)
		(l/min)	ppm	vol %	vol %	vol %	vol %	
B6	700 ºC	0,4	526400	0,10	0,30	0,99	0,00	1,77
B6	800ºC	0,4	526400	0,43	0,70	1,10	0,00	2,43
B6	900ºC	0,4	526400	0,68	0,90	1,10	0,02	2,22
H13	700ºC	0,5	2957	0,04	0,02	0,48	0,00	1,51
H13	800ºC	0,5	2957	0,34	0,30	0,47	0,00	1,80
H13	900ºC	0,5	2957	0,07	0,01	0,39	0,00	1,22
H13	700ºC	0,5	10560	0,06	0,10	0,44	0,00	1,49
H13	800ºC	0,5	10560	0,16	0,20	0,45	0,00	1,61
H13	900ºC	0,5	10560	0,37	0,30	0,48	0,00	1,78

It was clear that there were no significant differences between the oxygen flux values with the toluene amount of 3000 ppm and 10560 ppm for H13 membrane. Based on table 6, the bottom flow rate of the nitrogen and toluene increased from 0.4 l/min to 0.5 l/min. It indicated that the toluene amount has less effect on the oxygen flux and the total flow rate of the toluene and nitrogen affected the oxygen flux. The toluene amount depended on the amount of oxygen permeated though the membrane. If the partial oxidation was assumed to be the main reaction, the oxygen flux was approximately 2 ml/min*cm^2 and it meant that there was approximately 2% of oxygen permeated that corresponded 0.57% of toluene. In this experiment, 52.6 % of toluene in the inlet gas exceeded the required amount of the toluene in the reaction and it resulted in either thermal cracking of the toluene under high temperature to form tar

residues staying in the line. The amounts of the 3000 ppm and 10560 ppm of toluene were in the required range in the reaction for toluene and therefore, they provided similar results for the oxygen flux.

6.5 Effect of the steam

12.4 vol % of steam was added to the bottom flow in the experiment with membrane H14. The results were compared with the normal run with only toluene and nitrogen in the bottom flow with H13 membrane. The results are presented in Table 7. Due to the lack of the FID-GC analysis during the experiment, only TCD-GC measurements were performed. Therefore, the oxygen flux with the steam could not be calculated because the lack of the data for hydrocarbons for the carbon and hydrogen balance.

Table 7. The effect of the steam with the constant air flow of 0.45 l/min

					OUTPUT(%)				O2 FLUX
Membrane	Temperature	C_7H_8&N_2	Toluene amount		H_2	CO	CO_2	CH_4	(ml/min*cm2)
		(l/min)	(ppm)		vol %	vol %	vol %	vol %	
H13	700ºC	0,5	2957		0,04	0,02	0,48	0	1,51
H13	800ºC	0,5	2957		0,07	0,01	0,39	0	1,22
H13	900ºC	0,5	2957		0,34	0,3	0,47	0	1,8
				H2O+++	H2	CO	CO2	CH4	
H14	700ºC	0,5	2526	12,43 %	0,94	0,3	0,53	0	
H14	800ºC	0,5	2526	12,43 %	1,36	0,7	0,54	0	
H14	900ºC	0,5	2526	12,43 %	2,51	0,9	0,83	0	
H14	700ºC	0,5	2526	12,43 %	0,24	0,1	0,39	0	

It is clear based on the results that the concentration of outlet gas composition with H14 membrane was much higher by adding the steam than in the normal test run for H13 membrane. However, there was no methane found in the products from 700 ºC to 900 ºC. Therefore, the reaction was more favourable to form hydrogen and carbon monoxide after adding the steam to the reactor, whereas the addition of steam enhanced the steam reforming reaction. The ratio of the hydrogen to carbon monoxide varied at different temperatures and for H13 membrane was 2:1 at 700 ºC, 7:1 at 800 ºC and 1.1:1 at 900 ºC. For H14 membrane, the ratio of hydrogen to carbon monoxide being 3.1:1 at 700 ºC, 1.9:1 at 800 ºC and 2.8:1 at 900 ºC. The ideal ratio between the

hydrogen and carbon monoxide in the outlet gases was 7:4 (=1.75:1) for partial oxidation.

Although the oxygen flux for H14 membrane could not be calculated due to the lack of the FID-GC, the relationship between the oxygen flux values to steam ratio can be extracted the literature. Xiong et al. [3] reported that the oxygen flux increased with adding the steam to the reactor and it increased with the increase of the steam/carbon ratio (W/C). The oxygen flux of 7.5 ml/min*cm^2 at 850 ^oC for simulated gasoline with the molecular ratio of W/C 0.26 and the air flow rate of 0.2 l/min was lower than the oxygen flux of 8 ml/min*cm^2 at V_{He} of 35 ml/min and W/C of 0.4 [3]. The oxidation reactions initially took place and subsequent steam reforming promoted the reaction for activating the membrane resulting in the high oxygen permeability value. In the beginning, a small amount of oxygen permeated through the membrane to react with the toluene to form carbon monoxide, carbon dioxide and water (partial oxidation or complete combustion). Steam took part in the reaction to react with the carbon monoxide to form more carbon dioxide and hydrogen. Finally, all the gases contributed mixed reforming for additional products. Therefore, adding the steam to the reactor made the reaction more complicated and provided positive effect on the membrane.

6.6 Effect of the gasification gas

Gasification gas (wet gas composition: CO 10.9 vol %, CO_2 13.1 vol %, H_2 9.6 vol %, N_2 47.6 vol %, C_2H_4 0.873 vol %, CH_4 5.24 vol % toluene 0.25 vol %, H_2O 12.4 vol %) was fed to the bottom of the membrane reactor with H15 membrane. Toluene mainly cracked to benzene and light hydrocarbons such as ethylene and methane at high temperatures and there was no other heavier hydrocarbons found than benzene found in FID-GC. The toluene conversions, tar conversions, selectivity of toluene to benzene and oxygen fluxes are calculated and shown in Table 8. The results at 700 °C and 900 °C were calculated based on the GC data and the result of the 800 °C was lacked due to the operation error occurred at 800 °C.

Table 8. Effect of the gasification gas for H15 membrane (air flow: 0.45 l/min, C_7H_8 & N_2: 0.5 l/min)

	OUTPUT					
Temperature	C_7H_8	C_6H_6	C_7H_8 conversion	Tar conversion	Selectivity of C_7H_8 to C_6H_6	O_2 FLUX
	(ppm)	(ppm)	(%)	(%)	(%)	(ml/min*cm^2)
700°C	2499	14,7	1,00	0,53	37,80	2,05
900°C	586	158	76,90	70,90	8,10	3,03

It is clear based on the table that the oxygen flux reached 3.03 ml/min*cm^2 at 900 °C with gasification gas, whereas the oxygen flux of normal run (toluene and nitrogen) was only 1.8 ml/min*cm^2 for H13 membrane. The presence of the strong reducing gases of CO and H_2 lower the oxygen partial pressure on the products side and result in the higher oxygen permeability. It was clear that the toluene conversion (76.9 %) at 900 °C was much higher than that at 700 °C (1 %). The toluene would either thermal cracked to other hydrocarbons at high temperature or oxidized to gases. Toluene cracked mainly to benzene and lighter compounds (C_2H_4, C_2H_6 and CH_4) and there was no other

heavier compound than benzene found in the FID-GC. The higher the temperature it was, the less toluene was cracked to benzene. The selectivity of the toluene to benzene was 37.8% at 700 ºC dropping to 8.1% at 900 ºC. One explanation could be that more toluene was oxidized than thermally cracked at higher temperature. The results also showed that the tar conversion (70.9 %) at 900 ºC was much higher than that at 700 ºC (0.53 %). It was due to the oxygen flux was increased with the increase of temperature reaching the highest value at 900 ºC. The higher the temperature it was, the more oxygen permeated through the membrane, which resulted in more toluene decomposing as a result of high tar conversion. Therefore, it can be concluded that the oxygen permeability reached highest value at 900 ºC, and at this temperature the highest toluene conversion and tar conversion were reduced.

6.7 Effect of the long-term test

The H15 membrane was tested with gasification gas applying following sequence of 700 ºC, 900 ºC, 800 ºC and 700 ºC. Each temperature was tested for 10 hours, total time being 40 hours. Due to the experiment operation error, there were only 700 ºC and 900 ºC performed in the long-term test. The results of input and output compositions for the gasification gas components at 700 ºC are presented in figure 25. The objective of the long term test was to observe if the membrane would have stable activity.

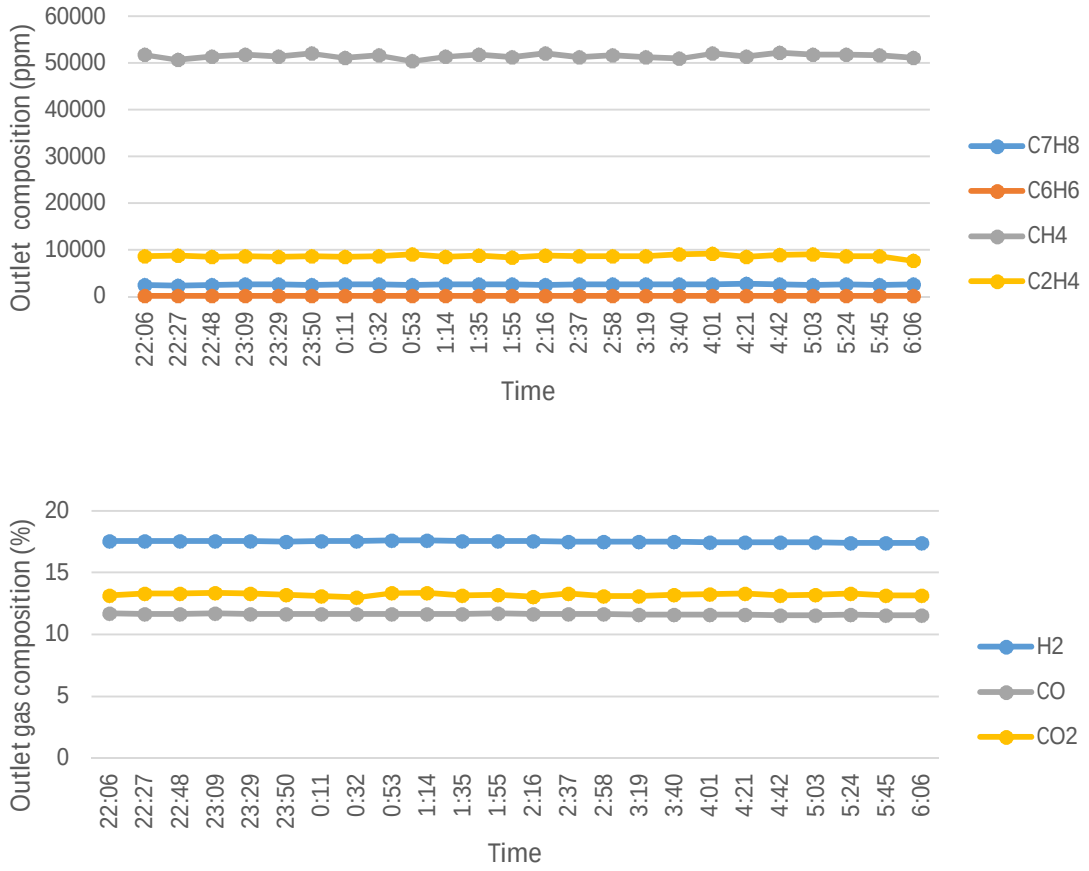

Figure 25. Effect of the long-term gasification gases testing at 700 ºC (Input value: C_7H_8: 2526ppm; CH_4: 52000 ppm, C_2H_4: 8645 ppm; CO 10.9 vol %; CO_2 13.1 vol %; H_2 9.6 vol %).

Based on the table 9, it is clear that there were only slight changes in the amounts toluene, benzene, methane and ethylene as well as the outlet gases (CO, CO_2 and H_2) after 10 hours. There was no significant change between the input value of toluene (2526 ppm) and output (2441ppm). It meant that toluene did not decompose on the membrane at 700 °C and there was only a small amount of oxygen permeated through the membrane. At 700 °C, only a small amount of the toluene was cracked into benzene and the output value of the methane and ethylene stayed similar as input. It can be concluded that the long-term test for 10 hours had very little effect for the oxygen permeability of the membrane as well as the toluene conversion. The same happened with the sequences for H16 membrane with steam for 40 hours at 700 °C, 900 °C, 800 °C and 700 °C and the results showed that at 700 °C, there was no significant change with the input and output values during the experiment time.

However, there was a significant change between the input and output values of the hydrocarbons at 900 °C for the gasification gas compared with those at 700 °C (Figure 26). The input value of the toluene was 2526 ppm and 593 ppm for output value. It meant that toluene had reacted at 900 °C. During the experiment, the amount of the benzene, methane and ethylene started to decrease. It might due to toluene has reacted more with the oxygen as a result of less thermal cracking. With the increasing of the time, the more oxygen permeated through the membrane to react with the toluene. Therefore, it can be concluded that long period of testing time at 900 °C has bigger effect than in 700 °C due to the increasing of the oxygen flux at higher temperature, which also resulted in less thermal cracking of the hydrocarbon. However, the results for the long time period testing at 800 °C was lacking due to the operation error.

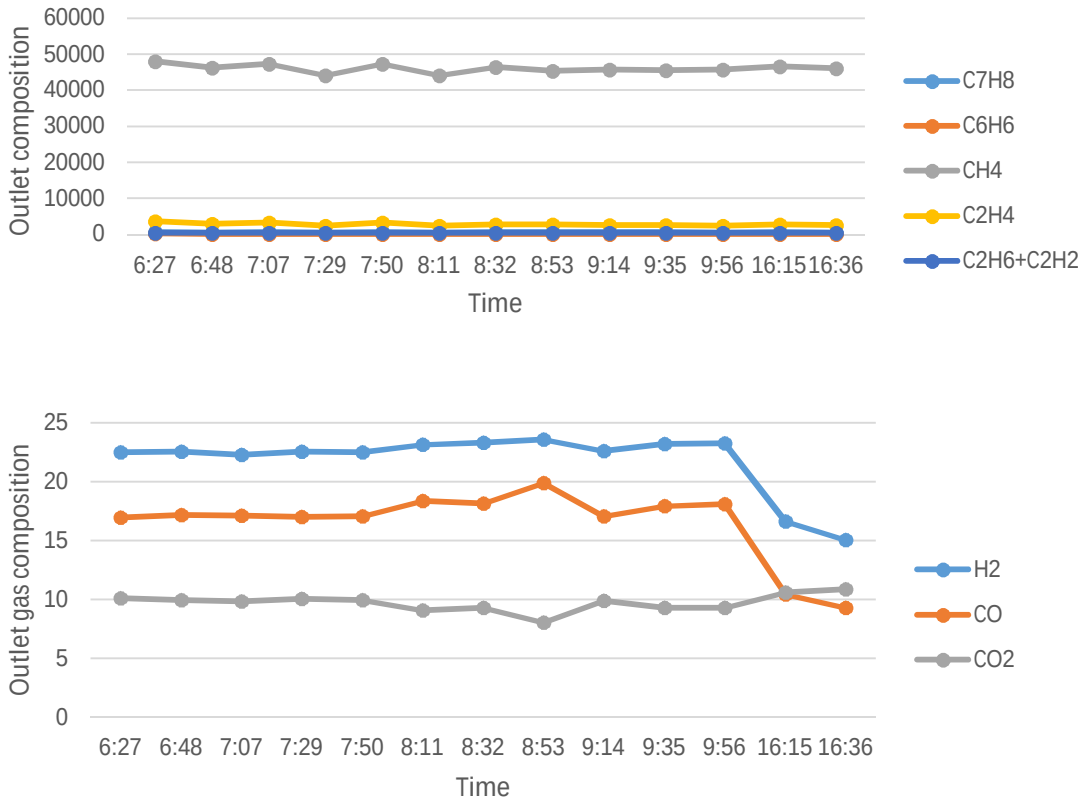

Figure 26. Effect of the long-term gasification gas testing at 900 ºC (Input value: C_7H_8: 2526ppm; CH_4: 52000 ppm, C_2H_4: 8645 ppm; CO 10.9 vol %; CO_2 13.1 vol %; H_2 9.6 vol %).

6.8 Comparison between standard run and runs with steam and gasification gas

H13 membrane was tested with a low amount of toluene (2957 ppm) and nitrogen fed to the reactor (air flow: 0.45 l/min, $V_{toluene+N2}$= 0.5 l/min). H14 and H15 membranes were tested using the steam and gasification gas, respectively (H14: C_7H_8: 2526 ppm, air flow: 0.45 l/min, $V_{toluene+N2}$= 0.5 l/min, H_2O: 12.4 %; H15: C_7H_8: 2526 ppm, air flow: 0.45 l/min, $V_{toluene+N2}$= 0.5 l/min). The results are presented in Figure 27, where the oxygen flux value for H14 with steam is missing due to the lack of the FID-GC measurements.

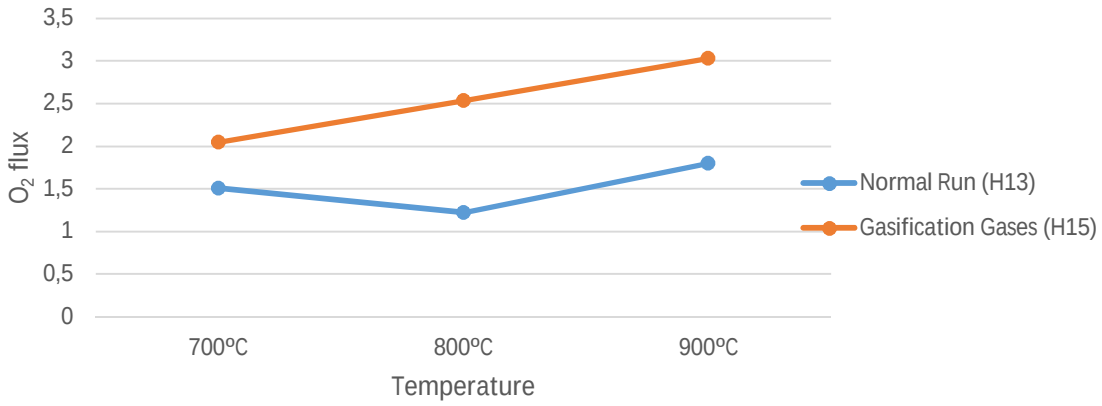

Figure 27. Comparison between normal run, steam reforming and gasification gases

Although the oxygen flux for H14 membrane was not presented in the table, the outlet gas composition indicates that the oxygen flux increased with the increased temperature. It can be explained by the presence of the strong reducing gases of CO and H_2, which made the contribution to the oxygen flux and steam reforming reaction activing the membrane. Both of the mixed reforming reactions increased the oxygen permeability by the oxidation, water gas-shift, methanation and steam reforming reactions between the carbon monoxide, carbon dioxide, hydrogen and water. However, in the normal test run with only nitrogen and toluene, the oxygen flux was

very low because there was no activating component, which resulted in lower partial pressure gradient between the two sides of the membrane.

H16 and H15 membranes were tested with the sequence runs with steam and gasification gas, respectively. (H16: C_7H_8: 10340 ppm, air flow: 0.45 l/min, $V_{toluene+N2}$= 0.5 l/min, H_2O: 12.4 %; H15: C_7H_8: 2526 ppm, air flow: 0.45 l/min, $V_{toluene+N2}$= 0.5 l/min). The results are shown in Figure 28.

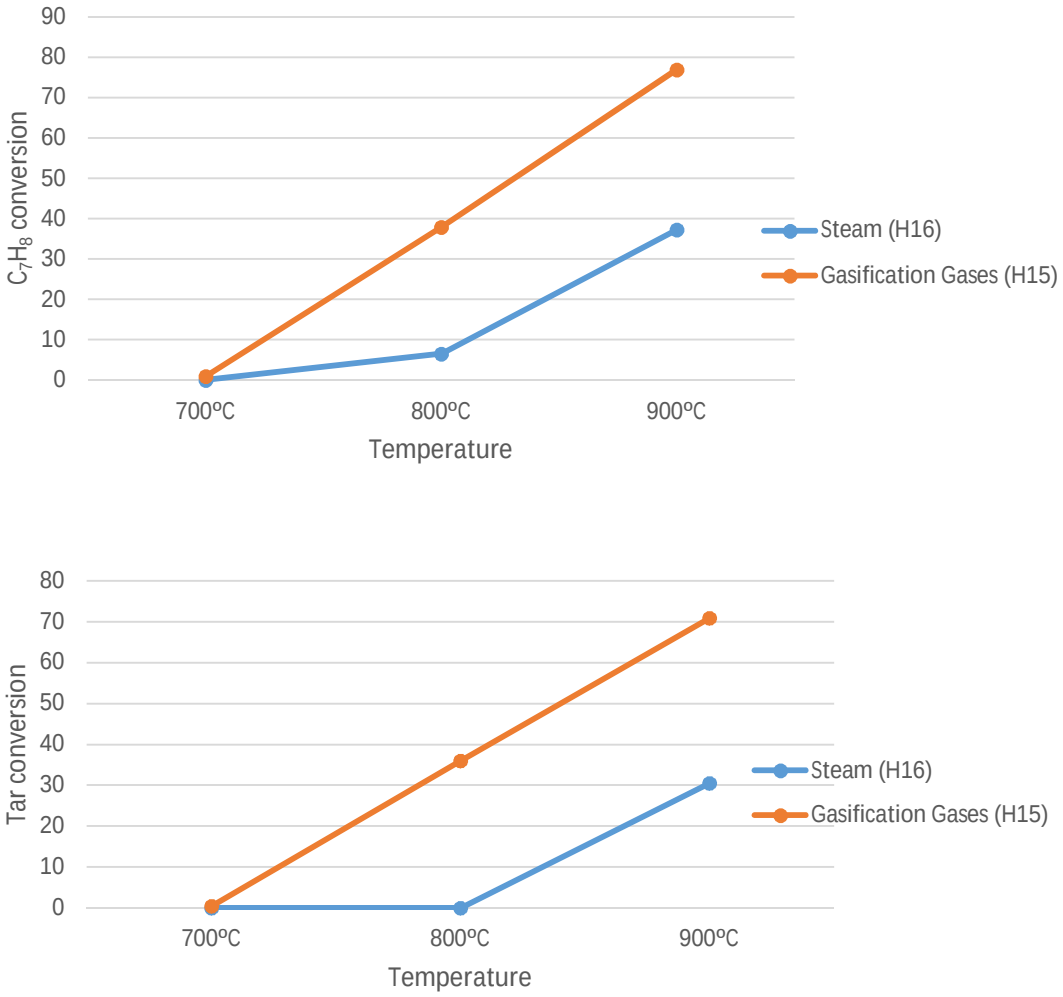

Figure 28. Comparison between steam and gasification gases

Considering the toluene conversion, it was clear that it increased with the increase of the temperature and it was higher with the gasification gases than with the steam. The higher toluene conversion could also be due to steam which reacted with toluene through steam reforming.

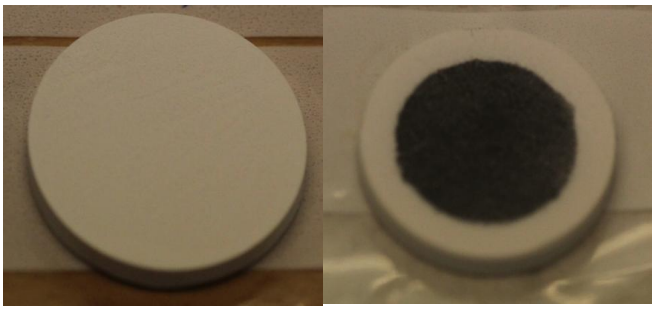

a) B6 before experiment b) B6 after experiment

c) H13 before experiment d) H13 after experiment e) H14 after experiment

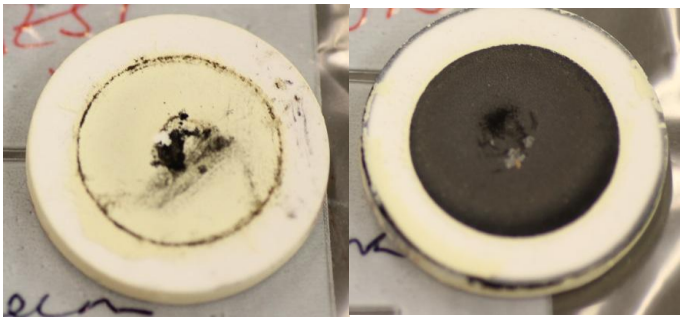

f) H15 after experiment g) H16 after experiment

Figure 29. The photographs of membranes before and after the runs

The photographs before and after the experiments on the reactions sides of the B6 and H type membranes are shown in Figure 29. The black color in the centre is coke, which was caused mainly by the thermal cracking of hydrocarbons on the membrane blocking the oxygen transforming through the membrane. There was also coke deposited on the H13, H14 and H16 membranes as well as B6 because of the relatively high concentration of the toluene. H14 and H16 membranes were both tested using the steam, of which H14 membrane was short run for 5 hours in total and H16 membrane was for 40 hours. However, H15 membrane tested for the gasification gas had excellent stability in long term run under a highly reducing atmosphere because of less coke deposition on the membrane. Therefore, it can be concluded that gasification gas had enough steam to inhibit coke formation. The short run with steam caused little coke on the membrane because the steam could prevent the coke from depositing on the membrane. However, the normal run and long-term tests for steam caused low performance of the membranes from the coke point of view.

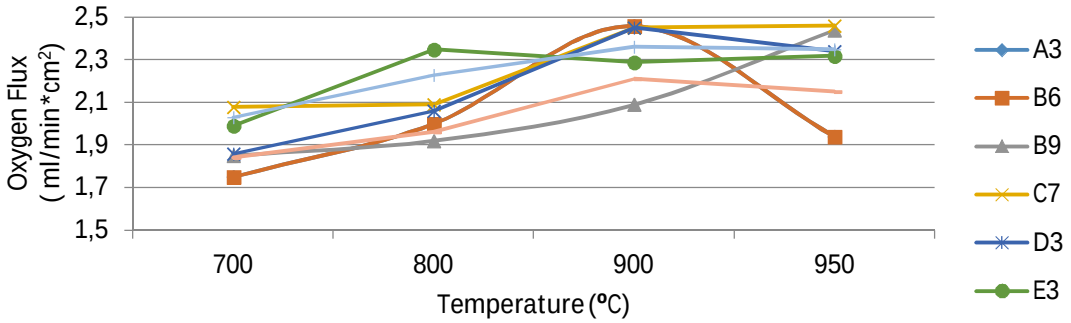

Figure 30. The effect of temperature (air flow rate: 0.45 l/min; toluene amount 52.74%, toluene and nitrogen flow: 0.4 l/min)

In standard run, A-G membranes were tested under various temperatures (700 °C to 950 °C). The performances of the membranes are shown in Figure 30. Among all the membranes (A-G), the oxygen fluxes were in the same range from 1.75 to 2.46 ml/min*cm^2 and C7 performed the best.

6.9 Error estimation

The most significant error sources were the reactor leakage, flow measurements, the reactor design, membrane preparation and oven temperature programme.

The pressure test was done after packing the membrane into the reactor to test that the gaskets were tight enough and there was no possibility for a leakage of dangerous compound such as carbon monoxide and carbon dioxide, during the experiment causing the hazardous incidents. It was performed by flushing the nitrogen to the top and bottom of the reactor for 1 min. The valve was closed and the pressure value was observed from the control screen. It was first tested for the quartz disc and the pressure stayed stable as shown in Figure 31. However, after changing a real perovskite membrane into the reactor, the pressure value was not stable.

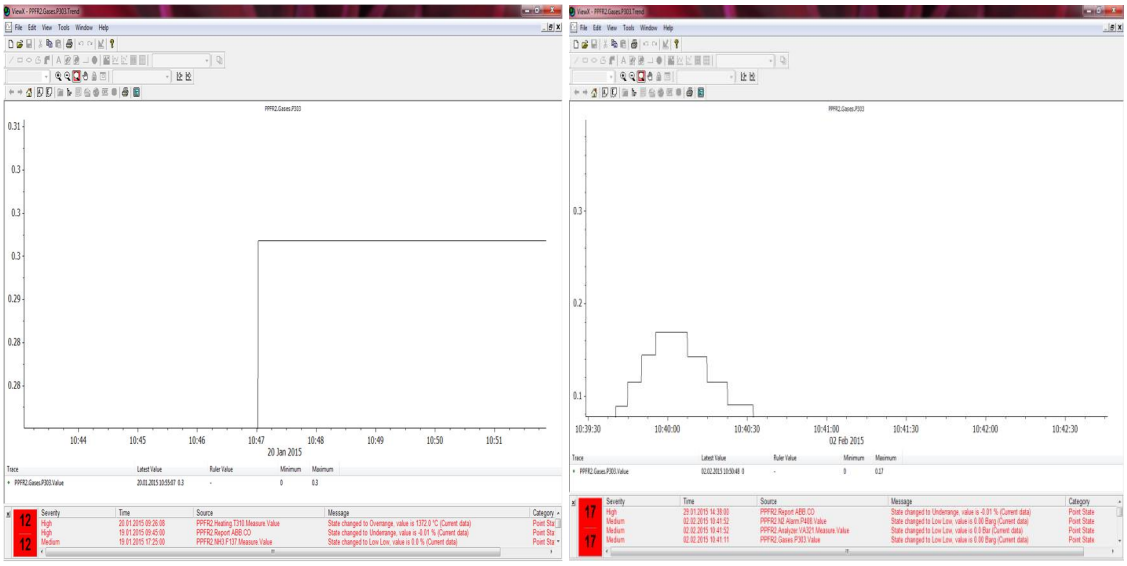

(a) (b)

Figure 31. Pressure test for (a) quartz disc; (b) membrane

It indicated that there were some leakage in the reactor. The small leakage might be caused by the defect of the reactor design that the reactor was oblique to the right side of the oven, which resulted in that the membrane was not placed horizontally between

the gaskets and the pressure from the gaskets was not evenly distributed on the membrane.

The membranes were tested for oxygen and nitrogen leakages before turning the oxygen to the membrane to make sure there was no nitrogen going through the membrane and the oxygen should accumulate near the membrane. It was performed by flushing air (0.45 l/min, 20% of O_2 and 80% of N_2) from the top and nitrogen to the bottom for oxygen test. The TCD-GC results showed that there was 0.01 % to 1.79% of oxygen found in the outlet gases and it varied between the membranes. There was no nitrogen going through. Reactor can be improved by the developing the manufacturing method.

The gas flow meter was used in the experiments to measure the outlet dry gas flow and the flow measurements contained a possibility for error. The oven temperature was measured by a thermocouple and the experiments were performed in order of 700 ^oC, 900 ^oC, 800 ^oC and 700 ^oC. However, the oven temperature control did not perform exactly the same way for each membrane with the same oven temperature set point value. E.g. if 900 ^oC was the set point, the temperature varied from 883 ^oC to 903 ^oC depending on the membrane. The temperature differences affected the results and were affected by the reaction. The higher reaction rate, the bigger effect on the temperature. The experiments were performed with significant high amount of toluene and the thermal cracking of hydrocarbons caused the coke formation as well as the tar remaining in the line. Both coke and tar stayed in the pipe line causing certain extent of blockage of the reactor, which might have led to the measurement errors.

7. Conclusions and recommendation for future studies

The objectives of the master's thesis were to have the tar decomposed on the perovskite membranes and find out the optimal reaction conditions for the highest oxygen permeability and the tar conversion. In this study, the theory and practice of the perovskite membranes were discussed in the literature study and twelve membranes (A-H) for toluene decomposition at the temperatures between 700 °C and 950 °C at atmospheric pressure were successfully tested in the laboratory scale. Different temperatures, air flow rates, total flow rates of toluene and nitrogen, toluene amounts as well as the effect of the steam and gasification gases were evaluated for perovskite membranes in order to investigate the optimal reaction conditions. The main target was to compare several perovskite materials and find the optimal conditions for the best material, where the toluene partial oxidation was the target reaction.

The tar removal from the gasification gases were considered to be important issue and oxygen permeable membranes could provide a solution for oxidation of the hydrocarbon with subsequent steam reforming enhances the hydrocarbon decomposition. However, the low oxygen flux value and stability were still limits to the application to the industrial scale. The good performance of the membrane material should exhibit high oxygen flux value and good stability under the reducing environment and CO_2 tolerance.

In the experimental part, membranes A to G were tested by feeding the synthetic air in the top part of the reactor and the toluene with nitrogen to the bottom of the reactor. The results showed that the oxygen fluxes were in the same range from 1.75 to 2.46 ml/min*cm^2 and C7 membrane had the highest oxygen flux among all membranes. The results also showed that the oxygen flux increased with the increase of temperature and air flow rate. Therefore, the membrane performed the best at highest temperature

(950 °C) and highest air flow rate (0.45 l/min). The bottom flow rate of nitrogen and toluene has effect on the oxygen flux value, of which the lower bottom total flow rate (0.5 l/min) has the higher oxygen flux value (1.5 ml/min*cm^2) due to the enough residence time for toluene led to more oxygen permeating through the membrane. The toluene amount has less effect on the oxygen flux value by comparing three different amount of toluene (527000 ppm, 3000 ppm and 10560 ppm). Moreover, the oxygen flux reached to 3.03 ml/min*cm^2 at 900 °C, air flow rate of 0.45 l/min and total bottom flow of 0.5 l/min by adding the gasification gas, of which oxygen flux value of 1.8 ml/min*cm^2 for a normal run under the same condition. Regarding to the toluene conversion, it was clear that the toluene conversion increased with the increase of the temperature and it was higher with the gasification gases than with the steam. Long-term tests for gasification gas and steam sequences at 700 °C, 900 °C, 800 °C and 700 °C of the total amount of the time being 40 hours were performed and the results show that that steam had less effect on the membrane than gasification gas and the oxygen flux value was little effected by the time. In summary, the optimal condition for the membrane was high temperature (900 °C), high air flow rate (0.45 l/min), with gasification gas.

The membrane materials in the experiment varied from A-H and it showed the same range of the oxygen flux value from 1.75 to 2.46 ml/min*cm^2. It was relatively low compared with the literature of 11.5 ml/min*cm^2 for the presence of the reforming catalyst of LiLaNiO/r-Al_2O_3 [67]. Deposited catalysts on the membrane surface would increase the chemical reaction rate, of which leads to a significant increase on the oxygen permeability performance. Moreover, addition of catalysts on the membranes can have the following effects and it can be recommended for the future studies.

1) To accelerate the adsorption and dissociation rate of CH_4 and O_2.
2) To accelerate the catalytic oxidation reaction rate (oxidation & reforming)
3) To increase the hydrocarbon conversion and H_2, CO selectivity.

4) To increase the oxygen permeability and membrane stability (in reducing environment)
5) To minimize the carbon decomposition on catalyst as much as possible

References

[1] Meng Kong, Jinhua Fei , Shuai Wang, Wen Lu and Xiaoming Zheng, “Influence of supports on catalytic behavior of nickel catalysts in carbon dioxide reforming of toluene as a model compound of tar from biomass gasification”, Bioresource Technology, vol. 102, pp. 2004-2008, 2011.

[2] Peter Vang Hendriksen, Peter Halvor Larsen, Mogens Mogensen, Finn Willy Poulsen and Kjell Wiik,” Prospects and problems of dense oxygen permeable membranes”, Catalysis Today, vol. 56, pp. 283-295, 2000.

[3] Yuwen Zhang, Jiao Liu, Weizhong Ding and Xionggang Lu, “Performance of an oxygen-permeable membrane reactor for partial oxidation of methane in coke oven gas to syngas”, vol. 90, pp. 324-330, 2011.

[4] Matthew M. Yung, Whitney S. Jablonski, and Kimberly A. Magrini-Bair, “Review of Catalytic Conditioning of Biomass-Derived Syngas”, Energy & Fuels, vol. 23, pp. 1874-1887, 2009.

[5] Ellett Anna Judith, “Oxygen Permeation and Thermo-Chemical Stability of Oxygen Separation Membrane Materials for the Oxyfuel Process”, Forschunszentrum Julich Zentralbibliothek, Verlag, 2010.

[6] Weishen Yang, Haihui Wang, Xuefeng Zhu and Liwu Lin, “Development and Application of Oxygen Permeable Membrane in Selective Oxidation of Light Alkanes”, Topics in Catalysis, vol. 35, pp.155-167, 2005.

[7] Marco van der Haar, "Mixed-conducting perovskite membrane for oxygen separation, towards the development of a supported thin-film membrane," Universiteit Twente, 2001.

[8] Liu Jizhong, Hongwei Cheng, Bo Jiang, Xionggang Lu and Weizhong Ding, “Effects of tantalum content on the structure stability and oxygen permeability of $BaCo_{0.7}Fe_{0.3-x}Ta_xO_{3-x}$ ceramic membrane, ” International Journal of Hydrogen Energy, vol. 38, pp. 11090-11096, 2013.

[9] T. Takahashi and T. Esaka, H. Iwahara, "Electrical conduction in the sintered oxides of the system Bi_2O_3–BaO, " J. Solid State Chem. Vol.16 , pp.317-323, 1976.

[10] Teroka, Y. et al, "Oxygen Permeation Through Perovskite Type Oxides, " Chemistry Letters, Chem. Soc. Japan, INT. Ed. pp. 1743-1746, 1985.

[11] J. Sunarso, S. Baumann, J.M. Serra, W.A. Meulenberg, S. Liu, Y.S. Lin, J.C and Diniz da Costa, "Mixed ionic–electronic conducting (MIEC) ceramic-based membranes for oxygen separation," Journal of Membrane Science, vol.320, pp.13–41,2008.

[12] G. Etchegoyen, “Oxyen permeation in $La_{0.6}Sr_{0.4}Fe_{0.9}Ga_{0.1}O_{3-\delta}$ dense membrane: effects of surface microstructure,” Journal of Solid State Electrochemistry, vol.10, pp.597-603, 2006.

[13] Joe da Costa, Simon Smart, Julius Motuzas, Shaomin Liu and Dongke Zhang, "State of Art (SOTA) Report on Dense Ceramic Membranes for Oxygen Separation from Air, "The University of Queensland , Curtin University and The University of Western Australia, 2013.

[14] Hong, W.K. and Choi, G.M. "Oxygen permeation of BSCF membrane with varying thickness and surface coating. Journal of Membrane Science, "vol.346. pp. 353-360, 2010.

[15] S. Smart, J.C. Diniz da Costa, S. Baumann and W.A. Meulenberg, "Oxygen transport membranes: dense ceramic membranes for power plant applications, in: A. Basile, S.P. Nunes (Eds.) Advance membrane science and technology for sustainable energy and environmental applications, " Woodhead Publishing Ltd, Cambridge, pp. 255-294, 2011.

[16] F.A. Kröger and H.J. Vink, "Relations between the concentrations of imperfections in solids," J. Phys. Chem. Solids, vol.5 (3), pp. 208, 1958.

[17] Y.S. Lin, W.Wang and J. Han, "Oxygen permeation through thin mixed-conducting solid oxide membranes,"AIChE J. vol.40 (5), pp.786, 1994.

[18] J.E. ten Elshof, H.J.M. Bouwmeester and H. Verweij, "Oxidative coupling of methane in a mixed-conducting perovskite membrane reactor," Applied Catalysis A, vol. 130, pp. 195-212, 1995.

[19] Qiying Jiang, "Mixed-Conducting Oxygen Permeable Ceramic Membrane and its Application in the Production of Synthesis Gas,” University of Kansas, Doctor thesis, 2010.

[20] P.M. Geffroy, J.Fouletier, N.Richet and T.Chartier, "Rational selection of MIEC materials in energy production processes," Chemical Engineering Science, vol. 87, pp. 408-433, 2013.

[21] Z. L. Wang and Z. C. Kang, "Functional and Smart Materials: Structural Evolution and Structure Analysis," Springer, pp. 514, 1998.

[22] Vivet, A..” Influence of glass and gold sealants materials on oxygen permeation performances in $La_{0.8}Sr_{0.2}Fe_{0.7}Ga_{0.3}O_{3-\delta}$ perovskite membranes”, Journal of Membrane Science, Vol. 366, pp. 132-138, 2011.

[23] Priscila Lemes-Rachadel, Giulliani Sachinelli Garcia, Ricardo Antonio Francisco Machado, Dachamir Hotza and João Carlos Diniz da Costa, "Current Developments of Mixed Conducting Membranes on Porous Substrates," Materials research, vol.17(1), pp. 242-249, 2014.

[24] J. Longo and R. Ward, "Magnetic Compounds of Hexavalent Rhenium with the Perovskite-type Structure," J. Am. Chem. Soc. Vol, 83 (13), pp 2816-2818, 1961.
[25] Xuefeng Zhu, Huanying Liu, You Cong and Weishen Yang, "Novel dual-phase membranes for CO_2 capture via an oxyfuel route,” Chem. Commun, vol.48, pp.251-253, 2012.

[26] Xueliang Dong, Jose´ Ortiz Landeros and Y. S. Lin, "An asymmetric tubular ceramic-carbonate dual phase membrane for high temperature CO2 separation,”Chem.Commun., vol.49, pp.9654, 2013.

[27] M Gateshki and J M Igartua, "Crystal structures and phase transitions of the double-perovskite oxides Sr_2CaWO_6 and Sr_2MgWO_6,”Journal of Physis: Condensed Matter, vol 16, pp.6639-6649, 2004.

[28] V. M. Goldschmidt, Skrifer Norske Videnskaps. Akad. Oslo I. Mat. Matur. Klasse, 1926, 8, 7–156.

[29] N. Ramadass, Mater. Sci. Eng., 1978, 36, 231–239.

[30] Kun Zhang, Jaka Sunarso, Zongping Shao,Wei Zhou, Chenghua Sun, Shaobin Wang and Shaomin Liu, "Research progress and materials selection guidelines on mixed conducting perovskite-type ceramic membranes for oxygen production," RSC advances, vol. 1, pp. 1661-1667, 2011.

[31] Xiaoyu Li, "Long Term Stability and Permeability of Mixed Ion Conducting Membranes under Oxyfuel Conditions," Doctor Thesis.

[32] Ali Alaee M.. “Preparation and characterisation of BaxSr1-x0.2Co0.8Fe0.2$O_{3-\delta}$ perovskite type membranes: Part 1 ”, Membrane Technology, vol. 2009, pp. 6-12, 2009.

[33] Huixia Luo, Bingbing Tian, Yanying Wei and Haihui wang, “Oxygen permeability and structural stability of a novel tantalum-doped perovskite $BaCo_{0.7}Fe_{0.2}Ta_{0.1}O_{3-\delta}$”, AIChE Journal 2009, vol. 56, pp. 604-610, 2009.

[34] John Sirman, “The evolution of Materials and Architecture for Oxygen Transport Membranes”, Nonporous Inorganic Membranes, 2006.

[35] Qiying Jiang, "Mixed-Conducting Oxygen Permeable Ceramic Membrane and its Application in the Production of Synthesis Gas,” University of Kansas, Doctor thesis, 2010.

[36] Yanying Wei, Weishen Yang, Jürgen Caro and Haihui Wang, “Dense ceramic oxygen permeable membranes and catalytic membrane reactors”, Chemical Engineering Journal, vol. 220, pp. 185-203, 2013.

[37] Irvine, J, I Metcalfe, A Thursfidel and A Kruth. “Defect Chemistry and Transport in Metal Oxides ”, Chemcial Industries, 2005.

[38] Kozo Ishizaki, “A hot isostatic process for fabricating porous materials”, Journal of Porous Materials, vol.1, pp. 19-27, 1995.

[39] J.L.G.Fierro, " Defect Chemistry and Transport in Metal Oxides,”A. Thursfield, I.S. Metcalfe, Kruth and J.T.S.Irvine. Ed. Metal Oxide: chemistry and Applications, pp.808 (78), 2005.

[40] H.P. Hsieh, "Materials and preparation of inorganic membranes,” Inorganic Membranes for Separation and Reaction, pp.587 (38), 1996.

[41] Korotcenkov, Ghenadii, "Handbook of Gas Sensor Materials Properties, Advantages and Shortcomings for Applications, “Volume 1: Conventional Approaches Series: Integrated Analytical Systems, pp 446, 2013.

[42] Stefan Diethelm, Jan Van herle, Joseph Sfeir and Philippe Buffat, "Correlation between oxygen transport properties and microstructure in $La_{0.5}Sr_{0.5}FeO_{3-\delta}$,” Journal of the European Ceramic Society, vol. 25, pp,2191–2196, 2005.

[43] V.V. Kharton and F.M.B., "Marques Mixed ionic–electronic conductors: effects of ceramic microstructure on transport properties,” Current Opinion in Solid State and Materials Science, vol. 6, pp. 261–269, 2002.

[44] Haihui Wang, Cristina Tablet, Armin Feldhoff and Jurgen Caro, “Investigation of phase structure, sintering, and permeability of perovskite-type $Ba_{0.5}Sr_{0.5}Co_{0.8}Fe_{0.2}O_{3-\delta}$ membranes”, Journal of Membrane Sceince, vol. 262, pp. 20-26, 2005.

[45] Weishen Yang, Haihui Wang, Xuefeng Zhu, and Liwu Lin, “Development and application of oxygen permeable membrane in selective oxidation of light alkanes”, Topics in Catalysis, Vol.35, pp. 155-167, 2005.

[46] B.A. van Hassel, J.E. ten Elshof and H.J.M. Bouwmeester, “Oxygen permeation flux through $La_{1-y}Sr_yFeO_3$ limited by carbon monoxide oxidation rate”, Applied Catalysis A: General, vol. 119, pp. 279-291, 1994.

[47] Peter Häussinger, Reiner Lohmüller and Allan M. Watson, ”Hydrogen”, Ullmann's Encyclopedia of Industrial Chemistry, 2000.

[48] Paolo Ciambelli, Vincenzo Palma, Emma Palo and Gaetano Iaquaniello, “Catalysis for Sustainable Energy Production, Chapter 9. Natural Gas Autothermal Reforming: an Effective Option for a Sustainable Distributed Production of Hydrogen”, 2009.

[49] Alessandro Trovarelli, “Catalytic Properties of Ceria and CeO_2-Containing Materials”, catalysis Reviews: Science and Engineering, vol. 38, 1996.

[50] F. Bimbela, D. Chen, J. Ruiza, L. García and J. Arauzo, “ Ni/Al coprecipitated catalysts modified with magnesium and copper for the catalytic steam reforming of model compounds from biomass pyrolysis liquids”, Applied Catalysis B: Environmental, vol. 119-120, pp. 1-12, 2012.

[51] Zongping Shao, Guoxing Xiong *, Hui Dong, Weishen Yang and Liwu Lin, “Synthesis, oxygen permeation study and membrane performance of a $Ba_{0.5}Sr_{0.5}Co_{0.8}Fe_{0.2}O_3$ oxygen-permeable dense ceramic reactor for partial oxidation of methane to syngas.” Separation and Purification Technology, vol. 25, pp. 97–116, 2001.

[52] Hongwei Cheng, Jizhong Liu, Xionggang Lu and Weizhong Ding, “Enhancing the Oxygen Permeability of $BaCo_{0.7}Fe_{0.2}Nb_{0.1}O_{3-\delta}$ Membranes by Coating $GdBaCo_{2-x}Fe_xO_{5+\delta}$ for Partial Oxidation of Coke Oven Gas to Syngas,” ACS Applied Materials & interfaces, 2011.

[53] Zongping Shao, Hui Dong, Guoxing Xiong, You Cong and Weishen Yang “Performance of a mixed-conducting ceramic membrane reactor with high oxygen permeability for methane conversion”, Journal of Membrane Science, vol. 183, pp. 181–192, 2000.

[54] Zongping Shao, Guoxing Xiong, Hui Dong, Weishen Yang and Liwu Lin, “Synthesis, oxygen permeation study and membrane performance of a $Ba_{0.5}Sr_{0.5}Co_{0.8}Fe_{0.2}O_3$ oxygen-permeable dense ceramic reactor for partial oxidation of methane to syngas.” Separation and Purification Technology, vol. 25, pp. 97–116, 2001.

[55] Zhibin Yang, Yuwen Zhang, Weizhong Ding, “Investigation on the reforming reactions of coke-oven-gas to H_2 and CO in oxygen-permeable membrane reactor”, Journal of Membrane Science, vol.470, pp.197–204, 2014.

[56] Dong Hui, Xiong Guoxing, Shao Zongping, Liu Shenglin and Yand Weishen, “Partial oxidation of methane to syngas in a mixed-conducting oxygen permeable membrane reactor,”

[57] Masayuki Ikeguchi, Tomohiro Mimura, Yasushi Sekine, Eiichi Kikuchi and Masahiko Matsukata, “Reaction and oxygen permeation studies in $Sm_{0.4}Ba_{0.6}Fe_{0.8}Co_{0.2}O_{3-\delta}$ membrane reactor for partial oxidation of methane to syngas”, Applied Catalysis A: General, vol. 290, pp. 212-220, 2005.

[58] Xuefeng Zhu, Mingrun Li, Huanying Liu, Tianyu Zhang, You Cong, Weishen Yang and State Key, “Design and experimental investigation of oxide ceramic dual-phase membranes”, Journal of Membrane Science, vol. 394-395, pp. 120.130, 2011.

[59] Zhibin Yang, Yuwen Zhang, Weizhong Ding, “Investigation on the reforming reactions of coke-oven-gas to H_2 and CO in oxygen-permeable membrane reactor”, Journal of Membrane Science, vol.470, pp.197–204, 2014.

[60] Wenliang Zhu, Wei Han, Guoxing Xiong and Weishen Yang, “Mixed reforming of heptane to syngas in the $Ba_{0.5}Sr_{0.5}Co_{0.8}Fe_{0.2}O_3$membrane reactor,” Catalysis Today, vol.104, pp.149–153, 2005.

[61] Yazhong Chen, Hengyong Xu, Yuzhong Wang, Xianglan Jin and Guoxing Xiong, “Hydrogen production from liquid hydrocarbon fuels for PEMFC application,” Fuel Processing Technology vol. 87, pp. 971–978, 2006.

[62] Wenliang Zhu, Guoxing Xiong, Wei Han and Wenshen Yang, “Catalytic partial oxidation of gasoline to syngas in a dense membrane reactor” Catalysis Today, vol. 93–95, pp.257–261, 2004.

[63] Thana Phuphuakrat, Tomoaki Namioka and Kunio Yoshikaw, “Tar removal from biomass pyrolysis gas in two-step function of decomposition and adsorption”, Applied Energy 87, pp. 2203-2211, 2010.

[64] Yazhong Chen, Hengyong Xu, Yuzhong Wang and Guoxing Xiong, “Hydrogen production from the steam reforming of liquid hydrocarbons in membrane reactor”, Catalysis Today, vol. 118, pp. 136-143, 2006.

[65] Yazhong Chen, Hengyong Xu, Yuzhong Wang and Guoxing Xiong, “Hydrogen production from the steam reforming of liquid hydrocarbons in membrane reactor”, Catalysis Today, vol.118, pp. 136-143, 2006.

[66] Zhang Yuwen, Liao Yong, Ding Weizhong and Lu Xionggang, “Perovskite-type oxygen-permeable membrane $BaCo_{0.7}Fe_{0.2}Nb_{0.1}O_{3-\delta}$ for partial oxidation of methane in coke oven gas to hydrogen”, Rare Metals, vol. 29, pp. 231-237, 2010.

[67] Wenliang Zhu, Guoxing Xiong∗, Wei Han, Wenshen Yang, “Catalytic partial oxidation of gasoline to syngas in a dense membrane reactor”, Catalysis Today, vol. 93-95, pp. 257-261, 2004.

APPENDICS

[68] Kovalevskii Andrel; Kharton, VV; Naumovich E.N., Tikhonovich V.N., Tonoyan A.A., Reut O.P. “Oxygen-ionic permeability of the $Sr_{0.7}Ln_{0.3}CoO_{3-\delta}$ (Ln = La, Nd, Sm, Gd) solid solutions with the perovskite structure”, Russian Journal of Electrochemistry, vol.33, pp.5, 1997.

[69] T.Nagai, W.Ito, T.Sakon, “Relationship between cation substitution and stability of perovskite structure in SrCoO3–δ-based mixed conductors, Solid State Ionics, vol. 177, pp. 3433-3444, 2007.

[70] Julia Martynczuk, Mirko Arnold and Armin Feldhoff,” Influence of grain size on the oxygen permeation performance of perovskite-type $(Ba_{0.5}Sr_{0.5})(Fe_{0.8}Zn_{0.2})O_{3-\delta}$ membranes, Journal of Membrane Science, Vol. 322, pp. 375-382, 2008.

[71] Liang Tan, Li Yang, Xuehong Gu, Wanqin Jin, Lixiong Zhang, Nanping Xu, “Influence of the size of doping ion on phase stability and oxygen permeability of $SrCo_{0.8}Fe_{0.2}O_{3-\delta}$ oxide”, Journal of Membrane Science, vol 230, pp. 21-27, 2004.

[72] Qin Guoli, Ding Weizhong, Zhang Yuwen, Shen Peijun, Wang Chenglei, “ Feasibility study of $SrFeCo_{0.5}O_{3-\delta-}$ oxygen permeable membrane on partial oxygen reforming of COG.” SHANGHAI METALS, vol.31, 2009.

[73] Li Qiming, Zhu Xuefeng, He Yufeng and Yang Weishen, ”Partial oxidation of methane in $BaCe_{0.1}Co_{0.4}Fe_{0.5}O_{3-\delta}$ membrane reactor,” Catalysis Today, Vol.149, pp, 185-190, 2010.

[74] V.V Kharton, A.A Yaremchenko, A.V Kovalevsky, A.P Viskup, E.N Naumovich and P.F Kerko, “Perovskite-type oxides for high-temperature oxygen separation membranes”, journal of Membrane Science, vol 163, pp. 307-317, 1999.

[75] Zhang Heng, Wang Tingting, Nie Yi, Zhang Xiangping, Linweiming,” Investigation of performance of $SrFe_{0.6}Cu_{0.3}Ti_{0.3}O_{3-\delta}$ mixed conducting membrane for partial oxidation of methane to syngas.

[76] Shidong Song , Peng Zhang, Minfang Han and Subhash C. Singhal, “ Oxygen permeation and partial oxidation of methane reaction in $Ba_{0.9}Co_{0.7}Fe_{0.2}Nb_{0.1}O_{3-\delta}$ oxygen

permeation membrane", Journal of Membrane Science, vol. 415-416, pp. 654-662, 2012.

[77] Hailei Zhao, Wei Shen, Zhiming Zhu, Xue Li and Zhifeng Wang, "Preparation and properties of $Ba_xSr_{1-x}Co_yFe_{1-y}O_{3-l}$ cathode material for intermediate temperature solid oxide fuel cells", Journal of Power Sources, vol. 182, pp. 503-509, 2008.

[78] Lei Ge, Wei Zhou, Ran Ran, Shaomin Liu, Zongping Shao, Wanqin Jin and Nanping Xu, "Properties and performance of A-site deficient $(Ba_{0.5}Sr_{0.5})_{1-x}Co_{0.8}Fe_{0.2}O_{3-\delta}$ for oxygen permeating membrane", Journal of Membrane Science, vol 306, pp. 318-328, 2007.

[79] Shao Zongping, Cong You, Xiong Guoxing and Sheng Shishan,"Perivskite-type B-site Bi-doped ceramic membranes for oxygen separation." Chinese Science Bulletin, vol.45, No.10, 2000.

[80] Jianhua Tong, Weishen Yang, Rui Cai, Baichun Zhu, Guoxing Xiong and Liwu Lin," Investigation on the structure stability and oxygen permeability of titanium-doped perovskite-type oxides of $BaTi_{0.2}Co_xFe_{0.8-x}O_{3-\delta}$ (x=0.2–0.6)," Separation and purification technology, vol.32, Issue 1-3, pp.289-299, 2003.

[81] C.H. Chen1, H.J.M. Bouwmeester, R.H.E. van Doorn, H. Kruidhof and A.J. Burggraaf, "Oxygen permeation of $La_{0.3}Sr_{0.7}CoO_{3-\delta}$, Solid State Ionics, "vol.98, pp.7–13, 1997.

[82] H. Kruidhof, H.J.M. Bouwmeester, R.H.E.v. Doorn and A.J. Burggraaf, "Influence of order-disorder transitions on oxygen permeability through selected nonstoichiometric perovskite-type oxides, "Solid State Ionics, vol. 63-65, pp.816-822, 1993.

[83] Norio Miura, Yasuo Okamoto, Jun Tamaki, Kenji Morinaga and Noboru Yamazoe, "Oxygen semipermeability of mixed-conductive oxide thick-film prepared by slip casting, "Solid State Ionics vol.79, pp. 195-200, 1995.

[84] Cui Meisheng, Li Minglai, Zhang shunli, Long Zhiqi, Cui Dali and Huang Xiaowei, "Preparation and physico-chemical characterisation of $La_{1-x}Ce_xCoO_{3-\delta}$ perovskite catalyst and its methane catalytic combustion", The Chinese Journal of Nonferrous Metals, vol.14, No. 9, 2004.

[85] Dengjie Chen, Chi Chen, Zarah Medina Baiyee, Zongping Shao, and Francesco Ciucci, "Nonstoichiometric Oxides as Low-Cost and Highly-Efficient Oxygen Reduction/Evolution Catalysts for Low-Temperature Electrochemical Devices", Chemical Reviews, vol. 115, pp. 9869-9921, 2015.

[86] V.V. Kharton, A.V. Kovalevsky, V.N. Tikhonovich, E.N. Naumovich and A.P. Viskup, "Mixed electronic and ionic conductivity of LaCo(M)O (M=Ga, Cr, Fe or Ni), II. Oxygen permeation through Cr- and Ni-substituted $LaCoO_3$, "Solid State Ionics, vol.110, pp.53–60, 1998.

[87] Ekaterina V. Tsipis and Vladislav V. Kharton, “Electrode materials and reaction mechanisms in solid oxide fuel cells: a brief review, I. Performance-determining factors”, Journal of Solid State Electrochem, vol. 12, pp. 1039-1060, 2008.

[88] Shao Zongping, Cong You, Xiong Guoxing, Sheng Shishan, Yang Weishen, ”Mixed-conducting perovskite-*type* $Sr_xBi_{1-x}FeO_{3-\delta}$ oxygen-permeating membranes,” Science China Chemistry, Vol.43, Issue (4), pp, 421-427, 2000.

[89] V.V. Kharton, A.P. Viskup, E.N. Naumovich, A.A. Tonoyan, and O.P. Reut,”Oxygen Ionic Transport in A-site-deficient Perovskites La(Pb)FeO_3. Vol.33, pp.1087-1093, 1998.

[90] Tong Jianhua, Yang Weishen, Ren Yanjie, Shao zongping, Xiong Guoxing and Lin Liwu,” Investigation on Ba, Fe Doped La-Co-O Series Mixed Conducting Membranes for Permeation of oxygen.” Chinese Journal of Catalysis, vol.21,No.5, 2000.

[91] Shaoli Guo , Hongjing Wu , Fabrizio Puleo and Leonarda F. Liotta, “B-Site Metal (Pd, Pt, Ag, Cu, Zn, Ni) Promoted $La_{1-x}Sr_xCo_{1-y}Fe_yO_{3-\delta}$ Perovskite Oxides as Cathodes for IT-SOFCs”, Cataltsts, vol. 5, pp. 366-391, 2015.

[92] ZHANG Yuwen, LIU Yong, Wang Chenglei, YANG Zhibin, DING Weizhong, and LU Xionggang, “Total conductivity, oxygen permeability and stability of perovskite-type oxide $BaCo_{0.7}Fe_{0.2}Nb_{0.1}O_{3-\delta}$”, Rare Metals, vol 28, pp. 202-208, 2009.

[93] Tingfang Tian, Minchuan Zhan, Wendong Wang and Chusheng Chen,” Surface properties and catalytic performance in methane combustion of $La_{0.7}Sr_{0.3}Fe_{1-y}Ga_yO_{3-d}$ perovskite-type oxides”, Catalysis Communications, vol. 10, pp. 513-517, 2009.

[94] A.A. Yaremchenko, V.V. Kharton, A.P. Viskup, E.N. Naumovich, V.N. Tikhonovich, and N.M. Lapchuk, “Mixed electronic and ionic conductivity of $LaCo(M)O_3$ (M=Ga, Cr, Fe or Ni). V. Oxygen permeability of Mg-doped La(Ga, Co)O perovskites, Solid State Ionics, vol. 120, pp, 65-74, 1999.

[95] V.V. Kharton, E.N. Naumovich and F.M.B. Marques, “Ionic and Electronic Transport in Perovskite-Type La(Ga,M)O3. 5 (M = Mg, Cr, Fe, Co, Ni, Nb), ” Ionics 5, 1999.

[96] Ekaterina V. Tsipis & Vladislav V. Kharton, “Electrode materials and reaction mechanisms in solid oxide fuel cells: a brief review”, Journal of Solid State Electrochemistry, vol. 12, pp.1039-1060, 2008.

TEST RUN	RUN DETAILS
TEST RUN-1	Temperature profile
TEST RUN-2	C_7H_8 feeding from bypass line
TEST RUN-3	Blank quartz disc, gasket and reactor leakage testing
TEST RUN-4	Al_2O_3 support high temperature testing
TEST RUN-5	O_2 permeability test for Al_2O_3 support
TEST RUN-6	Continue Run-5
TEST RUN-7	High temperature toluene cracking test (800-900 C);Toluene feeding from the bottom (52.7 vol % toluene)
TEST RUN-8	Micro-GC calibration practice 1
TEST RUN-9	Micro-GC calibration practice 2
TEST RUN-10	Micro-GC calibration practice 3
TEST RUN-11	Reactor broken and repaired again
TEST RUN-12	Micro-GC calibration curve practice 4 due to the software break
TEST RUN-13	High temperature toluene cracking test (800-950 ^oC.)
TEST RUN-14	Membrane A3 testing (52.7vol % toluene, 0.4l/min of total flow)
TEST RUN-15	Membrane B6 testing (52.7 vol % toluene, 0.4l/min of total flow)
TEST RUN-16	Membrane B9 testing (52.7 vol % toluene, 0.4l/min of total flow)
TEST RUN-17	Membrane C7 testing (52.7 vol % toluene, 0.4l/min of total flow)
TEST RUN-18	Membrane D3 testing (52.7 vol % toluene, 0.4l/min of total flow)
TEST RUN-19	Membrane E3 testing (52.7 vol % toluene, 0.4l/min of total flow)
TEST RUN-20	Membrane F16 testing (52.7 vol % toluene, 0.4l/min of total flow)
TEST RUN-21	Membrane G10 testing (52.7 vol % toluene, 0.4l/min of total flow)
TEST RUN-22	Membrane H13 testing (2643ppm of toluene, 2 l/min of total flow)
TEST RUN-23	Membrane H13 testing (3174 ppm of toluene, 1 l/min of total flow)
TEST RUN-24	Membrane H13 testing (2957 ppm of toluene, 0.5 l/min of total flow) Membrane H13 testing (10560 ppm of toluene, 0.5 l/min of total flow)
TEST RUN-25	Membrane H13 testing (10580 ppm of toluene, 1 l/min of total flow)
TEST RUN-26	Membrane H14 testing, effect of steam. (2957 ppm of toluene, 0.5 l/min of total flow, 12.4% H_2O)
TEST RUN-27	Membrane H14 testing, effect of steam. (9298 ppm of toluene, 0.5 l/min of total flow, 12.4% H_2O)
TEST RUN-28	Membrane H15 testing, effect of gasification gas, sequence for 40 hours
TEST RUN-29	Membrane H16 testing, effect of steam, sequence for 40 hours
TEST RUN-30	Membrane C8 testing, effect gasification gas, sequence for 40 hours

Appendix B. Data from all the runs

Table A. The outlet gases composition and oxygen flux for all the membranes

		INPUT			OUTPUT(%)				O2 FLUX
	Temperature	Air flow	Toluene&Nitrogen	Toluene amount	H2	CO	CO2	CH4	
	(ºC)	(l/min)	(l/min)	(ppm)					(ml/min*cm2)
A3	700	0,25	0,4	527400	0,03	0,2	0,92	0	1,8
		0,3	0,4	527400	0,1	0,2	1	0	1,67
		0,45	0,4	527400	0,1	0,2	1	0	1,75
	800	0,2	0,4	527400	0,3	0,4	1	0	1,91
		0,25	0,4	527400	0,3	0,4	1	0	2,1
		0,3	0,4	527400	0,2	0,3	1,03	0	1,86
		0,4	0,4	527400	0,3	0,4	1	0	1,98
		0,45	0,4	527400	0,3	0,4	1	0	2
	900	0,4	0,4	527400	0,6	0,7	1	0,01	2,39
		0,45	0,4	527400	0,6	0,7	1,1	0,01	2,46
	950	0,25	0,4	527400	0,3	0,4	1	0,08	2,07
		0,3	0,4	527400	0,3	0,3	1,1	0,1	2,15
		0,4	0,4	527400	0,4	0,4	1	0,1	1,92
		0,45	0,4	527400	0,4	1,4	1,9	0,1	1,94

		INPUT			OUTPUT(%)				O2 FLUX
	Temperature	Air flow	Toluene&Nitrogen	Toluene amount	H2	CO	CO2	CH4	
	(ºC)	(l/min)	(l/min)	(ppm)					(ml/min*cm2)
B6	700 ºC	0,2	0,4	527400	0,08	0,3	0,89	0	1,59
		0,3	0,4	527400	0,1	0,3	0,9	0	1,79
		0,45	0,4	527400	0,1	0,3	0,99	0	1,77
	800 ºC	0,3	0,4	527400	0,4	0,6	1	0	1,85
		0,45	0,4	527400	0,43	0,7	1,1	0	2,43
	900 ºC	0,2	0,4	527400	0,77	0,6	0,93	0	2,01
		0,3	0,4	527400	0,71	0,9	0,98	0,03	2,12
		0,45	0,4	527400	0,68	0,9	1,1	0,02	2,22
	950 ºC	0,4	0,4	527400	0,83	1,06	0,9	0,1	2,1
		0,45	0,4	527400	0,95	1,2	0,9	0,1	2,25

B9	700ºC	0,2	0,4	527400	0,15	0,3	0,92	0	1,71
		0,3	0,4	527400	0,1	0,2	1	0	1,77
		0,45	0,4	527400	0,1	0,2	1,02	0	1,85
	800ºC	0,2	0,4	527400	0,28	0,4	0,92	0	1,78
		0,3	0,4	527400	0,28	0,4	0,97	0	1,83
		0,45	0,4	527400	0,28	0,4	1,03	0	1,92
	900ºC	0,2	0,4	527400	0,34	0,58	0,91	0,01	1,83
		0,45	0,4	527400	0,36	0,61	1,01	0,01	2,09
	950ºC	0,2	0,4	527400	0,77	0,85	0,9	0,1	1,9
		0,45	0,4	527400	1,73	1,59	0,9	0,1	2,44

		INPUT			OUTPUT(%)				O2 FLUX
	Temperature	Air flow	Toluene&Nitrogen	Toluene amount	H2	CO	CO2	CH4	
	(ºC)	(l/min)	(l/min)	(ppm)					(ml/min*cm2)
C7	700ºC	0,2	0,4	527400	0,07	0,02	1,02	0	1,67
		0,45	0,4	527400	0,1	0,01	1,2	0	2,08
	800ºC	0,2	0,4	527400	0,23	0,2	1,12	0	2,47
		0,45	0,4	527400	0,22	0,2	1,2	0	2,09
	900ºC	0,2	0,4	527400	1,2	1,36	0,83	0,01	2,18
		0,45	0,4	527400	1,22	1,45	0,94	0,02	2,45
	950ºC	0,2	0,4	527400	1,03	1,46	0,8	0,1	2,12
		0,45	0,4	527400	1,36	1,71	0,9	0,1	2,46

		INPUT			OUTPUT(%)				O2 FLUX
	Temperature	Air flow	Toluene&Nitrogen	Toluene amount	H2	CO	CO2	CH4	
	(ºC)	(l/min)	(l/min)	(ppm)					(ml/min*cm2)
D3	700ºC	0,2	0,4	527400	0,19	0,1	1,01	0	1,76
		0,45	0,4	527400	0,1	0,02	1,1	0	1,86
	800ºC	0,2	0,4	527400	0,32	0,3	1,05	0	1,87
		0,45	0,4	527400	0,35	0,3	1,17	0	2,06
	900ºC	0,2	0,4	527400	0,97	1,06	0,87	0	2,09
		0,45	0,4	527400	1	1,12	1,07	0,03	2,45
	950ºC								
		0,45	0,4	527400	0,09	1,21	0,9	0,1	2,34

		INPUT			OUTPUT(%)				O2 FLUX
	Temperature	Air flow	Toluene&Nitrogen	Toluene amount	H2	CO	CO2	CH4	
	(ºC)	(l/min)	(l/min)	(ppm)					(ml/min*cm2)
E3	700ºC	0,2	0,4	527400	0,51	0,6	0,94	0	1,89
		0,45	0,4	527400	0,5	0,7	1	0	1,99
	800ºC	0,2	0,4	527400	1,12	1,8	0,55	0	2,05
		0,45	0,4	527400	1,06	1,6	0,75	0	2,35
	900ºC	0,2	0,4	527400	1,4	2,15	0,44	0	2,03
		0,45	0,4	527400	1,34	2,21	0,54	0	2,29
	950ºC	0,2	0,4	527400	1,33	2,2	0,4	0,1	2,03
		0,45	0,4	527400	1,48	2,37	0,5	0,1	2,32

		INPUT			OUTPUT(%)				O2 FLUX
	Temperature	Air flow	Toluene&Nitrogen	Toluene amount	H2	CO	CO2	CH4	
	(ºC)	(l/min)	(l/min)	(ppm)					(ml/min*cm2)
F16	700ºC	0,2	0,4	527400	0,16	0,1	1,06	0	1,82
		0,45	0,4	527400	0,3	0,2	1,02	0	2,03
	800ºC	0,2	0,4	527400	0,31	0,2	1,1	0	1,93
		0,45	0,4	527400	0,31	0,2	1,28	0	2,23
	900ºC	0,2	0,4	527400	1,04	0,98	0,93	0	2,08
		0,45	0,4	527400	1,22	0,99	1,01	0	2,36
	950ºC								
		0,45	0,4	527400	1,28	1,5	0,9	0	2,35

		INPUT			OUTPUT(%)				O2 FLUX
	Temperature	Air flow	Toluene&Nitrogen	Toluene amount	H2	CO	CO2	CH4	
	(ºC)	(l/min)	(l/min)	(ppm)					(ml/min*cm2)
G10	700ºC	0,2	0,4	527400	0,12	0,2	0,9	0	1,64
		0,45	0,4	527400	0,1	0,3	1	0	1,84
	800ºC	0,2	0,4	527400	0,17	0,3	0,95	0	1,72
		0,45	0,4	527400	0,19	0,3	1,09	0	1,96
	900ºC	0,2	0,4	527400	0,71	0,64	0,91	0,02	1,88
		0,45	0,4	527400	0,66	0,63	1,05	0,03	2,21
	950ºC	0,2	0,4	527400	0,67	0,51	0,9	0,1	1,8
		0,45	0,4	527400	0,5	0,37	1,1	0,1	2,15

		INPUT			OUTPUT(%)				O2 FLUX
	Temperat	Air flow	Toluene&Nitrogen	Toluene Amount	H2	CO	CO2	CH4	
	ºC	(l/min)	(l/min)	(ppm)					(ml/min*cm2)
A3	700ºC	0,25	0,4	527400	0,03	0,2	0,92	0	1,8
		0,3	0,4	527400	0,1	0,2	1	0	1,67
		0,45	0,4	527400	0,1	0,2	1	0	1,75
B6	700 ºC	0,2	0,4	527400	0,08	0,3	0,89	0	1,59
		0,3	0,4	527400	0,1	0,3	0,9	0	1,79
		0,45	0,4	527400	0,1	0,3	0,99	0	1,77
B9	700ºC	0,2	0,4	527400	0,15	0,3	0,92	0	1,71
		0,3	0,4	527400	0,1	0,2	1	0	1,77
		0,45	0,4	527400	0,1	0,2	1,02	0	1,85
C7	700ºC	0,2	0,4	527400	0,07	0,02	1,02	0	1,67
		0,45	0,4	527400	0,1	0,01	1,2	0	2,08
D3	700ºC	0,2	0,4	527400	0,19	0,1	1,01	0	1,76
		0,45	0,4	527400	0,1	0,02	1,1	0	1,86
E3	700ºC	0,2	0,4	527400	0,51	0,6	0,94	0	1,89
		0,45	0,4	527400	0,5	0,7	1	0	1,99
F16	700ºC	0,2	0,4	527400	0,16	0,1	1,06	0	1,82
		0,45	0,4	527400	0,3	0,2	1,02	0	2,03
G10	700ºC	0,2	0,4	527400	0,12	0,2	0,9	0	1,64
		0,45	0,4	527400	0,1	0,3	1	0	1,84

			INPUT		OUTPUT(%)				O2 FLUX
	Temperature		Air flow	Toluene& Nitrogen	H2	CO	CO2	CH4	
	ºC		(l/min)	(l/min)					(ml/min*cm2)
A3	800	ºC	0,2	0,4	0,3	0,4	1	0	1,91
			0,25	0,4	0,3	0,4	1	0	2,1
			0,3	0,4	0,2	0,3	1,03	0	1,86
			0,4	0,4	0,3	0,4	1	0	1,98
			0,45	0,4	0,3	0,4	1	0	2
B6	800	ºC	0,3	0,4	0,4	0,6	1	0	1,85
			0,45	0,4	0,43	0,7	1,1	0	2,43
B9	800	ºC	0,2	0,4	0,28	0,4	0,92	0	1,78
			0,3	0,4	0,28	0,4	0,97	0	1,83
			0,45	0,4	0,28	0,4	1,03	0	1,92
C7	800	ºC	0,2	0,4	0,23	0,2	1,12	0	2,47
			0,45	0,4	0,22	0,2	1,2	0	2,09
D3	800	ºC	0,2	0,4	0,32	0,3	1,05	0	1,87
			0,45	0,4	0,35	0,3	1,17	0	2,06
E3	800	ºC	0,2	0,4	1,12	1,8	0,55	0	2,05
			0,45	0,4	1,06	1,6	0,75	0	2,35
F16	800	ºC	0,2	0,4	0,31	0,2	1,1	0	1,93
			0,45	0,4	0,31	0,2	1,28	0	2,23
G10	800	ºC	0,2	0,4	0,17	0,3	0,95	0	1,72
			0,45	103 0,4	0,19	0,3	1,09	0	1,96

		INPUT		OUTPUT(%)				O2 FLUX
	Temperat	Air flow	Toluene&Nitrogen	H2	CO	CO2	CH4	
	ºC	(l/min)	(l/min)					(ml/min*cm2)
A3	900ºC	0,4	0,4	0,6	0,7	1	0,01	2,39
		0,45	0,4	0,6	0,7	1,1	0,01	2,46
B6	900 ºC	0,2	0,4	0,77	0,6	0,93	0	2,01
		0,3	0,4	0,71	0,9	0,98	0,03	2,12
		0,45	0,4	0,68	0,9	1,1	0,02	2,22
B9	900ºC	0,2	0,4	0,34	0,58	0,91	0,01	1,83
		0,45	0,4	0,36	0,61	1,01	0,01	2,09
C7	900ºC	0,2	0,4	1,2	1,36	0,83	0,01	2,18
		0,45	0,4	1,22	1,45	0,94	0,02	2,45
D3	900ºC	0,2	0,4	0,97	1,06	0,87	0	2,09
		0,45	0,4	1	1,12	1,07	0,03	2,45
E3	900ºC	0,2	0,4	1,4	2,15	0,44	0	2,03
		0,45	0,4	1,34	2,21	0,54	0	2,29
F16	900ºC	0,2	0,4	1,04	0,98	0,93	0	2,08
		0,45	0,4	1,22	0,99	1,01	0	2,36
G10	900ºC	0,2	0,4	0,71	0,64	0,91	0,02	1,88
		0,45	0,4	0,66	0,63	1,05	0,03	2,21

		INPUT		OUTPUT(%)				O2 FLUX
	Temperature	Air flow(l/min)	Toluene/Nitrogen(l/min)	H2	CO	CO2	CH4	(ml/min*cm2)
A3	950ºC	0,25	0,4	0,3	0,4	1	0,08	2,07
		0,3	0,4	0,3	0,3	1,1	0,1	2,15
		0,4	0,4	0,4	0,4	1	0,1	1,92
		0,45	0,4	0,4	1,4	1,9	0,1	1,94
B6	950 ºC	0,4	0,4	0,83	1,06	0,9	0,1	2,1
		0,45	0,4	0,95	1,2	0,9	0,1	2,25
B9	950ºC	0,2	0,4	0,77	0,85	0,9	0,1	1,9
		0,45	0,4	1,73	1,59	0,9	0,1	2,44
C7	950ºC	0,2	0,4	1,03	1,46	0,8	0,1	2,12
		0,45	0,4	1,36	1,71	0,9	0,1	2,46
D3	950ºC							
		0,45	0,4	0,09	1,21	0,9	0,1	2,34
E3	950ºC	0,2	0,4	1,33	2,2	0,4	0,1	2,03
		0,45	0,4	1,48	2,37	0,5	0,1	2,32
F16	950ºC							
		0,45	0,4	1,28	1,5	0,9	0	2,35
G10	950ºC	0,2	0,4	0,67	0,51	0,9	0,1	1,8
		0,45	0,4	0,5	0,37	1,1	0,1	2,15

		INPUT			OUTPUT(%)				O2 FLUX
	Temperature	Air flow	Toluene&Nitrogen	Toluene amount	H2	CO	CO2	CH4	
		(l/min)	(l/min)	(ppm)					(ml/min*cm2)
H13	700ºC	0,2	2	2643	0,01	0	0,06	0	0,6
		0,45	2	2643	0,01	0	0,06	0	0,6
	800ºC	0,2	2	2643	0	0	0,06	0	0,58
		0,45	2	2643	0	0	0,08	0	0,8
	900ºC	0,2	2	2643	0,05	0	0,08	0	0,8
		0,45	2	2643	0,04	0	0,1	0	1,01
	950ºC	0,2	2	2643	0,06	0	0,08	0	0,86
		0,45	2	2643	0,04	0	0,1	0	1
H13	700ºC	0,45	1	3174	0,02	0,02	0,14	0	0,76
	900ºC	0,45	1	3174	0,09	0	0,21	0	1,16
H13	700ºC	0,45	0,5	2957	0,04	0,02	0,48	0	1,51
	900ºC	0,45	0,5	2957	0,34	0,3	0,47	0	1,8
	800ºC	0,45	0,5	2957	0,07	0,01	0,39	0	1,22
H13	700ºC	0,45	0,5	10560	0,06	0,1	0,44	0	1,49
	900ºC	0,45	0,5	10560	0,37	0,3	0,48	0	1,78
	800ºC	0,45	0,5	10560	0,16	0,2	0,45	0	1,61
H13	700ºC	0,45	1	10580	0,03	0	0,12	0	0,66
	900ºC	0,45	1	10580	0,12	0,03	0,15	0	0,89
	800ºC	0,45	1	10580	0,04	0	0,12	0	0,64

		INPUT					OUTPUT(%)			
	Temperat	Air flow	Toluene&Nitroger	Toluene amount			H2	CO	CO2	CH4
		(l/min)	(l/min)	(ppm)						
H14					H2O+++					
52min	700ºC	0,45	0,5	2526	12,43 %		0,1	0,02	0,42	0
50min	900ºC	0,45	0,5	2526	12,43 %		1,53	0,7	0,62	0
50min	800ºC	0,45	0,5	2526	12,43 %		1,04	0,5	0,48	0
H14 (longer run)					H2O+++					
2h10	700ºC	0,45	0,5	2526	12,43 %		0,94	0,3	0,53	0
2h20	900ºC	0,45	0,5	2526	12,43 %		2,51	0,9	0,83	0
1h10	800ºC	0,45	0,5	2526	12,43 %		1,36	0,7	0,54	0
44min	700ºC	0,45	0,5	2526	12,43 %		0,24	0,1	0,39	0
H14					H2O+++		H2	CO	CO2	CH4
	700ºC	0,45	0,5	9289	12,43 %		0,46	0,2	0,4	0
	900ºC	0,45	0,5	9289	12,43 %		8,03	4,2	0,89	0
	800ºC	0,45	0,5	9289	12,43 %		2,89	1,4	0,49	0
	700ºC	0,45	0,5	9289	12,43 %		0,6	0,3	0,36	0

H15	TCD (%)								FID-GC (ppm)			
	H2	N2	CH4	CO	CO2	C2H4	C2H6		C7H8	C6H6	CH4	C2H4
700 GASIFICATION GAS 23.3.2015 21_45_213.	17,54	49,97	5,67	11,68	13,16	3,64	0,01		2441,29	16,35733	5,13E+04	8328,81525
700 GASIFICATION GAS 23.3.2015 22_06_213.	17,56	50,06	5,65	11,67	13,31	3,55	0,01		2295,934	16,41607	5,19E+04	8557,30281
700 GASIFICATION GAS 23.3.2015 22_27_213.	17,56	50,03	5,65	11,67	13,32	3,56	0,01		2415,11	17,07751	5,07E+04	8660,58499
700 GASIFICATION GAS 23.3.2015 22_48_213.	17,55	49,95	5,67	11,68	13,35	3,78	0,01		2524,701	17,95096	5,14E+04	8378,19122
700 GASIFICATION GAS 23.3.2015 23_09_213.	17,55	50,11	5,64	11,65	13,32	3,61	0,01		2487,38	18,13455	5,19E+04	8550,81908
700 GASIFICATION GAS 23.3.2015 23_29_213.	17,49	50,09	5,64	11,65	13,19	3,63	0,02		2454,157	17,52435	5,14E+04	8392,79337
700 GASIFICATION GAS 23.3.2015 23_50_213.	17,52	50,08	5,64	11,65	13,08	3,61	0,02		2484,065	17,81147	5,21E+04	8647,95291
700 GASIFICATION GAS 24.3.2015 0_11_213.	17,55	50,07	5,64	11,64	12,99	3,62	0,02		2485,109	16,84035	5,11E+04	8393,40609
700 GASIFICATION GAS 24.3.2015 0_32_213.	17,6	50,18	5,64	11,64	13,38	3,3	0,02		2458,495	16,40502	5,17E+04	8548,6086
700 GASIFICATION GAS 24.3.2015 0_53_213.	17,6	49,92	5,66	11,67	13,35	3,67	0,02		2605,271	16,31275	5,04E+04	8990,26558
700 GASIFICATION GAS 24.3.2015 1_14_213.	17,56	49,87	5,66	11,67	13,16	3,7	0,02		2606,726	15,94444	5,14E+04	8434,48051
700 GASIFICATION GAS 24.3.2015 1_35_213.	17,54	49,94	5,65	11,69	13,18	3,68	0,02		2550,008	15,37362	5,18E+04	8671,46255
700 GASIFICATION GAS 24.3.2015 1_55_213.	17,54	49,8	5,65	11,66	13,07	3,74	0,02		2409,46	13,67848	5,13E+04	8370,87847
700 GASIFICATION GAS 24.3.2015 2_16_213.	17,49	49,85	5,64	11,65	13,3	3,67	0,02		2563,01	14,21841	5,21E+04	8736,69626
700 GASIFICATION GAS 24.3.2015 2_37_213.	17,5	49,87	5,63	11,65	13,09	3,64	0,02		2546,268	13,29926	5,13E+04	8513,88225
700 GASIFICATION GAS 24.3.2015 2_58_213.	17,48	49,81	5,62	11,61	13,09	3,62	0,02		2503,72	12,69695	5,16E+04	8580,32784
700 GASIFICATION GAS 24.3.2015 3_19_213.	17,47	49,8	5,62	11,6	13,2	3,63	0,02		2529,771	12,54239	5,13E+04	8521,34875
700 GASIFICATION GAS 24.3.2015 3_40_213.	17,46	49,65	5,63	11,61	13,24	3,7	0,02		2528,516	12,0471	5,10E+04	8940,9891
700 GASIFICATION GAS 24.3.2015 4_01_213.	17,45	49,69	5,62	11,59	13,3	3,64	0,02		2654,263	12,75178	5,21E+04	9139,5903
700 GASIFICATION GAS 24.3.2015 4_21_213.	17,43		5,59	11,53	13,13	3,49	0,02		2503,589	11,87138	5,14E+04	8508,48681
700 GASIFICATION GAS 24.3.2015 4_42_213.	17,42	49,64	5,61	11,56	13,2	3,62	0,02		2463,157	12,09907	5,22E+04	8809,88936
700 GASIFICATION GAS 24.3.2015 5_03_213.	17,38	49,65	5,62	11,59	13,3	3,63	0,02		2514,237	11,8529	5,18E+04	9011,34844
700 GASIFICATION GAS 24.3.2015 5_24_213.	17,37	49,6	5,61	11,56	13,15	3,66	0,02		2465,04	11,88997	5,18E+04	8634,1602
700 GASIFICATION GAS 24.3.2015 5_45_213.	17,39	49,56	5,59	11,55	13,17	3,62	0,02		2509,727	12,21505	5,17E+04	8641,09235
700 GASIFICATION GAS 24.3.2015 6_06_213.	23,54	43,07	4,18	18,58	9,15	0,92	0,05		2215,383	48,03386	5,11E+04	7614,05486

			TCD (%)								FID-GC(ppm)				
H15			H2	N2	CH4	CO	CO2	C2H4	C2H6		C7H8	C6H6	CH4	C2H6+C2H2	C2H4
900 GASIFICATION GAS 24.3.2015 6_27_213.			22,52	44,1	4,81	16,95	10,14	1,18	0,06		593,373	230,5422	4,80E+04	527,06869	3592,887
900 GASIFICATION GAS 24.3.2015 6_48_213.			22,58	44	4,76	17,18	9,93	1,22	0,06		531,0081	174,1662	4,64E+04	458,14424	2949,92
900 GASIFICATION GAS 24.3.2015 7_07_213.			22,28	44,25	4,79	17,11	9,87	1,29	0,06		628,2108	183,9234	4,73E+04	485,97131	3330,764
900 GASIFICATION GAS 24.3.2015 7_29_213.			22,57	44	4,8	17,02	10,05	1,18	0,05		524,8955	140,0626	4,42E+04	408,43141	2440,197
900 GASIFICATION GAS 24.3.2015 7_50_213.			22,53	44,05	4,78	17,07	9,95	1,21	0,06		628,2108	183,9234	4,73E+04	485,97131	3330,764
900 GASIFICATION GAS 24.3.2015 8_11_213.			23,18	43,25	4,49	18,39	9,11	0,87	0,05		524,8955	140,0626	4,42E+04	408,43141	2440,197
900 GASIFICATION GAS 24.3.2015 8_32_213.			23,32	43,2	4,47	18,16	9,29	0,84	0,05		609,5988	148,0578	4,64E+04	445,10923	2853,747
900 GASIFICATION GAS 24.3.2015 8_53_213.			23,63	42,51	4,24	19,88	8,04	0,65	0,04		669,0636	154,7233	4,53E+04	441,1185	2778,367
900 GASIFICATION GAS 24.3.2015 9_14_213.			22,63	43,83	4,74	17,07	9,9	1,14	0,06		614,4168	140,0213	4,58E+04	433,828	2645,083
900 GASIFICATION GAS 24.3.2015 9_35_213.			23,2	43,29	4,57	17,96	9,32	0,8	0,05		602,7112	140,5832	4,55E+04	449,13465	2593,256
900 GASIFICATION GAS 24.3.2015 9_56_213.			23,28	43,14	4,48	18,1	9,29	0,75	0,05		548,7486	133,0222	4,57E+04	439,30358	2461,621
900 GASIFICATION GAS 24.3.2015 16_15_213.			16,64	43,13	5,05	10,44	10,6	3,05			606,1125	151,525	4,67E+04	474,97126	2810,316
900 GASIFICATION GAS 24.3.2015 16_36_213.			15,07	38,49	4,5	9,32	10,87	3,15			541,3046	140,6531	4,62E+04	457,70802	2549,292
900 GASIFICATION GAS 24.3.2015 16_57_213.			16,19	41,94	4,94	10,12	12,23	3,59			15,69934	3,7618	1,23E+04	15,48325	51,54988

H16			TCD (%)						GC(ppm)				
	,		H2	N2	CH4	CO	CO2	O2	C7H8	C6H6	CH4	C2H6+C2H2	C2H4
700C STEAM LONG RUN H1625.3.2015 18_33_31			0,14	95,54	0,09	0	0,37	0	1,03E+04	238,8612	122,95298	8,10644	
700C STEAM LONG RUN H1625.3.2015 18_54_31			0,15	94,4	0	0,11	0,47	0,07	9810,99414	178,77149	107,66492	7,30225	
700C STEAM LONG RUN H1625.3.2015 19_15_31			0,13	94,05	0	0,11	0,42	0	1,03E+04	152,57474	106,23995	21,18344	
700C STEAM LONG RUN H1625.3.2015 19_36_31			0,13	94,12	0	0,11	0,44	0	1,02E+04	149,67634	103,18783	19,32018	
700C STEAM LONG RUN H1625.3.2015 19_56_31			0,14	94,14	0	0,11	0,43	0	1,03E+04	148,65995	96,34225	6,1952	4,32863
700C STEAM LONG RUN H1625.3.2015 20_17_31			0,14	95,36	0	0,11	0,46	0	1,04E+04	147,67396	94,30244		6,08247
700C STEAM LONG RUN H1625.3.2015 20_38_31			0,15	95,64	0	0,11	0,44	0	1,03E+04	151,07281	89,49869		4,53478
700C STEAM LONG RUN H1625.3.2015 20_59_31			0,15	95,65	0	0,12	0,44	0	9875,4092	149,60228	84,34243		4,43982
700C STEAM LONG RUN H1625.3.2015 21_20_31			0,15	95,67	0	0,11	0,45	0	1,04E+04	152,91179	81,66872		5,07471
700C STEAM LONG RUN H1625.3.2015 21_41_31			0,15	95,63	0	0,11	0,44	0	1,04E+04	147,54055	75,56341		4,46425
700C STEAM LONG RUN H1625.3.2015 22_02_31			0,15	95,7	0	0,11	0,44	0	1,05E+04	150,03258	73,20087		6,13377
700C STEAM LONG RUN H1625.3.2015 22_22_31			0,15	95,7	0	0,11	0,45	0	1,04E+04	150,36532	67,90067		4,19119
700C STEAM LONG RUN H1625.3.2015 22_43_31			0,16	95,69	0	0,11	0,45	0	1,04E+04	147,9572	62,83325		4,31851
700C STEAM LONG RUN H1625.3.2015 23_04_31			0,16	95,66	0	0,11	0,45	0	1,03E+04	155,93581	61,10353		6,16327
700C STEAM LONG RUN H1625.3.2015 23_25_31			0,16	95,64	0	0,11	0,45	0	1,04E+04	150,20232	56,31468		6,12056
700C STEAM LONG RUN H1625.3.2015 23_46_31			0,16	95,68	0	0,11	0,44	0	1,04E+04	154,4718	50,54853		4,01672
700C STEAM LONG RUN H162´6.3.2015 00_07_31			0,16	95,71	0	0,11	0,44	0	1,04E+04	151,18203	46,28873		3,94631
700C STEAM LONG RUN H1626.3.2015 00_28_31			0,16	95,63	0	0,11	0,46	0,01	1,04E+04	153,83936	42,60729		3,92027
700C STEAM LONG RUN H1626.3.2015 00_49_31			0,16	95,65	0	0,11	0,45	0,01	1,04E+04	153,13587	38,64758		4,03051
700C STEAM LONG RUN H1626.3.2015 01_10_31			0,16	95,6	0	0,11	0,45	0,01	1,05E+04	152,55735	35,20976		4,12166
700C STEAM LONG RUN H1626.3.2015 01_30_31			0,16	95,62	0	0,11	0,45	0,01	1,03E+04	154,95792	30,87251		3,67197
700C STEAM LONG RUN H1626.3.2015 01_51_31			0,16	95,63	0	0,11	0,44	0,01	1,04E+04	150,05892	28,04876		3,92681
700C STEAM LONG RUN H1626.3.2015 02_12_31			0,16	95,66	0	0,1	0,44	0,01	1,04E+04	154,9202			3,77555
700C STEAM LONG RUN H1626.3.2015 02_33_31			0,16	95,62	0	0,11	0,44	0,01	1,04E+04	150,65137	22,93247		4,1497
700C STEAM LONG RUN H1626.3.2015 02_54_31			0,16	95,64	0	0,11	0,42	0,01	1,04E+04	158,04598			3,6368
700C STEAM LONG RUN H1626.3.2015 03_15_31			0,16	95,6	0	0,11	0,45	0,01	1,04E+04	154,65758			3,74369
700C STEAM LONG RUN H1626.3.2015 03_35_31			0,16	95,57	0	0,1	0,43		1,04E+04	153,1591			3,4565
700C STEAM LONG RUN H1626.3.2015 03_56_31			0,16	95,6	0	0,11	0,44	0,01	1,04E+04	156,22297			3,37825
700C STEAM LONG RUN H1626.3.2015 04_17_31			0,16	95,6	0	0,11	0,44	0,01	1,05E+04	154,52254			2,92849

H16			TCD (%)						GC(ppm)				
	,		H2	N2	CH4	CO	CO2	O2	C7H8	C6H6	CH4	C2H6+C2H2	C2H4
900C STEAM LONG RUN H1626.3.2015 04_59_31			3,28	91,48	0,02	1,36	0,88		6652,18676	936,41903	540,16605		6,66775
900C STEAM LONG RUN H1626.3.2015 05_20_31			3,12	91,63	0,02	1,24	0,89	0,01	6836,57284	757,1701	377,27838		6,44341
900C STEAM LONG RUN H1626.3.2015 05_40_31			3,11	91,65	0,02	1,21	0,87	0,01	6649,34976	734,74136	367,38144		6,12005
900C STEAM LONG RUN H1626.3.2015 06_01_31			3,24	91,42	0,01	1,32	0,87	0,01	6806,94312	730,24496	358,95254		6,20176
900C STEAM LONG RUN H1626.3.2015 06_22_31			3,14	91,55	0,02	1,29	0,86	0,01	6898,8311	729,24393	362,36433		6,70948
900C STEAM LONG RUN H1626.3.2015 06_43_31			3,26	91,39	0,01	1,34	0,85	0,01	6759,04531	722,38725	366,42682		6,08697
900C STEAM LONG RUN H1626.3.2015 07_04_31			3,32	91,25	0,01	1,43	0,83	0,01	5634,00447	613,43549	326,00178		5,05357
900C STEAM LONG RUN H1626.3.2015 07_25_31			3,6	90,78	0,01	1,62	0,84	0,01	6627,78416	699,84245	351,15103		6,21025
900C STEAM LONG RUN H1626.3.2015 07_46_31			3,49	90,93	0,01	1,57	0,83	0,01	6634,97614	711,81135	356,56312		6,22552
900C STEAM LONG RUN H1626.3.2015 08_06_31			3,73	90,54	0,01	1,72	0,83	0,01	6268,96431	685,20606	353,43144		6,23253
900C STEAM LONG RUN H1626.3.2015 08_27_31			3,57	90,67	0,01	1,62	0,8	0,01	6626,10247	709,05248	358,7711		6,19165
900C STEAM LONG RUN H1626.3.2015 08_48_31			3,38	90,9	0,01	1,51	0,8	0,01	6596,77427	710,20897	361,08924		6,14654
900C STEAM LONG RUN H1626.3.2015 09_09_31			3,42	90,81	0,01	1,55	0,79	0,01	6583,27466	701,49519	354,53782		6,27573
900C STEAM LONG RUN H1626.3.2015 09_30_31			3,42	90,73	0,01	1,57	0,78	0,01	6382,25985	695,77562	355,82629		6,10787
900C STEAM LONG RUN H1626.3.2015 09_50_31			3,82	90,01	0,01	1,79	0,82	0,01	6428,83771	722,89688	379,58713		6,22469
900C STEAM LONG RUN H1626.3.2015 10_11_31			3,6	90,29	0,02	1,66	0,8	0,01	6442,4013	696,01022	350,99416		6,27258
900C STEAM LONG RUN H1626.3.2015 10_32_31			3,5	90,43	0,01	1,59	0,79	0,01	6389,21992	692,02022	354,77386		6,40982
900C STEAM LONG RUN H1626.3.2015 10_52_31			3,67	90,08	0,01	1,71	0,77	0,01	6436,14541	698,38941	351,68885		6,32038
900C STEAM LONG RUN H1626.3.2015 11_14_31			3,78	90,17	0,01	1,74	0,68	0,01	6306,35238	736,13434	383,11779		5,7617
900C STEAM LONG RUN H1626.3.2015 12_58_31			3,95	90,31	0,01	1,87	0,77	0	5934,22626	613,23204	336,9847		5,35386
900C STEAM LONG RUN H1626.3.2015 13_19_31			3,74	90,65	0,01	1,74	0,78	0	6163,88248	613,93831	319,60508		5,50013
900C STEAM LONG RUN H1626.3.2015 13_40_31			3,52	90,95	0,01	1,61	0,77	0	6385,18716	643,52103	338,3924		5,65314
900C STEAM LONG RUN H1626.3.2015 14_00_31			3,4	91,06	0,02	1,56	0,77	0	6547,97799	647,7436	333,05048		5,96055
900C STEAM LONG RUN H1626.3.2015 14_20_31			3,29	91,2	0,01	1,49	0,77	0	6634,75223	667,03416	340,94221		5,98262

H16			TCD (%)						GC(ppm)				
	,		H2	N2	CH4	CO	CO2	O2	C7H8	C6H6	CH4	C2H6+C2H2	C2H4
800C STEAM LONG RUN H1626.3.2015 15_03_31			1,02	94,31	0	0,46	0,51	0	9448,66933	225,13768	28,93241		3,49725
800C STEAM LONG RUN H1626.3.2015 15_24_31			0,92	94,52	0	0,4	0,52	0	9521,22141	244,95935	31,74849		3,29714
800C STEAM LONG RUN H1626.3.2015 15_45_31			0,87	94,56	0	0,37	0,53	0	9669,39636	254,60635	31,99916		3,61739
800C STEAM LONG RUN H1626.3.2015 16_05_31			0,86	94,64	0	0,35	0,53	0	9478,86071	261,04151	32,63739		3,30282
800C STEAM LONG RUN H1626.3.2015 16_26_31			0,85	94,62	0	0,35	0,53	0	9672,57629	266,14903	33,78196		12,65972
800C STEAM LONG RUN H1626.3.2015 16_47_31			0,86	94,65	0	0,34	0,53	0	9543,21932	260,24721	32,14883		3,55711
800C STEAM LONG RUN H1626.3.2015 17_08_31			0,84	94,67	0	0,33	0,53	0	9579,19007	268,68428	34,25201		3,70056
800C STEAM LONG RUN H1626.3.2015 17_29_31			0,83	94,65	0	0,34	0,54	0	9636,19158	271,74351	33,80273		3,5591
800C STEAM LONG RUN H1626.3.2015 17_50_31			0,82	94,66	0	0,33	0,53	0	9635,80491	272,86957	33,60349		3,28438
800C STEAM LONG RUN H1626.3.2015 18_10_31			0,81	94,58	0	0,32	0,53	0	9841,47341	280,80021	33,73053		3,6691
800C STEAM LONG RUN H1626.3.2015 18_31_31			0,8	94,52	0	0,32	0,53	0	9582,37752	273,13514	34,02464		3,30643
800C STEAM LONG RUN H1626.3.2015 18_52_31			0,8	94,53	0	0,31	0,52	0	9720,74363	274,68324	33,7396		3,46947
800C STEAM LONG RUN H1626.3.2015 19_13_31			0,79	94,55	0	0,31	0,53	0	9668,37277	272,85298	33,5924		3,51684
800C STEAM LONG RUN H1626.3.2015 19_34_31			0,78	94,52	0	0,31	0,52	0	9689,32262	270,55725	33,65696		3,51577
800C STEAM LONG RUN H1626.3.2015 19_55_31			0,79	94,62	0	0,3	0,52	0	9706,82912	276,73581	33,84176		3,36036
800C STEAM LONG RUN H1626.3.2015 20_15_31			0,79	94,62	0	0,31	0,53	0	9654,93148	271,68392	34,04508		3,35747
800C STEAM LONG RUN H1626.3.2015 20_36_31			0,79	94,66	0	0,31	0,52	0	9712,59626	275,222	33,63852		3,28017
800C STEAM LONG RUN H1626.3.2015 20_57_31			0,78	94,6	0	0,31	0,54	0	9680,49128	274,81683	34,18039		3,28153
800C STEAM LONG RUN H1626.3.2015 21_18_31			0,78	94,63	0	0,31	0,54	0	9645,38513	270,277	33,87048		3,27666
800C STEAM LONG RUN H1626.3.2015 21_39_31			0,78	94,59	0	0,31	0,54	0	9765,19857	275,22982	34,25069		3,28925
800C STEAM LONG RUN H1626.3.2015 22_00_00			0,78	94,62	0	0,31	0,54	0	9695,01355	267,56999	32,54595		3,13991
800C STEAM LONG RUN H1626.3.2015 22_21_00			0,78	94,64	0	0,3	0,54	0	9774,24065	277,59618	33,98238		3,27043
800C STEAM LONG RUN H1626.3.2015 22_41_00			0,77	94,59	0	0,3	0,53	0	9671,50753	269,60967	33,0799		3,36941
800C STEAM LONG RUN H1626.3.2015 23_02_00			0,78	94,6	0	0,31	0,52	0	9872,8869	275,01694	33,43219		3,38579
800C STEAM LONG RUN H1626.3.2015 23_23_00			0,78	94,57	0	0,3	0,53	0	9597,00516	269,20239	33,52454		3,20375
800C STEAM LONG RUN H1626.3.2015 23_44_00			0,78	94,65	0	0,3	0,53	0	9832,77943	275,19763	34,37462		3,25814
800C STEAM LONG RUN H1627.3.2015 0_05_00			0,78	94,57	0	0,3	0,53	0	9674,19635	274,2351	34,14054		3,00594
800C STEAM LONG RUN H1627.3.2015 0_26_00			0,77	94,6	0	0,3	0,52	0	9726,4101	269,97174	32,98113		3,05161

H16			TCD (%)						GC(ppm)				
	,		H2	N2	CH4	CO	CO2	O2	C7H8	C6H6	CH4	C2H6+C2H2	C2H4
800C STEAM LONG RUN H1627.3.2015 0_43_00			0,28	95,1	0	0,13	0,43	0	9723,59522	274,91582	32,79486		3,08077
800C STEAM LONG RUN H1627.3.2015 1_07_00			0,3	95,26	0	0,14	0,41	0	1,04E+04	96,75843			1,33971
800C STEAM LONG RUN H1627.3.2015 1_28_00			0,28	94,98	0	0,15	0,43	0	1,05E+04	104,17273			1,25868
700C STEAM LONG RUN H1627.3.2015 1_49_00			0,28	94,88		0,14	0,42	0	1,03E+04	113,07134		4,0561	1,26756
700C STEAM LONG RUN H1627.3.2015 2_10_00			0,27	94,75		0,13	0,43	0	1,03E+04	119,45011		4,53164	1,18131
700C STEAM LONG RUN H1627.3.2015 2_31_00			0,27	94,79		0,14	0,42	0	1,03E+04	123,55884		5,16944	1,2425
700C STEAM LONG RUN H1627.3.2015 2_52_00			0,26	94,69		0,14	0,42	0	1,04E+04	126,05598		4,95647	1,15378
700C STEAM LONG RUN H1627.3.2015 3_13_00			0,26	94,62		0,13	0,42	0	1,03E+04	129,627		5,61145	1,12129
700C STEAM LONG RUN H1627.3.2015 3_33_00			0,26	94,59		0,12	0,42	0	1,03E+04	128,74801		5,64999	1,19569
700C STEAM LONG RUN H1627.3.2015 3_54_00			0,26	94,57		0,13	0,42	0	1,04E+04	135,07179		6,10109	1,22695
700C STEAM LONG RUN H1627.3.2015 4_15_00			0,26	94,47		0,13	0,42	0	1,03E+04	134,19615		6,04126	1,07969
700C STEAM LONG RUN H1627.3.2015 4_36_00			0,25	94,43		0,13	0,42	0	1,03E+04	135,44641		6,81751	1,11506
700C STEAM LONG RUN H1627.3.2015 4_57_00			0,25	94,47		0,13	0,41	0	1,05E+04	139,08218		6,42891	1,3131
700C STEAM LONG RUN H1627.3.2015 5_18_00			0,25	94,33		0,13	0,42	0	1,05E+04	137,57444		6,79519	1,07032
700C STEAM LONG RUN H1627.3.2015 5_38_00			0,25	94,3		0,13	0,42	0	1,05E+04	141,34904		6,722	1,03487
700C STEAM LONG RUN H1627.3.2015 5_59_00			0,25	94,26		0,13	0,42	0	1,04E+04	138,30209		6,50344	1,1158
700C STEAM LONG RUN H1627.3.2015 6_20_00			0,25	94,36		0,13	0,41	0	1,04E+04	143,51055		6,70E+00	1,22105
700C STEAM LONG RUN H1627.3.2015 6_41_00			0,25	94,35		0,13	0,42	0	1,04E+04	141,51707		7,61792	9,49E-01
700C STEAM LONG RUN H1627.3.2015 7_02_00			0,24	94,27		0,13	0,41	0	1,01E+04	138,82343		6,9096	1,02394
700C STEAM LONG RUN H1627.3.2015 7_23_00			0,25	94,27		0,12	0,42	0	1,05E+04	1,43E+02		7,1997	9,23E-01
700C STEAM LONG RUN H1627.3.2015 7_43_00			0,25	94,29		0,13	0,42	0	1,04E+04	143,14894		6,77483	9,08E-01
700C STEAM LONG RUN H1627.3.2015 8_04_00			0,24	94,21		0,13	0,42	0	1,03E+04	146,85893		7,20582	1,02936
700C STEAM LONG RUN H1627.3.2015 8_25_00			0,25	94,21		0,13	0,42	0,01	1,03E+04	144,27709		6,98954	1,05854
700C STEAM LONG RUN H1627.3.2015 8_46_00			0,24	94,15		0,12	0,41	0	1,04E+04	148,90937		7,09983	1,00983
700C STEAM LONG RUN H1627.3.2015 9_07_00			0,24	94,13		0,12	0,41	0	1,05E+04	145,79662		7,87408	9,87E-01
700C STEAM LONG RUN H1627.3.2015 9_28_00			0,24	94,09		0,12	0,42	0,01	1,04E+04	149,79769		7,21324	9,92E-01
700C STEAM LONG RUN H1627.3.2015 9_47_00			0,24	94,07		0,13	0,42	0,01	1,04E+04	148,41774		7,45296	1,04303
700C STEAM LONG RUN H1627.3.2015 10_09_00			0,24	94,06		0,12	0,42	0,01	1,03E+04	146,18757		7,66262	1,0894

Appendix C. Single phase materials with the $ABO_{3-\delta}$ perovkite-type

Perovskite type: Sr (Co, Fe)$O_{3-\delta}$ (SCFO)

$SrCoO_{3-\delta}$: $SrCoO_3$ or $SrFeO_3$ exhibits both good ionic and electronic conductivity for high oxygen flux, therefore it has been studied intensively. The oxygen permeability can be improved by either doping metal ions on the A-site or partially substituting transition metals to the B-site (Co), which has great influence on the thermal/chemical stability. [68]

$Sr_{0.7}Ln_{0.3}CoO_{3-\delta}$: Partial doping of metals on the A-site has stronger influence on the oxygen flux value than doping on the B-site. The oxygen vacancies in the lattice can be achieved by partial substitution of Ln metal ion by Sr^{2+} in the A-site, whereas the higher oxygen permeability flux due to the larger ionic radius doped metal on the A-site [11] &[30]. The oxygen fluxes of $Sr_{0.7}Ln_{0.3}CoO_{3-\delta}$ (Ln=La, Nd, Sm, Gd) increases as follows: La> Nd> Sm> Gd. [68]

$SrCoBO_{3-\delta}$ (B=Zn, Cu, Ni, Cr, Zr, Fe): The high thermal expansion coefficient of cobalt results in the low thermal stability. Therefore, doping higher activation energy transition metals to the B-site with cobalt result in the stable perovskite structure. It was found that Sr-Co-Zr, Sr-Co-Cr and Sr-Co-Cu have higher oxygen capacity; moreover the oxygen capacity of Sr-Co-Zr is almost twice as much as that of Sr-Co-Ni and Sr-Co-Zn. The oxygen permeability decreases as follows: SCF< $SrCo_{0.9}Fe_{0.1}O_{3-\delta}$ <$SrCo_{0.9}Ti_{0.1}O_{3-\delta}$ <$SrCoO_{3-\delta}$< $SrCo_{0.9}Nb_{0.1}O_{3-\delta}$. [69]

$Sr_{1-x}Bi_xFeO_{3-\delta}$: Bi^{3+} is partially substituted by Sr^{2+} to increase oxygen vacancies, while the iron shows the electrical conductivity by the mixed valence state transferred from Fe^{4+} to Fe^{3+} to keep electrical neutrality. The oxygen permeation flux of SBF increases with the increasing of the content of bismuth (when $1-x\leq0.5$); if $1-x\geq0.5$, the oxygen flux decreases as the increasing with content of Bi. It is known that the oxygen flux depends on the surface exchange rate and the oxygen vacancies. When $1-x\leq0.5$, the oxygen flux,

which is controlled by the surface exchange rate. The increasing amount of Bi leads to increase the cavity size (rc) and lattice free volume (Fv) makes the surface exchange easy resulting in high oxygen permeability. While 1-x≥0.5, the influence of the oxygen flux is determined by the bulk diffusion of the concentration of oxygen vacancies and the increasing the content of Bi leads to decrease the oxygen vacancies. In addition, Bi-doped materials (Bi_2O_3) causes the phase inversion under high temperature due to the melting point (824°C), therefore it is suitable for middle temperature or lower temperature membrane materials. [70]

$SrCo_{0.8}Fe_{0.2}O_{3-\delta}$: This material exhibit highest oxygen flux value among $La_{0.6}Sr_{0.4}Co_{0.8}Fe_{0.2}O_{3-\delta}$ under an air/helium oxygen partial gradient at 900°C, however they have poor stability under the reducing atmosphere that restricts its applications. Under the reducing atmosphere, the transformation from Co^{3+} to Co^{2+} would result in thermal expansion of the lattice volume, which causes distortion or breaking of the membrane materials leading to poor thermal/chemical stability. For Co doped membranes, structural failure occurs easily under oxygen chemical potential gradient across the membranes because of their high thermal expansion coefficients and poor stability. The iron ions are used to restrain this transformation and the increasing amount of Fe will limit the formation of the concentration of oxygen vacancies, which will decrease the oxygen flux. Therefore, the oxygen permeability flux follows: $SrCo_{0.5}Fe_{0.5}O_{\delta} > SrCo_{0.5}Fe_{0.75}O_{\delta} > SrCo_{0.5}FeO_{\delta} > SrCo_{0.5}Fe_{1.25}O_{\delta}$. [71]

$SrFeCo_{0.5}O_{3-\delta}$: The possibility of producing hydrogen by partial oxidation of coke oven gas (COG) with mixed conductor SFCO oxygen permeable membrane was studied and the experiment result showed that SCFO it could be stable when operated in the pure methane but would be damaged in H_2-rich COG. The metal Fe phase and little of $Sr_3Fe_3O_{10-x}$ phase appeared on the reforming side and the metal-Co, Fe and $Sr_4Fe_3O_{3-x}$ phases appeared on the atmosphere side. Finally, the results showed that the SCFO

material was easily damaged in H_2-rich COG and it was not stable for COG-reforming reactor. [72]

$Sr(Co,M)O_{3-\delta}$ (M=Ti or Cr): Doping higher valence transition metal cations (Cr or Ti) on B-site with cobalt will increase the phase stability, while decreasing the oxygen flux by the lowering the electronic conductivity. The stability follows the order: Ni, Cu, Zn, In, Ce < Cr, Al, Ga, Zr, Sn, V < La < Fe <Ti < Nb. [73]& [74]

$SrFe_{0.6}Cu_{0.3}Ti_{0.3}O_{3-\delta}$: SFCT membrane was synthesized for partial oxidation of methane to syngas and the resulted that show the crystallinity of both side of SFCT membrane declined significantly after catalytic reaction. The decomposition of the perovskite structure and the formation of $SrCoO_3$ and other phases were found in the reaction-side surface of the membrane, along with the emergence of loose porous morphology. [75] & [76]

$Sr(Co_{0.8}Fe_{0.2})_{1-x}$ $M_xO_{3-\delta}$ (M=Mg^{2+}, Ca^{2+}, Sr^{2+}, Ba^{2+}, Ti^{4+}, and Zr^{4+}): The alkaline earth ions (Mg^{2+}, Ca^{2+}, Sr^{2+} and Ba^{2+}) doped on B-cations, while Zr^{4+} and Ti^{4+} partially substitute the B-cations resulting in the formation of $SrTiO_3$ and $SrZrO_3$ phases, respectively. SCF doped with Zr and Ti has higher phase stability than undoped SCF, because Zr^{4+} (Ti^{4+}) can restrain the inclined transformation from Co^{3+} to Co^{2+} at high temperature in reducing environment or CO_2 atmosphere resulting in high thermal/chemical stability. Higher radius of doping ions in alkaline earth metal group result in more phase stability, whereas SCF-Ba performs the highest phase stability due to the highest radius size among the alkaline earth metal group. Doped SCF membrane has lower oxygen flux value than the undoped SCF membrane due to the transition metals of Ti and Zr decreases the oxygen vacancies in the lattice. Therefore, doping alkaline metals and transition metals on B-site will increase the phase stability but decrease the oxygen permeability. It was found that oxygen per-selectivity of $Sr(Co_{0.4}Fe_{0.6-x}Zr_{x)}O_{3-\delta}$ decrease as Zr and Co content increase, and thermal/chemical stability increase as Zr decrease. [71]

$Ba_xSr_{1-x}Co_yFe_{1-y}O_{3-\delta}$: The introduction of bigger ionic radius size Ba^{2+} to A-site will lower the activation energy bond between Ba-O, increase the lattice free volume (Fv) and enhance the phase stability with being t nearly to 1. The electronic neutrality is compensated by multivalent changes of Co and Fe metal ions, with the actual amount of Fe^{4+} ion decreasing, while that of Fe^{3+} ions increases with the rise of Co content. The doped Fe ions restrain the transformation of Co^{3+} to Co^{2+} reducing oxygen vacancy concentration, while increasing the phase stability by increasing the bond energy. Therefore, doped Ba will increase the oxygen permeation flux and doped Fe will increase the thermal/chemical stability due to Fe ion having a stable state under reducing environment. [77]

$Ba_{0.5}Sr_{0.5}Co_{0.8}Fe_{0.2}O_{3-\delta}$: This material exhibits good oxygen permeability and higher thermal/chemical stability than $La_{0.2}Sr_{0.8}Co_{0.2}Fe_{0.8}O_{3-\delta}$ and $SrCo_{0.8}Fe_{0.2}O_{3-\delta}$ especially in the reducing environment. Partial doping Sr to Ba in A- side, which was a greater ionic radius resulting in the rise of oxygen vacancies, providing the high oxygen permeability. Although the alkaline earth metals will have phase conversion caused by reaction with CO_2 in the formation of $BaCO_3$ and $SrCO_3$ and with H_2 in the form of BaO, FeO, SrO and $BaFeO_3$ in reducing environment, the BSCF is oxidized again to keep the structure stable. The rank of oxygen flux follows the order: BCF>BSCF>SCF>SCCF>MCF. Therefore, according to A-site doping, bigger ionic radius and smaller ionic potential of alkaline earth metal like Ba should be taken into account. [78]

$BaCe_{0.1}Co_{0.4}Fe_{0.5}O_{3-\delta}$: Ba-Ce-O based perovskite oxide is usually employed for hydrogen permeable membrane in POM, because it has high resistance for the reducing environment. They exhibit good phase stability and high oxygen permeability due to the doped large radius of cerium ions and changeable valence from Ce^{4+} to Ce^{3+}. They achieves high conversion of CH_4 and selectivity of CO and still survives in the long-term operation above 1000h good performance. [74]

$BaBi_{0.2}Co_yFe_{0.8-y}O_{3-\delta}$ ($y \leq 0.4$), $BaBi_xCo_{0.2}Fe_{0.8-x}O_{3-\delta}$($x=0.1-0.5$): Bi_2O_3 is a typical type of fluorite compound, which has very high oxygen ionic conductivity. Doping Bi to the B-site in the perovskite type exhibits considerable high oxygen permeability at high temperature due to Bi-O having low average bond energy (ABE) value. The oxygen flux value of $BaBi_{0.2}Co_{0.35}Fe_{0.45}O_{3-\delta}$ could reach $0.77*10^{-6}$ mol s^{-1} cm^{-2} under an air/helium oxygen partial gradient at 900°C, which is much greater than with other doped Bi conducting membranes. The oxygen permeability increases with the content of Co and no simply related to Bi content was observed. [79]

$BaTi_{0.2}Co_xFe_{0.8-x}O_{3-\delta}$: Doping titanium to B-site could improve the phase stability at the same time has less influence on the oxygen permeability due to the higher stabilized energy of Ti results in high activation energy between Ti-O bonds. In B-site of BTCF, the presence of Co^{3+} ions with smaller ion radii could compensate the electronic of Ti^{4+}, the electronic conduction proceeds via B-O-B bonds. The oxygen permeability flux of 0.9 ml $cm^{-2}min^{-1}$ at 950 °C under air/He in steady state was achieved. With the BTCF membranes performs high phase stability and oxygen permeability. [80]

Usually, the perovskite-type membranes containing alkaline earth metals have good oxygen permeability; however, they could react with CO_2, SO_2 or water vapor. Moreover, cobalt containing oxides have poor stability under the reducing atmosphere and high coefficient of thermal expansion limiting their application in reality. For practical industries, a dense ceramic membrane reactor has to show considerably high oxygen permeability under operation conditions and high stability under the harsh atmosphere, especially in CO_2-containing atmosphere or the reducing atmosphere.

Perovskite type: La (Co, Fe)$O_{3-\delta}$ (LCFO)

$La_{1-x}Sr_xCo_{1-y}Fe_yO_{3-\delta}$ was another type of perovskite material with high ionic conductivity and electric conductivity (1000 $S.cm^{-1}$), which was first investigated to overcome the poor stability of Sr (Co, Fe)$O_{3-\delta}$. The results shows the oxygen flux value was lower than with SCFO due to the low surface exchange rate. The oxygen fluxes raised with the increased content of Co. At the same time, charge neutrality was achieved by the valence state transformation of Co (Co-O-Co) and Fe on B-cations. The oxygen vacancies concentration in the lattice could be riased by partial substitute Ba, Sr, Ca to A-site of La to increase the oxygen permeation flux, while high electronic conductivity was enhanced by doping with low valence state cations such as Ga, Cr, Fe, Pb, or Ni for partial substitute of Co. [30]

$LaBO_3$ (B=V, Cr,Mn, Fe, Co, Ni): The stability of peroskite material follows of the doped metal oxides stability. The higher stability of a doping metals resulting in the higher stability of the perovskite membrane due to the high metal-oxygen bond energy. In the reducing environment, the stability follows the sequence of: $LaCrO_3 > LaFeO_3 > LaMnO_3 > LaCoO_3 > LaNiO_3$. [71]

$La_{0.3}Sr_{0.7}CoO_{3-\delta}$ membrane oxygen permeability is predominantly controlled either by bulk diffusion (L>10Lc) or surface exchange (L<0.1Lc). When it is controlled by the bulk diffusion (0.057<Lc<0.215 cm), the thinner thickness (Lc=0.057cm) provides a larger oxygen flux and higher temperature results in the lower oxygen flux. While it is controlled by the surface exchange (68 µm<Lc<87 µm), the oxygen permeability increases with the thicker material and higher temperature results in large oxygen flux due to the increase of ionic conductivity [81]. $La_{0.6}Sr_{0.4}CoO_{3-\delta}$ membrane operating the temperature range (750-940°C), the oxygen flux increased sharply in the magnitude up to $3*10^7$ mol s^{-1} $cm^{-2}$and decreased after 400 h [82]. Similar value of oxygen flux of approximately $3\text{-}4*10^7$ mol s^{-1} cm^{-2} was reported by other authors [82] & [83].

$La_{1-x}Ce_xCoO_{3-\delta}$: La partially substituted with Ce will increase the oxygen vacancies and the amount of Ce determines the phase stability and morphology structure of the membrane. When x<0.3, the phase structure is stable under air/He oxygen partial gradient at 900°C, Increasing the Ce content will result in the formation of Co_3O_4 (x>0.5), along with the emergence of loose porous morphology (x>0.7). Therefore, to keep the tolerance factor close to 1, the suitable amount of Ce is about 0.3. [84]

(Ln, Sr)$CoO_{3-\delta}$: Doping lanthanide metals on the A-site will increase the oxygen flux and the order of flux follows the metal radius size: La>Pr>Nd>Sm>Gd. Doping with metal with the large radius will increase the tolerance factor (t), consequently resulting the better oxygen permeability flux value. However, the Co metal ion has a low average Co-O bonding energy and high thermal expansion coefficient resulting in high creep especially in the reducing environment. Therefore, it is necessary to partially substituted of B ions with Ga, Cr, Fe, Pb, Ni. [85]

La(Co,Cr)$O_{3-\delta}$: The oxygen flux, electrical conductivity and thermal expansion of $La(Co_{1-x}M_x)O_{3-\delta}$ (x=0.1-0.4) decreases with the increasing chromium concentration, due to the lower polarization site energy at Co site than the Cr. [86]

La(Co,Ni)$O_{3-\delta}$: Doping nickel into the cobalt on B-site will increase the electrical conductivity with the increase of the nickel content due to the increasing mobility of itinerant electrons. However, it will result in decline of the oxygen ionic conductivity. Therefore, increasing Ni and Cr will both increase phase stability by decreasing of thermal expansion coefficient. [86]

*(La,*A)$FeO_{3-\delta}$: Oxygen flux follows the sequence of: $La_{0.6}Ba_{0.4}FeO_{3-\delta}$ > $La_{0.6}Ca_{0.4}FeO_{3-\delta}$ > $La_{0.6}Sr_{0.4}FeO_{3-\delta}$. [87]

$La_{1-x}Sr_xFeO_{3-\delta}$(x=0.1-0.3): Lower valency cations (Sr^{2+}) can be introduced into the crystal lattices on A-site to increase the oxygen vacancies and the ionic conductivity, which lead to increase the oxygen permeability; while the iron shows the electrical

conductivity by mixed valence state transferred from Fe^{4+} to Fe^{3+} to keep the electrical neutrality and oxygen per-selectivity. The experiment performed under the air/He gradient at the temperature between 1123-1323K, resulted in which the oxygen permeation reaching 5.3-9.3*10^{-6} mol s^{-1} cm^{-2} with the thickness between 0.5mm and 2mm. [88]

$La_{1-x}Pb_xFeO_{3-\delta}$(x=0.1-0.3): Doping with Pb in order to partial substitution of lanthanide metals on the A-site will not only increase the electrical conductivity and oxygen permeability with increasing the content of Pb, but also increase the phase stability of the membrane. Compared with the pervoskite type of (La,Sr) $O_{3-\delta,}$ it has better performance for sulfur dioxide poisoning resistance. However, oxygen permeability value of $La_{1-x}Pb_xFeO_{3-\delta}$ was less than $La_{1-x}Sr_xFeO_{3-\delta}$ since the oxygen flux limited by the bulk ionic conductivity. [89]

La $(Fe_{1-x}$ $M_x)O_{3-\delta}$ M=Ga, Cr, Fe, Pb, Ni: The oxygen per-selectivity increases as Cr content increase, while oxygen per-selectivity decrease as Ni content decrease. [19]

$La_{0.6}Sr_{0.4}Co_{0.8}Fe_{0.2}O_{3-\delta}$: The increase of La content results in valence state transformation of Fe and Co ions, which leads to the high oxygen permeability flux value. The introduction of Fe ions to Co will restrain the transformation of Co (Co^{3+} to Co^{2+}) leading to stable phase. However, the oxygen flux value of the LSCF membrane decreased significantly with the time whereas an air stream containing sweeping gas of both CO_2 and H_2O impurities was introduced at a temperature of 810°C. The membrane decomposed partially and the oxygen flux slightly decreased by the formation of bicarbonate on the membrane surface. It can even cause a crack and deactivation resulting in phase instability under the high Air/CH_4 partial pressure gradient in long-term operation. [30]

$La_{0.6}A_{0.4}Co_{0.8}Fe_{0.2}O_{3-\delta}$: The oxygen permeability follows the order Ba > Ca > Sr > Na > La and the chemical/thermal stability: LaSrCoFe < LaBaCoFe. [19]

$La_{0.6}Sr_{0.4}Fe_{0.2}B_{0.8}O_{3-\delta}$: the oxygen flux value decreases in the sequence of Cu>Ni>Co>Fe>Cr>Mn. [30]

$La(Ba)Co(Fe)O_{3-\delta}$: $La(Ba)Co(Fe)O_{3-\delta}$ was synthesized by liquid citrate method showed good crystal structure, oxygen desorption ability and high permeation flux value. It was indicated that the introduction of Ba contributing to lower the oxygen permeation activation energy leading to the rise of the oxygen flux. Doping Fe in the materials with higher Ba content has not clear correlation with oxygen permeability, but provided the perovskite structure stability by decreasing the thermal expansion coefficient. The oxygen permeability follows the order: $La_{0.2}Ba_{0.8}Co_{0.2}Fe_{0.8}O_{3-\delta}$ > $La_{0.3}Ba_{0.7}Co_{0.2}Fe_{0.8}O_{3-\delta}$ > $La_{0.6}Ba_{0.4}Co_{0.8}Fe_{0.2}O_{3-\delta}$ > $La_{0.6}Ba_{0.4}Co_{0.2}Fe_{0.8}O_{3-\delta}$ With the increase content of Ba, the oxygen permeability increases due to the formed high oxygen vacancies and low average bond energy (ABE) of $La_{0.2}Ba_{0.8}Co_{0.2}Fe_{0.8}O_{3-\delta}$. [90] &[91].

$BaCo_{0.7}Fe_{0.2}Nb_{0.1}O_{3-\delta}$: BCFN exhibits more stability than any other membrane materials in the Ar, H_2, and CO_2 atmosphere, which has been widely used for partial oxidation studies of the coke oven gas recently. The total conductivity of BCFN was 3.6S/cm at 600°C, which declined with the rise of temperature (600-650°C) due to the oxygen desorption consuming the electron holes. However, the conductivity increased again with the rise of temperature above 650°C . Finally, the oxygen permeability was 5.5 ml/(min.cm^2) in an experimental apparatus at 870°C under the air/helium oxygen partial pressure gradient. Large radius size of Ba contributes to the tolerance factor to be 1 as well as the increase the lattice free volumn (Fv). [90]& [92]

Perovskite type: $LaGaO_{3-\delta}$ (LGO)

Currently, cobalt containing perovskite membranes are limited in practical industry due to [30]:

1) Low structure stability: collapses of membrane and unstability under high oxygen partial pressure and reducing environment.

2) High thermal expansion coefficient: may lead to crack easily, especially under a large oxygen gradient resulting unstable of the phase structure.

Therefore, cobalt-free perovskite compounds such as $LaGaO_3$ have been developed, which incorporated with alkaline metals (Ba, Ca, and Sr) on A-site and transition metals Fe, Co, Ti, Cr, Ni on Ga (B-site) can form $La(A)Ga(B)O_3$.

$La_{1-x}M_xGaO_3$(M=Ba, Ca, Sr): Doping alkali metals to A-site will decrease the overall electric conductivity, but could also increase ionic conductivity value which depends on the doping metal type. The ionic conductivity follows the order: Sr>Ba>Ca. Doping Sr will increase the electric conductivity and electric conductivity is highest with x=1. [93]

$(La,Sr)Ga_{1-z}M_zO_{3-\delta}$ (z=0-0.2): Doping Fe, Co, Ni metals on B-site will increase the ionic conductivity, but adding Ti, Cr to Ga-site will decrease the ionic conductivity. $(La,Sr)Ga_{1-z}Ni_zO_{3-\delta}$has high oxygen permeability but low chemical stability. [93]

$La_xSr_{1-x}Ga_yFe_{1-y}O_{3-\delta}$: The oxygen permeability follows the order $La_{0.2}Ba_{0.8}Co_{0.2}Fe_{0.8}O_{3-\delta}$> $La_{0.3}Sr_{0.7}Ga_{0.2}Fe_{0.8}O_{3-\delta}$ > $La_{0.6}Sr_{0.4}Ga_{0.8}Fe_{0.2}O_{3-\delta}$> $La_{0.6}Sr_{0.4}Ga_{0.2}Fe_{0.8}O_{3-\delta}$. With the increasing of Ba content, the activation energy will decrease and less energy is required to overcome the force for oxygen ion migration leading to increase in the oxygen flux. Doping Fe into B-site provides the perovskite structure stability. [94]

$La_{0.15}Sr_{0.85}Ga_{0.3}Fe_{0.7}O_{3-\delta}$: Due to $La_{0.6}Sr_{0.4}Co_{0.8}Fe_{0.2}O_{3-\delta}$ membrane having low thermal/chemical stability, doping high valent Ga to partial substitute Co metal could improve their thermal/chemical stability performance because Ga only shows +3 valent

in the membrane (low expansion coefficient). Ga provides more stable valance bond than Co. LSGFO has higher oxygen permeability than LSCFO due to Ga increasing the oxygen vacancies in the membrane. It was found that doping Fe metals to B-site has more thermal stability than doping Co and Ni, however, it shows low oxygen flux value. [90]

$La_{0.7}Sr_{0.3}Fe_{1-y}Ga_yO_{3-\delta}$ (y=0, 0.3, 0.5, 0.7, 1): was investigate as catalysts for methane combustion of which it shows the highest activity. At 600°C, 90% methane conversion was attained with $La_{0.7}Sr_{0.3}Fe_{0.7}Ga_{0.3}O_{3-\delta,}$ while the conversion of methane was as low as 10% with $La_{0.7}Sr_{0.3}GaO_{3-\delta}$. The Fe content in the mixed oxides had strong influence on their structures and surface characteristics, however, the high cost and unstable of phase stability limits its application. [73]& [95]

$LaGa_{1-x-y}Co_xMg_yO_{3-\delta}$: Using Mg, Al as partial substitution of Ga increases electric conductivity and especially doping with Mg leads to an increase in oxygen nonstoichiometry, electronic and oxygen ionic conductivity because of the transformation of transition metal ions [26]. Increasing the amount of the cobalt content results in the increase in the electrical conductivity and thermal expansion coefficient, while increasing amount of magnesium concentration leads to oxygen permeation limited by bulk diffusion [96].

$La_{1-x}A_xM_{1-y}B_yO_{3-\delta}$ (A=Sr^{2+}, Ln^{3+}, Ce^{4+}; M= Fe, Co, Ga; B=Co, Fe, Mg, x=0.1-1mol, y=0.1-0.5mol), the electric conductivity will increase by doping with Fe and Co.

$La_{0.85}Ce_{0.1}Ga_{0.3}Fe_{0.65}Al_{0.05}O_{3-\delta}$: Under 900°C, perovskite structure is stable in the condition of 20 vol% CO_2 + He atmosphere for 100h and the oxygen flux reaches $1.23*10^{-7}$mol s^{-1} cm^{-2}.

$BaCe_{0.15}Fe_{0.85}O_{3-\delta}$: The oxygen flux of $BaCe_{0.15}Fe_{0.85}O_{3-\delta}$ increases with the increasing content of Fe and has high thermal/chemical stability.

$Ba_{0.5}Sr_{0.5}Zn_{0.8}Fe_{0.2}O_{3-\delta}$: has good thermal/chemical stability and the highest oxygen flux among the cobalt free membranes.

$BaZr_{0.5}Co_{0.8}Fe_{0.2}O_{3-\delta}$ (BZCF): The thermal/chemical stability of this membrane is greater than of BSCF, however, its oxygen flux is half of BSCF. It provides good stability under an air/helium oxygen chemical gradient for partial oxidation of methane at 900°C and the methane conversion reaches 96-98%, with CO selectivity being with 98-99%. After the experiment, the membrane was characterized by XRD, SEM and EDX. It was shown that the perovskite structure has phase inversion but the perovskite structure was maintained. [45]

$BaCo_{0.4}Fe_{0.4}Zr_{0.2}O_{3-\delta}$: It was found that it was difficult to synthesize the pure phase BCFZ since the Zr^{4+} ion is relatively large for occupation of B-site. Therefore Zn, which exhibits constant state, was chosen to substitute Zr in BCFZ. [70]